

**High Yield Functional Expression, Purification,
and Reconstitution of Human Sodium/D-
Glucose Cotransporter 1 (hSGLT1) in *Pichia
pastoris***
&
**Pilot Studies for Photoaffinity Labeling of Functional
Domains of SGLT1**

Dissertation

Submitted to the Department of Chemistry
University of Dortmund, Germany
For the Degree of Doctor of Natural Sciences

Completed at

Max Planck Institute for Molecular Physiology, Dortmund, Germany

By

Navneet Kumar Tyagi

Dortmund 2005

The research work described in this thesis was carried out in the period from November 2001 to November 2004 at the Max Planck Institute for Molecular Physiology, Dortmund, Germany, under the supervision of Prof. Dr. Dr. h.c. Rolf K.H. Kinne in the department of Epithelial Cell Physiology.

1. Referee: Prof. Dr. Dr. h.c. Rolf K.H. Kinne
2. Referee: Prof. Dr. Herbert Waldmann

*“This thesis work is dedicated to
My wonderful, awesome and precious parents
Siyawati and Vijai
Who have demonstrated the true meaning of the word
`Love`
By their endless sacrifices, bountiful care, and unshakable
determination for my well being throughout every day of
their lives”.*

*“The beauty and frustration of science
is that it constantly produces surprises”*

“Unknown”

Abbreviations.....	v
1. Introduction	1
1.1. Transporters.....	1
1.2. Solute carrier (SLC) families of transporters	2
1.2.1. Sodium/glucose cotransporter family (SLC5).....	3
1.2.2. Sodium/glucose cotransporter protein (SGLT1)	8
1.3. <i>Pichia pastoris</i> as an expression host.....	10
1.4. Photoaffinity labeling	11
2. Aim of the study	13
3. Materials and methods.....	14
3.1. General equipments.....	14
3.2. Materials.....	15
3.2.1. Chemicals	15
3.2.2. Enzymes and reagents for molecular biology	16
3.2.3. Antibodies	16
3.2.4. Commercial Kits and other materials.....	16
3.2.5. Primers for preparation of cDNA inserts	17
3.2.6. Plasmids.....	17
3.2.6.1. Original plasmids	17
3.2.6.2. Plasmid with insert	18
3.3. Work with <i>E.coli</i>	19
3.3.1. <i>E.coli</i> strains	19
3.3.2. Media for bacterial culture	19
3.3.3. General	20
3.3.4. Transformation of plasmid in <i>E.coli</i>	20
3.3.4.1. Preparation of competent cells by CaCl ₂ method.....	20
3.3.4.2. Heat shock transformation of the plasmid.....	20
3.4. Work with <i>P. pastoris</i>	20
3.4.1. <i>P. pastoris</i> strains	20
3.4.2. Media for <i>P. pastoris</i> culture.....	21
3.4.3. General	21
3.4.4. Electroporation of <i>P. pastoris</i> with plasmid pPICZB or pPICZB-hSGLT1	22
3.5. Recombinant DNA processing and manipulation.....	22
3.5.1. Buffers and solutions.....	22
3.5.2. Restriction endonuclease digestion of DNA	23
3.5.3. Purification of the digested DNA.....	23
3.5.4. Ethanol precipitation of DNA	23
3.5.5. Dephosphorylation of linearized plasmid DNA by CIP.....	23
3.5.6. Ligation of DNA fragments	24

3.5.7. Miniprep: small-scale preparation of plasmid DNA	24
3.5.8. Large scale preparation of plasmid DNA	24
3.5.9. Quantification of DNA and RNA solutions	25
3.5.10. Agarose gel electrophoresis	25
3.5.11. DNA recovery from agarose gel	26
3.5.12. DNA sequencing	26
3.5.13. DNA amplification of hSGLT1 gene by PCR for cloning into different expression systems	26
3.5.14. Addition or deletion mutagenesis in hSGLT1 gene	27
3.5.14.1. Addition of 30 base pairs long spacer at the C-terminal of hSGLT1 gene ...	29
3.5.14.2. Addition of FLAG tag in hSGLT-spacer gene	29
3.5.14.3. Deletion of N-terminal half of hSGLT1 gene	29
3.5.15. Addition of Unc-F gene at the N-terminal of hSGLT1 gene	30
3.6. Protein expression and analysis.....	30
3.6.1. Growth conditions of <i>E.coli</i> for hSGLT1 expression.....	30
3.6.2. Growth condition of <i>P. pastoris</i> for hSGLT1 expression	31
3.6.3. hSGLT1 purification from <i>P. pastoris</i>	31
3.7. Protein analysis.....	32
3.7.1. Buffers and solutions.....	32
3.7.2. Measurement of protein concentration.....	33
3.7.2.1. Enhanced alkaline copper (Lowry) protein assay	33
3.7.3. SDS-PAGE	33
3.7.4. Coomassie staining of the polyacrylamide gels.....	34
3.7.5. Western blot analysis.....	34
3.8. Functional analysis of recombinant hSGLT1.....	35
3.8.1. Membrane preparations for transport studies.....	35
3.8.2. Reconstitution of recombinant hSGLT1	36
3.8.3. Transport assay of hSGLT1 in membranes and in proteoliposomes.....	36
3.9. Chemical synthesis of photoaffinity probes	37
3.9.1. [(2'-Iodo-4'-(3''-trifluoromethyldiaziriny) phenoxy]-D-glucopyranoside (TIPDG)	
.....	37
3.9.1.1. 4-Methoxytrifluoroacetophenone (1)	37
3.9.1.2. 3-Iodo-4-methoxytrifluoroacetophenone (2).....	37
3.9.1.3. 4-Hydroxy-3-iodo-trifluoroacetophenone (3)	37
3.9.1.4. [(2'-Iodo-4'-trifluoroacetyl) phenoxy]-2,3,4,6-tetra-O-acetyl-D-	
glucopyranoside (5).....	37
3.9.1.5. [(2'-Iodo-4'-trifluoroacetyloxime) phenoxy]-2,3,4,6-tetra-O-acetyl-D-	
glucopyranoside (6).....	38

3.9.1.6. [(2'-Iodo-4'-(3''-trifluoromethyldiaziridinyl) phenoxy]-2,3,4,6-tetra-O-acetyl-D- glucopyranoside (7).....	38
3.9.1.7. [(2'-Iodo-4'-(3''-trifluoromethyldiaziriny) phenoxy]-2,3,4,6-tetra-O-acetyl-D- glucopyranoside (8).....	39
3.9.1.8. [(2'-Iodo-4'-(3''-trifluoromethyldiaziriny) phenoxy]-D-glucopyranoside (9)	40
3.9.2. [(4'-Benzoyl) phenoxy]-D- glucopyranoside (BzG).....	40
3.9.2.1. [4'-Benzoyl) phenoxy] -2,3,4,6-tetra-O-acetyl-D- glucopyranoside (11).....	40
3.9.2.2. [(4'-Benzoyl) phenoxy]-D- glucopyranoside (12)	40
3.9.3. 3-Azidophlorizin (3-AP)	41
3.9.3.1. 3-Nitrophlorizin (14)	41
3.9.3.2. 3-Aminophlorizin (15).....	41
3.9.3.3. 3-Azidophlorizin (16).....	42
3.9.4. n-Methyl-6C- (Azimethyl)-D- glucopyranoside (6-AG)	42
3.9.4.1. Methyl-2,3,4-tri-O-benzyl-7-deoxy-DL-glycero-D-glucohepta-1,5- pyranoside (18)	42
3.9.4.2. Methyl-2,3,4-tri-O-benzyl-7-deoxy-D-glucohepto-1,5-pyranoside-6-ulose (19)	43
3.9.4.3. Methyl- 7- deoxy-D-glucohepta- 1, 5- pyranoside-6- ulose (20).....	43
3.9.4.4. n-Methyl-6C-(Azimethyl)-D-glucopyranoside (22).....	44
3.10. Photoaffinity labeling of loop 13.....	45
3.10.1. Isolation of small intestine brush border membrane vesicles (BBMV).....	45
3.10.2. Transport measurements.....	45
3.10.3. Photoaffinity labeling of truncated loop 13 protein with TIPDG or BzG.....	45
3.10.4. Photoaffinity labeling of truncated loop 13 protein with 3-AP.....	46
4. Results	48
4.1. <i>E.coli</i> as an expression host.....	48
4.1.1. Construction of different clones of hSGLT1 in pET22b vector.....	48
4.1.2. Construction of pET22b-Unc-F and pET22b-Unc-F-hSGLT1 clones.....	49
4.1.3. hSGLT1 expression in <i>E.coli</i>	50
4.1.4. β -subunit of E.coli ATPase expression in pET22b-Unc-F and pET22b-Unc-F-hSGLT1 plasmids.....	51
4.1.5. Messenger RNA stability of hSGLT1 in <i>E.coli</i>	52
4.2. <i>Pichia pastoris</i> as an expression host.....	54
4.2.1. Construction of expression plasmid pPICZB-hSGLT1.....	54
4.2.2. Identification of positive clones of hSGLT1 showing protein expression.....	55
4.2.3. Optimization of feeding and induction in the shake flask cultures	55
4.2.4. Purification of hSGLT1 from <i>Pichia pastoris</i>	56

4.2.5. Functional analysis of recombinant hSGLT1 in right-side-out membrane vesicles	57
4.2.6. Functional analysis of recombinant hSGLT1 in prteoliposomes	58
4.3. Synthesis and Characterization of different photoaffinity probes	63
4.3.1. Synthesis of labels BzG and 3-AP for the identification of phlorizin interaction sites	63
4.3.2. Synthesis of label TIPDG for the identification of arbutin ineraction sites	64
4.3.3. Synthesis of label 6-AG for the identification of D-glucose interaction sites.....	64
4.3.4. Photochemical properties and stability of TIPDG, BzG, 3-AP and 6-AG	65
4.3.5. Inhibition of glucose uptake in rabbit small intestine BBMV by BzG and 3-AP ..	66
4.3.6. Inhibition of glucose uptake in rabbit small intestine BBMV by TIPDG	67
4.3.7. Inhibition of glucose uptake in rabbit small intestine BBMV by 6-AG	68
4.4. Photoaffinity labeling of truncated loop 13 with TIPDG, BzG, and 3-AP	70
4.4.1. Photoaffinity labeling of truncated loop 13 with TIPDG and BzG.....	70
4.4.2. Photoaffinity labeling of truncated loop 13 with 3- Azidophlorizin	71
4.4.3. Identification of the ligand contact points	72
5. Discussion	74
5.1. <i>E. coli</i> as an expression host.....	75
5.1.1. Probable reasons for not getting hSGLT1 expression in <i>E. coli</i>	75
5.1.1.1. Codon usage	75
5.1.1.2. Signal sequences.....	76
5.1.1.3. Degradation of hSGLT1 mRNA in <i>E.coli</i>	76
5.1.1.4. Comparison to other attempts to express hSGLT1 in <i>E. coli</i>	78
5.2. <i>P. pastoris</i> as an expression host.....	80
5.2.1. Expression of hSGLT1 in <i>P. pastoris</i>	80
5.2.2. Protein purification.....	81
5.2.3. Reconstitution and functional analysis of recombinant hSGLT1	82
5.2.4. Reasons for getting functional expression of hSGLT1 in <i>P. pastoris</i>	82
5.2.5. Advantages of our expression method	83
5.3. Photoaffinity labeling of truncated loop 13.....	84
5.4. Future prospective	87
6. Summary	89
7. Zusammenfassung	91
8. Reference list.....	93

Erklärung

Acknowledgements

Curriculum Vitae

Abbreviations

aa	Amino Acids
Ac	Acetate
6-AG	n-Methyl-6C- (azimethyl)-D- glucopyranoside
Amp	Ampicillin
3-AP	3- Azidophlorizin
Arg	Arginine
ATP (ADP, AMP)	Adenosine-5'-tri (Di, Mono-) Phosphate
BBMV	Brush border membrane vesicles
bp	Base Pair
BSA	Bovine Serum Albumin
BzG	[(4'-Benzoyl)phenoxy]-D- glucopyranoside
cDNA	Complimentary DNA
CIAP	Calf Intestine Alkaline Phosphatase
DMSO	Dimethylsulphoxide
DNA	Deoxyribonucleic acid
dNTP	Deoxy-Nucleotriphosphate
DTT	Dithiothreitol
EDTA	Ethylenediaminetetraacetate
EST	Expressed Sequence Tag
EtBr	Ethidium bromide
g	Gram
h	Hours
hSGLT1	Human sodium/D- glucose cotransporter 1
IPTG	Isopropyl- β -D-Thiogluconide
K_i	Inhibition constant
M	Molar
MALDI-TOF	Matrix-assisted laser desorption ionization –time of flight
MCS	Multiple Cloning Site
Min	Minute
ml	Milliliter
mM	Milli Molar
NC	Nitro Cellulose membrane
OD	Optical Density
PAGE	Polyacrylamide Gel Electrophoresis
PCR	Polymerase Chain Reaction
RNA	Ribonucleic acid
RT	Room Temperature

SDS	Sodium Dodecylsulphate
TCA	Trichloroacetic acid
TEMED	<i>N, N, N', N'</i> Tetramethylethylenediamine
TIPDG	[(2'-Iodo-4'-(3''-trifluoromethyldiaziriny)phenoxy]-D-glucopyranoside
TMH	Trans Membrane Helices
Tris	Tris (hydroxymethy) amino methane
Trp	Tryptophan
U	Unit
UV	Ultraviolet

1. Introduction

1.1. Transporters

Transporters are the gatekeepers for all cells and organelles, facilitating influx and efflux of crucial compounds such as sugars, amino acids, nucleotides, inorganic ions and drugs. Transporters can be divided into passive and active transporters (Figure 1.1). Passive transporters, allow passage of solutes (e.g., glucose, amino acid, urea) across membranes down their electrochemical gradients. Active transporters create ion/solute gradients across membranes, utilizing diverse energy-coupling mechanisms. These active transporters are classified as primary- or secondary-active transporters according to the directness of coupling to cellular energy (e.g., ATP hydrolysis, or ion gradients).

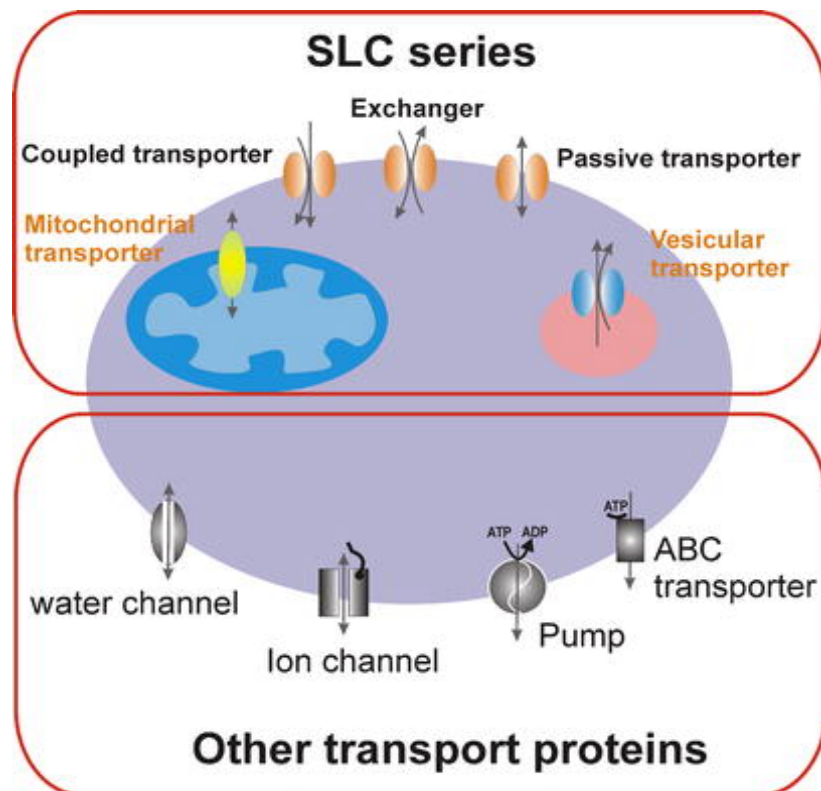


Figure 1.1 Cartoon showing a cell with different transporters. Solute carrier (SLC)- and non-SLC transporters expressed in the plasma membrane or in intracellular compartment membranes are shown.

Primary-active, ATP-dependent transporters include members of the ATP-binding cassette (ABC) transporter family and ion pumps (ATPases). Mammalian ABC transporters [e.g., P-glycoprotein/multi-drug resistance (MDR) proteins and transporter associated with antigen processing (TAP)] bind or hydrolyze ATP as a control gate for the transport of a variety of substances such as ions, carbohydrates, lipids, xenobiotics and drugs, out of cells or into organelles (Borst and Elferink, 2002). Ion pumps hydrolyze ATP to pump ions such as Na^+ , K^+ , H^+ , Ca^{2+} and Cu^{2+} out of cells or into organelles, for review see (Dunbar and Caplan,

2000; Muller and Gruber, 2003). These pumps also generate and maintain electrochemical ion gradients across membrane, and are thus called active transporters. Such ion gradients are used in turn by secondary-active, ion-coupled transporters to drive uphill transport of nutrients across biological membranes.

Similar to transporter, channels allow movement of solute down their electrochemical gradients, for review see (Armstrong, 2003; Chen, 2003; Decoursey, 2003; Jiang et al., 2003; Yu and Catterall, 2003). Transporters typically have a fixed stoichiometry of ion/solute movement per translocation cycle. Ion or solute flow through channels, on the other hand, is controlled by open probability of the channel via gating mechanisms.

1.2. Solute carrier (SLC) families of transporters

The solute carrier (SLC) series includes genes encoding passive transporters, ion coupled transporters and exchangers (Hediger et al., 2004; Wright and Turk, 2004). A transporter has been assigned to a specific SLC family if it has at least 20-25% amino acid sequence identity to other members of that family (Turk and Wright, 1997). The list of currently approved SLC human gene symbols is shown in Table 1.1. The table comprises 43 different SLC transporter families of the SLC series and the number of members in each family.

Table 1.1 List of currently approved solute carrier (SLC) families.

The HUGO SLC Family Series		Total
SLC1	The high-affinity glutamate and neutral amino acid transporter family	7
SLC2	The facilitative GLUT transporter family	14
SLC3	The heavy subunits of the heteromeric amino acid transporters	2
SLC4	The bicarbonate transporter family	10
SLC5	The Na ⁺ /glucose cotransporter family	8
SLC6	The sodium- and chloride-dependent neurotransmitter transporter family	16
SLC7	The cationic amino acid transporter/glycoprotein-associated amino-acid transporter family	14
SLC8	The Na ⁺ /Ca ²⁺ exchanger family	3
SLC9	The Na ⁺ /H ⁺ exchanger family	8
SLC10	The sodium bile salt cotransport family	6
SLC11	The proton-coupled metal ion transporter family	2
SLC12	The electroneutral cation-Cl cotransporter family	9
SLC13	The human Na ⁺ -sulfate/carboxylate cotransporter family	5
SLC14	The urea transporter family	2
SLC15	The proton oligopeptide cotransporter family	4
SLC16	The monocarboxylate transporter family	14
SLC17	The vesicular glutamate transporter family	8
SLC18	The vesicular amine transporter family	3
SLC19	The folate/thiamine transporter family	3
SLC20	The type-III Na ⁺ -phosphate cotransporter family	2

SLC21/SLCO	The organic anion transporting family	11
SLC22	The organic cation/anion/zwitterion transporter family	18
SLC23	The Na ⁺ -dependent ascorbic acid transporter family	4
SLC24	The Na ⁺ /(Ca ²⁺ -K ⁺) exchanger family	5
SLC25	The mitochondrial carrier family	27
SLC26	The multifunctional anion exchanger family	10
SLC27	The fatty acid transport protein family	6
SLC28	The Na ⁺ -coupled nucleoside transport family	3
SLC29	The facilitative nucleoside transporter family	4
SLC30	The zinc efflux family	9
SLC31	The copper transporter family	2
SLC32	The vesicular inhibitory amino acid transporter family	1
SLC33	The acetyl-CoA transporter family	1
SLC34	The type-II Na ⁺ -phosphate cotransporter family	3
SLC35	The nucleoside-sugar transporter family	17
SLC36	The proton-coupled amino acid transporter family	4
SLC37	The sugar-phosphate/phosphate exchanger family	4
SLC38	The System A and N, sodium-coupled neutral amino acid transporter family	6
SLC39	The metal ion transporter family	14
SLC40	The basolateral iron transporter family	1
SLC41	The MgtE-like magnesium transporter family	3
SLC42	The Rh ammonium transporter family (pending)	3
SLC 43	The Na ⁺ -independent, system-L-like amino acid transporter family	2
Total		298

In general the genes are named using the root symbol SLC, followed by a numeral (e.g., SLC1, solute carrier family 1), the letter A (which act as a divider between the numerals) and finally the number of the individual transporter (e.g., SLC5A1, sodium/glucose cotransporter protein). These general rules of SLC gene nomenclature have been elaborated further for a couple of families. In the nucleotide-sugar transporter family SLC35, the letter between SLC35 and family member number has been exploited to specify specific subfamilies, called A, B, C, D and E (Ishida and Kawakita, 2004). In another family, originally named SLC21, encoding the organic anion-transporting (OATP) proteins, the “21” and the “A” have been replaced by the letter “O”, which stands for organic transporter. This modification has occurred to accommodate a unique, species-independent classification and naming system that has been introduced, because this family has been the subject of rapid evolution, giving rise to new isoforms within a given species (Hagenbuch and Meier, 2004).

1.2.1. Sodium/glucose cotransporter family (SLC5)

The sodium/glucose cotransporter family (SLC5) has 220 members in animal and bacterial cells (Wright and Turk, 2004). An unrooted phylogenetic tree of 11 human members of the SLC5 family of cotransporters and two other vertebrate members of known function is shown

in Figure 1.2. The 11 human genes (Table 1.2) are expressed in tissues such as the small intestine, kidney, brain, muscle, and thyroid gland. Despite the homology among the proteins (21-70% amino acid identity to SGLT1) there is diversity in gene structure: in eight of ten genes mapped the coding sequences are found in 14-15 exons (SGLT1-6, NIS, and the Na⁺-dependent multivitamin transporter SMVT) (Turk et al., 1994; Wang et al., 1999). On the other hand the coding sequences for the choline transporter (CHT) and SMIT are contained in eight and one exons respectively (Mallee et al., 1997; Okuda et al., 2000). In SGLT4-6 and SMIT there is evidence for alternative splicing (Roll et al., 2002).

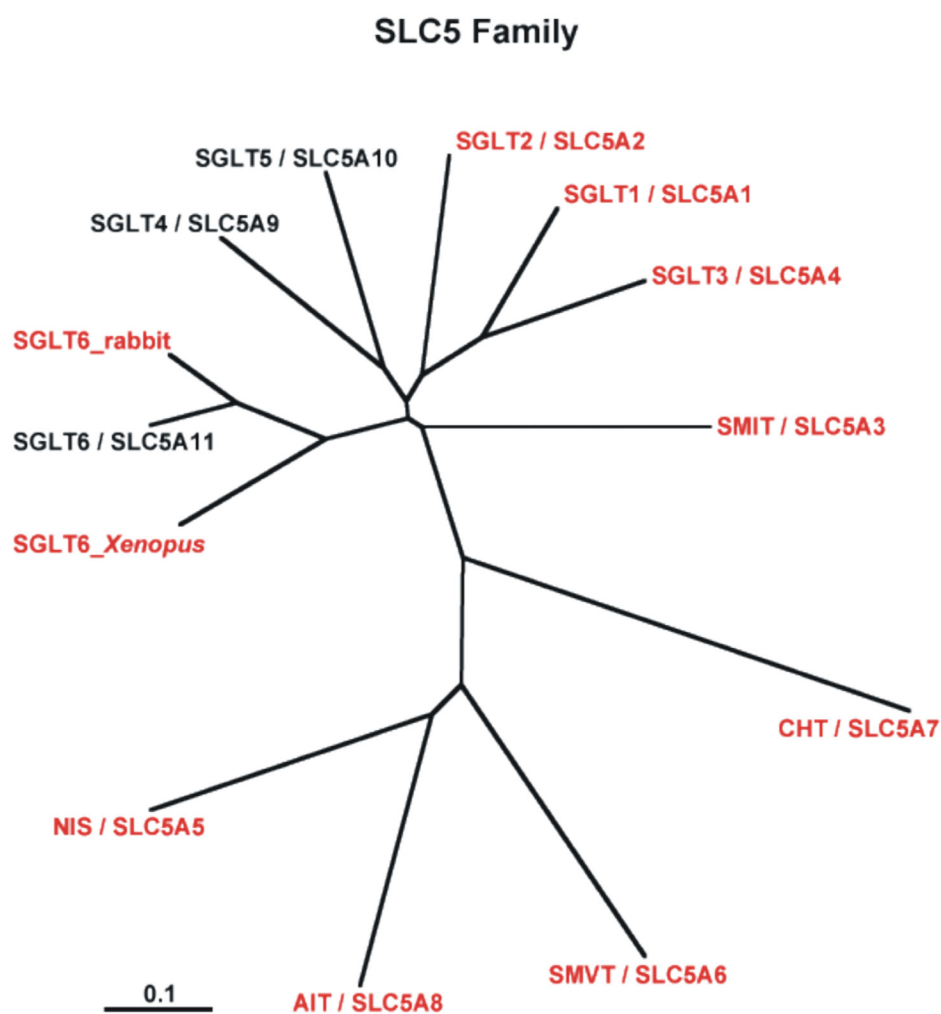


Figure 1.2 Unrooted phylogenetic tree of the 11 human members of the SLC5 family of cotransporters and two other vertebrate members of known function. Members for which transport functions have been demonstrated experimentally are shown in *red*. Members shown in *black* have yet to have their function determined. In a pairwise basic local alignment search tool (BLAST) analysis the amino acid identities relative to SGLT1 were 59% SGLT2, 70% SGLT3, 56% SGLT4, 57% SGLT5, 50% SGLT6, 55% SMIT, 24% SMVT, 24% CHT, and 21% NIS (*SGLT* Na⁺/glucose transporter, *SMIT* Na⁺/*myo*-inositol transporter, *SMVT* Na⁺/multivitamin transporter, *CHT* choline transporter, *AIT* apical iodide transporter, *NIS* Na⁺/iodide transporter).

Table 1.2 The SLC5 sodium/glucose cotransporter family (OMIM Online Mendelian Inheritance in Man Database, *TMH* transmembrane helix, *aa* amino acids).

Human gene name	Protein name	Aliases	Predominant substrates	Transport type/coupling ion*	Tissues distribution and cellular/subcellular expression ^r	Link to disease	Human gene locu	Sequence Accession ID	Splice variants and their specific features ^s
SLC5A1	SGLT1	None	Glucose and galactose (urea and water)	C/Na ⁺ (H ⁺) F/Na ⁺ (H ⁺) Channel: urea and water	Small intestine>>trachea, kidney and heart; plasma membranes	Glucose galactose malabsorption ^G OMIM 182380	22q13.1	NM_000343	
SLC5A2	SGLT2	None	Glucose	C/Na ⁺	Kidney cortex	Familial renal glycosuria ^G OMIM 182381	16p12-p11	NM_003041	
SLC5A3	SMIT	None	myo-inositol (glucose)	C/Na ⁺	Brain, heart, kidney and lung; plasma membranes	Down's syndrome? OMIM 600444	21q22.12	NM_006933	
SLC5A4	SGLT3	SAAT1	Na ⁺ (H ⁺)	Glucose activated Na ⁺ (H ⁺) channel	Small intestine (cholinergic neurons), skeletal muscle, kidney, uterus and testis; plasma membranes		22q12.2-q12.3	NM_14227	
SLC5A5	NIS		I ⁻ (ClO ₄ ⁻ , SCN ⁻ , NO ₃ ⁻ , Br ⁻)	C/Na ⁺ Uniporter Na ⁺ channel Urea water	Thyroid, breast, colon and ovary; plasma membranes	Thyroid hormonogenesis ^G OMIM 601843	19p13.2-p12	NM_000453	
SLC5A6	SMVT		Biotin, lipoate and pantothenate	C/Na ⁺	Brain, heart, kidney, lung and placenta; plasma membranes		2p23	NM_021095	
SLC5A7	CHT	CHT1	Choline	C/Na ⁺ /Cl ⁻	Spinal cord and medulla		2q12	NM_021815	

SLC5A8**	SGLT4				(intracellular vesicles) Small intestine, kidney, liver, lung and brain		1p32	HCT1951464	Internal splice in Exon 14 adds either 38 or 53 aa between TMHs13-14
SLC5A9	SGLT5	Rabbit RK-D			Kidney		17p11.2	XM_064487	Exon 7 may be spliced out deleting 26 aa between TMHs 5-6; internal splice in exon 10 means either 36 or 52 aa between TMHs 8-9; and an internal splice in exon 12 adds

SLC5A10	SGLT6	KST1 Rabbit ST1 Rabbit SMIT2	Rabbit ortholog: myo-inositol, chiro- inositol, glucose and xylose. Xenopus laevis ortholog: myo-inositol and glucose	C/Na ⁺	Small intestine, brain, kidney, liver, heart, and lung	16p12.1	NM_052944	either 12 or 37 aa between TMHs 11-12
SLC5A11	AIT		Iodide		Thyroid; apical plasma membrane	12q23.1	NM_145913	Splicing eliminates exon 6 and TMH 4

*C cotransporter; F uniporter. Function based on results obtained with heterologous expression systems

** Provisional SGLT4 exons identified by mining the Celera databases

^T Tissue distribution of SGLT1-6 was determined RNAase protection assays using gene specific probes. Also includes data from the original cloning papers and GeneCard (EST, and/or DNA array)

^G Gene defect

^S Potential alternative splice sites

Note: single nucleotide polymorphisms (SNPs) and variants in the NCBI SNP database are not included.

1.2.2. Sodium/glucose cotransporter protein (SGLT1)

SGLT1 (SLC5A1) was expression-cloned in 1987 (Hediger et al., 1987). SGLT1 is expressed primarily in the brush border membrane of mature enterocytes in the small intestine where it plays a central role for the homeostasis of glucose, galactose, salt and water (Kinne, 1976; Wright et al., 1994; Wright and Loo, 2000; Wright et al., 2001). The most well known genetic disease caused by SGLT1 is glucose-galactose malabsorption (GGM) (Kasahara et al., 2001; Lam et al., 1999; Martin et al., 1997; Martin et al., 1996; Turk et al., 1991; Wright et al., 2001; Wright et al., 2002). This is a rare autosomal recessive disease (Online Mendelian Inheritance in Man database accession No. *OMIM* 182380) that presents in newborn infants as a life-threatening diarrhea. The diarrhea ceases promptly on removing dietary glucose, galactose and lactose, but returns immediately on reintroducing one of the offending sugars into the child's diet. In some 46 patients tested so far mutations have been identified in the SGLT1 gene that cause the defect in sugar transport. These include missense, nonsense, frame-shift, and splice-site mutations. The missense mutations were studied using the oocytes expression system, where the defect in transport in 22 out of 23 mutants was due to missorting of the protein in the cell. Surprisingly, some very conservative GGM mutations cause the trafficking defect; e.g., four are alanine to valine trafficking mutants. Normal trafficking is restored when valine is replaced by cysteine, suggesting that slight conformational changes in the protein interfere with interactions between the transport vesicles containing SGLT1 and motor proteins responsible for delivery of the vesicle to plasma membrane.

Human isoforms of SGLT1 are 664 amino acids long with 14 transmembrane α -helices and both the N- and C-terminals facing the extracellular fluid (Turk and Wright, 1997) (Figure 1.3). A secondary structure model as shown in Figure 1.3 is indicating position of loop 13 as intracellular (Turk and Wright, 1997), while our group (Lin et al., 1999) results with 6 \times Histidine tagged mutant in COS-7 cells indicates that the last large loop (loop13) towards the C-terminal end faces the cell exterior where it might be involved in substrate recognition. However both the secondary structure models are not able to explain all the functional properties of SGLT1, so both models are not 100% correct, but it might be the case that this loop exists in dynamic equilibrium between extracellular and intracellular orientations, which takes place during the interaction with substrates.

Extensive molecular biological and biophysical studies of hSGLT1 in *Xenopus laevis* oocytes revealed that the N-terminal half of the protein contains the Na⁺-binding sites (Meinild et al., 2001) while the solutes and inhibitors binding sites lies in the C-terminal half of protein (Panayotova-Heiermann et al., 1997; Panayotova-Heiermann et al., 1996). Further studies in this direction indicate that residue Gln-457, Thr-460 (Diez-Sampedro et al., 2001; Napoli et al., 1995) and negative charge at residue Asp-454 form the sugar-binding and translocation pathway (Diez-Sampedro et al., 2004). The mechanism by which SGLT1 couple their substrates across the cell membrane is still unknown. A commonly proposed kinetic model for

sodium/glucose cotransport is a six-state ordered kinetic model (Loo et al., 1993; Loo et al., 1998; Parent et al., 1992a; Parent et al., 1992b; Peerce and Wright, 1984). The model describes sodium/glucose cotransport as a series of ligand-induced conformational changes (Figure 1.4). On the external surface of the membrane, two Na^+ ions bind to the transporter before sugar. The empty transporter C (states 1 and 6), Na^+ -loaded transporter CNa_2 (states 2 and 5), and the sugar-loaded transporter CNa_2S (states 3 and 4) can “cross” the membrane. Membrane voltage affects Na^+ -binding and translocation of the empty transporter.

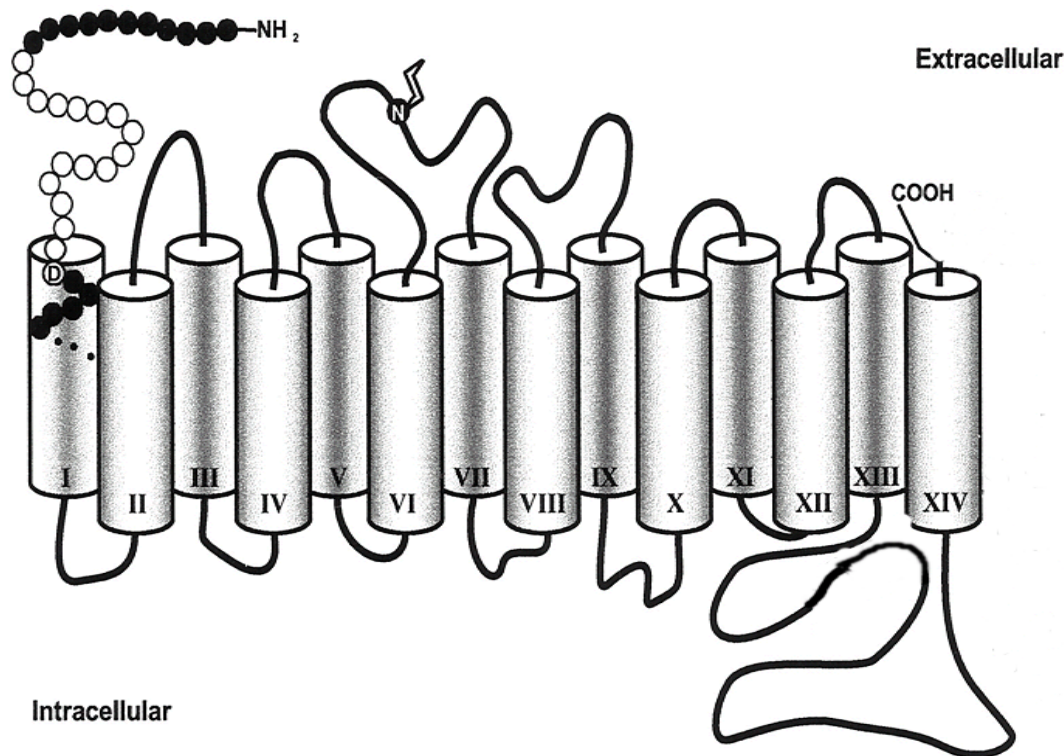


Figure 1.3 Tentative secondary structure model of hSGLT1. hSGLT1 consists of 14 α -helical transmembrane domains (shaded columns) with the N- and C-terminal located on the extracellular phase of membrane. The N-glycosylation site (Asn-248; N) is indicated (Quick and Wright, 2002).

Heterologous expression of hSGLT1 has been described in *Xenopus laevis* oocytes (Hediger et al., 1987), COS-7 cells (Birnir et al., 1990), CHO cells (Lin et al., 1998), Sf9 cells (Smith et al., 1992), and *Escherichia coli* (Quick and Wright, 2002) and has increased our knowledge about functions of transporter significantly but the amount of protein produced in the above mentioned systems is not sufficient for most of the biochemical, biophysical and structural studies which need tens or some times hundreds of milligrams of highly purified protein. In view of these difficulties our group's previous success in the expression and purification of different fragments of SGLT1 (Raja et al., 2003; Xia et al., 2003) and their subsequent use as a model for the identification of phlorizin-binding site and alkyl glucosides-binding site as studied by fluorescence spectroscopy and affinity labeling (Raja et al., 2004; Raja et al., 2003; Tyagi and Kinne, 2003; Xia et al., 2003) provided valuable information about different inhibitors mechanism. However there lies an urgent need to express hSGLT1 in full-length

and sufficient quantity. To achieve high-level expression of hSGLT1 we chose to use the methylotropic yeast *Pichia pastoris* because in the last 15 years this expression system has emerged as the most successful expression system for the heterologous expression of a wide variety of foreign proteins (Cereghino and Cregg, 2000; Cregg et al., 2000; Higgins and Cregg, 1998), especially membrane proteins, which were either not possible to express in *E. coli* or if possible, express in very low amounts often with loss of functionality.

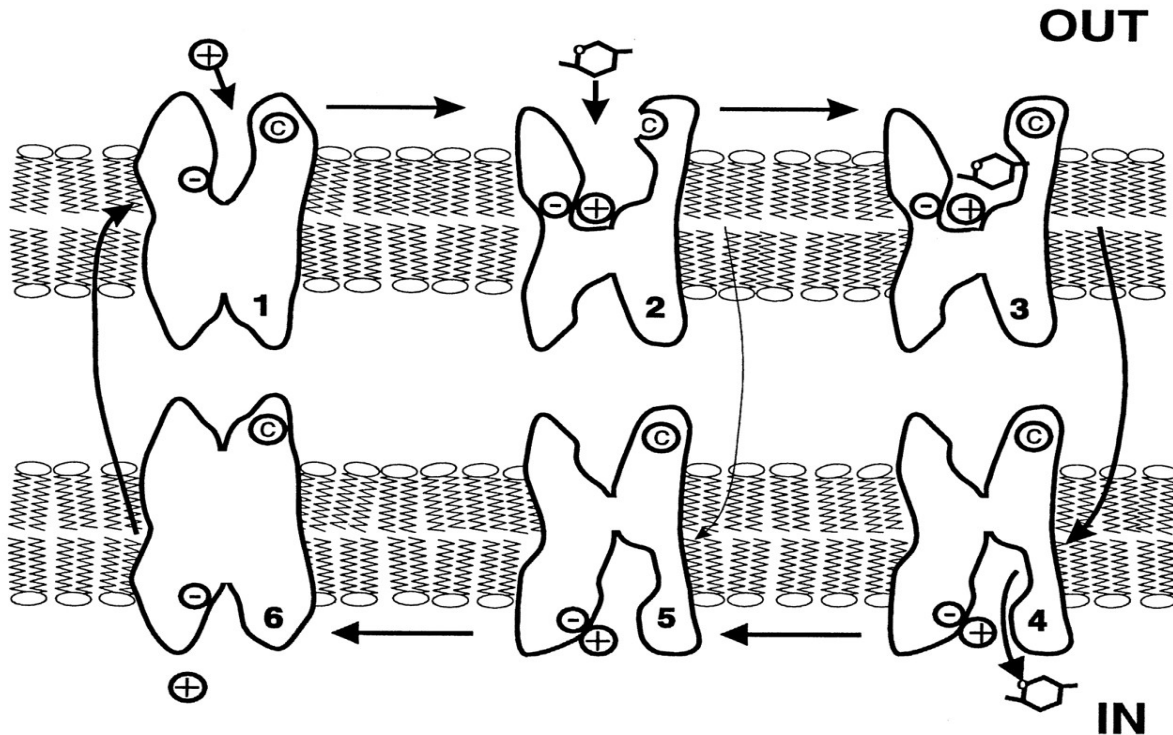


Figure 1.4 Cartoon of the 6-state ordered kinetic model for sodium/glucose cotransport. States 1-3 face the external and states 4-6 internal membrane surfaces, respectively. In the absence of ligands, the transporter exists in 2 states (1 and 6). At the external surface, 2 Na^+ ions bind to the transporter to form the complex CNa_2 (state 2). The fully loaded transporter CNa_2S (state 3) undergoes a conformational change (states 3 to 4) resulting in sodium/glucose cotransport. The reaction from state 2 to 5 represents a uniport (“leak”) pathway for the sugar (Loo et al., 1998).

1.3. *Pichia pastoris* as an expression host

Pichia pastoris has become a highly successful system for the expression of heterologous genes. Several factors have contributed to its rapid acceptance, the most important of which include:

1. A promoter derived from the alcohol oxidase I (*AOX1*) gene of *P. pastoris* that is uniquely suited for the controlled expression of foreign genes;
2. The similarity of techniques needed for the molecular genetic manipulation of *P. pastoris* to those of *Saccharomyces cerevisiae*, one of the most well-characterized experimental systems in modern biology;

3. The strong preference of *P. pastoris* for respiratory growth, a key physiological trait that greatly facilitates its culturing at high cell densities relative to fermentative yeasts; and
4. A 1993 decision by Phillips Petroleum Company to release the *P. pastoris* expression system to academic research laboratories, the consequences of which has been an explosion in the knowledge base of the system.

As a yeast, *P. pastoris* is a single-celled microorganism that is easy to manipulate and to culture. However, it is also a eukaryote and capable of many of the posttranslational modifications performed by higher eukaryotic cells, such as proteolytic processing, protein folding, and disulfide bond formation. Thus many proteins that end up as inactive inclusion bodies in *E. coli* are produced as biologically active molecules in *P. pastoris*. The *P. pastoris* system is also generally regarded as being faster, easier, and less expensive to use than expression systems derived from higher eukaryotes, such as insect and mammalian tissue culture cell systems, and usually gives higher expression levels.

A second role played by *P. pastoris* in research is not directly related to its use as a protein expression system. *P. pastoris* serves as a useful model system to investigate certain areas of modern cell biology, including the molecular mechanisms involved in import and assembly of peroxisomes, the selective autophagic degradation of peroxisomes, and the organization and function of the secretory pathway in eukaryotes. More detailed information on the *P. pastoris* system can be found in the numerous reviews describing the system (Cereghino and Cregg, 2000; Cregg et al., 2000; Higgins and Cregg, 1998) and the *Pichia* Expression Kit Manual (Invitrogen Corporation, Carlsbad, CA, USA). The DNA sequence of many *P. pastoris* expression vectors and other useful information can be found on the Invitrogen web site (<http://www.invitrogen.com>).

In the last few years the following membrane proteins have been successfully expressed in *P. pastoris*, Na⁺, K⁺-ATPase (Strugatsky et al., 2003), multidrug resistance protein1 (Cai et al., 2001), ATP-binding cassette transporter (Cai and Gros, 2003), NOP-1 (Bieszke et al., 1999), mammalian intestinal peptide transporter (Doring et al., 1998), human μ -opioid receptor (Talmont et al., 1996) and 5HT_{5A}-serotonergic receptor (Weiss et al., 1998).

1.4. Photoaffinity labeling

Photoaffinity labeling and cross-linking refer to a variety of important biochemical techniques that are used to investigate structural and functional properties of biological systems, for review see (Bayley, 1983; Bayley and Knowles, 1977; Brunner, 1993; Dorman and Prestwich, 2000). These techniques make use of reagents, which, after targeting to a biological system or component, can be activated with UV light to generate highly reactive intermediates capable of forming covalent bonds with adjacent molecules. Labeling reagents can be divided into three main classes: first, probes designed to report on general properties of a system (for

example, small apolar molecules and lipids which partition into membranes and, upon activation, label selectively integral membrane proteins) (Brunner et al., 1980; Do et al., 1996; D'Silva and Lala, 2000; Heinrich et al., 2000; Mothes et al., 1997), second, affinity labeling reagents intended to interact with and label components (receptors, cotransporters, and channels) in a specific, functionally relevant manner (Addona et al., 2002; Jahn et al., 2002; Kipp et al., 1997; Leite et al., 2003; Thiele et al., 2000; Tyagi and Kinne, 2003), and third, heterobifunctional photo cross-linkers, containing a photactivatable and a conventional (thermal) reactive functional group, preferentially connected via a cleavable linker. These later reagents are primarily used to study the spatial relationship between components in complex systems.

Several successful examples of photoaffinity labeling of membrane proteins have been reported; among these are the glucose transporters in the plasma membrane of erythrocytes and of adipocytes (Trosper and Levy, 1977), the β -galactoside transport in *E. coli* membrane vesicles (Rudnick et al., 1975), the dipeptide and oligopeptides transporters in *E. coli* (Staros and Knowles, 1978), rhodopsin (Borhan et al., 2000), the ATP-binding cassette transporter LmrA (van Veen et al., 2000), fatty acid binding proteins in *E. coli* (Mangroo and Gerber, 1992), alpha 1-adrenergic receptors of rat heart (Terman and Insel, 1986), anion channel-1 in rat brain (Darbandi-Tonkabon et al., 2003), the ion channel of F-ATP synthase (von Ballmoos et al., 2004), the synaptic vesicle protein SV2A (Lynch et al., 2004), the bovine γ -aminobutyric acid type receptor (Sawyer et al., 2002), and nicotinic acetylcholine receptor (Chiara et al., 2003; Pratt et al., 2000; Wang et al., 2000; Ziebell et al., 2004).

2. Aim of the study

Large-scale purification of recombinant human membrane proteins represents a rate-limiting step towards understanding their role in health and disease. There are only four mammalian membrane proteins of known structure and these were isolated from natural sources. However, heterologous expression of hSGLT1 has been described in *Xenopus laevis* oocytes, COS-7, CHO, Sf9 cells, and *Escherichia coli* but the amount of protein produced in the above mentioned systems is not sufficient for most of the biochemical, biophysical and structural studies. In order to shed more light on the structure-functions of hSGLT we intend to express full-length transporter in high yield to fulfill our requirements of protein amount, which is necessary for most of the biochemical and biophysical experiments.

The elucidation of molecular interactions leading to transport of sugar and its translocation pathway through SGLT1 is a major objective of this work. Different methods have been widely used for the identification of sugar translocation pathway into SGLT1, but all methods were unable to provide an insight into protein structure at molecular level. To overcome this problem we proposed the use of photoaffinity labeling of functional domains of SGLT1 with different ligands and inhibitors based photoaffinity probes for the identification of sugar translocation pathway and inhibitor binding sites. To achieve this aim we proposed the synthesis and application of four new photoaffinity probes.

Therefore the main objectives of this work are:

1. To achieve high-level heterologous expression, purification and reconstitution of full-length functional hSGLT1.
2. Functional characterization of recombinant hSGLT1 by sugar uptake assays.
3. Synthesis of sugar and phlorizin based photoaffinity probes for the identification of sugar translocation pathways and inhibitor binding sites.
4. Photoaffinity labeling of loop 13 with [(2'-Iodo-4'-(3''-trifluoromethyldiazirinyloxy)-D-glucopyranoside (TIPDG), [(4'-Benzoyloxy)-D-glucopyranoside (BzG), and 3-Azidophlorizin (3-AP).
5. Photoaffinity labeling of recombinant full-length hSGLT1.

3. Materials and methods

Protocols were adapted from standard methods (Sambrook and Russell, 2001) unless otherwise mentioned.

All solutions and media were prepared with ultra-pure water (Milli-Q Plus ultra purification pak, Milli-RO Plus purification pak; Millipore, Molsheim, France).

3.1. General equipments

Autoclave	Autoclave 23; MELAG Medizintechnik (Berlin, Germany) Bioclav; Schütt Labortechnik GmbH (Göttingen, Germany)
Centrifuges	Biofuge pico, Omnifuge 2.OR, Megafuge 1.ORS, Heraeus (Osterode, Germany) Centrikon H-401, with Rotors A8.24 and A6.9; Kontron-Hermle (Gosheim, Germany)
Chromatography System	Automated Econo System; Biorad (Hercules, CA)
Electroporation apparatus	Gene pulser II; Biorad (Hercules, CA)
Freezer, -70°C	ULT1706; Revco Scientific (Asheville, NC),
Gel documentation camera	Polaroid MP-4 land camera; Polaroid USA
Gel Electrophoresis	Biorad (Hercules, CA)
Incubators	WTB Binder (Tuttlingen, Germany), Forma Scientific (USA) JULABO Labortechnik GmbH
Liquid nitrogen tank	BT40; L'air liquide (Champigny, France)
Magnetic stirrer	MR3001; heidolph (Kelheim, Germany)
MALDI-MS	PE-Biosystems, Shelton, USA
Microscope	IX50; Olympus Optical GmbH (Hamburg, Germany)
Oriel photochemical reactor	Oriel, Stratford, CT, USA
Rayonet photochemical reactor	Southern New England, Branford, CT, USA
pH meter	Model 765 Calimatic; Knick (Berlin, Germany)
Scales	Model BP 2100S; Sartorius (Göttingen, Germany)
Sonicator	SONOPLUS Bandelin electronic GmbH (Berlin, Germany)
Spectrophotometer	UVICON 930; Kontron instruments (Echingen, Germany)
Thermocycler	Mastercycler gradient; Eppendorf (Hamburg, Germany)
Thermomixer	Thermomixer compact; Eppendorf (Hamburg, Germany)
Ultracentrifuge	Optima™ TLX, with rotor TLA 100.4; BeckMan Instruments Fullerton, CA
Vortexer	REAX top; Heidolph (Kelheim, Germany)
Water baths	GFL GmbH (Burgwedel, Germany)

Densitometer	Pharmacia LKB (Sweden)
UV illuminator	Model N90M; UniEquip (Martinsried, Germany)

3.2. Materials

3.2.1. Chemicals

Acryl/Bis 37.5:1; 40% (w/v) Solution	AMRESKO Inc. USA
α -D-Acetobromoglucose	Mo Bio Laboratories, USA
Agar	Mo Bio Laboratories, USA
Agarose	Sigma, Munich, Germany
Ammonium persulphate	Sigma, Munich, Germany
Ampicillin	Sigma, Munich, Germany
Bromophenol blue	Sigma, Munich, Germany
4-Bromoanisol	Sigma, Munich, Germany
BSA (bovine serum albumin)	Sigma, Munich, Germany
G250 Brilliant Blue	Serva, Heidelberg, Germany
α -Cyano-4-hydroxycinnamic acid	Sigma, Munich, Germany
Dideoxynucleotides	Stratagene Inc USA
2,5-dihydroxybenzoic acid	Sigma, Munich, Germany
3,5-Dimethoxy-4-hydroxycinnamic acid	Sigma, Munich, Germany
DMSO	Sigma, Munich, Germany
DTT	Sigma, Munich, Germany
EDTA	Sigma, Munich, Germany
Ethidium Bromide	Sigma, Munich, Germany
Formamide	Fluka AG, Neu-Ulm, Germany
FosCholine-12	Anatrace, Maumee, OH, USA
D-[6- ³ H] Glucose	Perkin-Elmer, LAS, Germany
Glycerol	Merck, Darmstadt, Germany
HEPES	Sigma, Taufkirchen, Germany
4-Hydroxybenzophenone	Sigma, Munich, Germany
IPTG	peqLab Biotechnologie, Erlangen, Germany
Methyl- α -D-[¹⁴ C] glucopyranoside	Perkin-Elmer, LAS, Germany
SDS	Sigma, Munich, Germany
Sodium Azide	Serva, Heidelberg
Phlorizin	Sigma, Munich, Germany
TEMED	Sigma, Munich, Germany
Triton X-100	Sigma, Munich, Germany
Tryptone	Sigma, Munich, Germany

Tween 20	Sigma, Munich, Germany
Yeast extracts	Sigma, Munich, Germany
Zeocin	Invitrogen, Carlsbad, USA

All other Chemicals were of analytical grade and obtained from commercial sources.

3.2.2. Enzymes and reagents for molecular biology

Restriction enzymes	New England Biolabs GmbH, Frankfurt, Germany
<i>Taq</i> DNA polymerase	New England Biolabs GmbH, Frankfurt, Germany
<i>Pfu</i> Ultra HF DNA polymerase	Stratagene, Netherlands
Thermoscript reverse transcriptase	Invitrogen GmbH, Karlsruhe, Germany
Calf Intestine alkaline phosphatase	Roche Diagnostic, Mannheim, Germany
T4 DNA ligase	New England Biolabs GmbH, Frankfurt, Germany
RNaseA	Sigma, Munich, Germany
DNase I	Roche Diagnostic, Mannheim, Germany
DNase (Rnase free)	Qiagen, Hiden, Germany
Lysozyme	Sigma, Munich, Germany
dNTP	Stratagene, Netherlands
T4 Polynucleotide kinase	New England Biolabs GmbH, Frankfurt, Germany

3.2.3. Antibodies

Anti-FLAG M2 monoclonal antibody peroxidase conjugate	Sigma, Munich, Germany
Mouse anti-His-tag (27E8) monoclonal antibody	Cell Signaling Technology Beverly, USA
Rabbit anti-human SGLT1 antibody	Acrris Antibodies, Hiddenhausen, Germany

3.2.4. Commercial Kits and other materials

QIAquick™ PCR-Purification kit	Qiagen, Hiden, Germany
QIAquick™ Gel-extraction kit	Qiagen, Hiden, Germany
QIA® Spin Miniprep kit	Qiagen, Hiden, Germany
QuickChange® XL Site directed mutagenesis kit	Stratagene, Netherlands
Rapid DNA ligation kit	Roche Diagnostic, Mannheim, Germany
Expend High Fidelity PCR system	Roche Diagnostic, Mannheim, Germany
Easy Select™ Pichia Expression Kit	Invitrogen, Carlsbad, USA
Lowry Protein assay kit	Sigma, Munich, Germany
Hybond™-C extra blotting membrane	Amersham Biosciences, Germany

SuperSignal [®] West Pico chemiluminiscent Substrate	Pierce, Rockland, USA
Photographic film	Polapan; Polaroid, Offenbach, Germany

3.2.5. Primers for preparation of cDNA inserts

Primer	Sequence	Type, restriction site
SGLT_F	TATTGAATTCGATGGACAGTAGCACCTG	Sense, <i>EcoR</i> I
SGLT_R	AATACTCGAGGGCAAATATGCATGGC	Antisense, <i>Xho</i> I
Δ N12-377SGLT_F	CTGCGAGGCCTGATGCTATCAGTCATGCTG	Sense
Δ N12-377SGLT_R	GGTGGTCTTGGGGCTCCAGGTGCTACTGTC	Antisense
Spacer_His_SGLT_F	GGTGGTAGCCCGGGTCACCACCACCACCAC CACTGAGAT	Sense
Spacer_His_SGLT_R	GCTTTTATACAGCACGGCAAATATGCATGG CAAAGAC	Antisense
T7 promoter_F	TAATACGACTCACTATAGGG	Sense
Unc-F_R	TTTATTACAGTTCAGCGACAAG	Antisense
SGLT_FLAG_F	GACGACGATAAGATCCAAGAAGGCCCTAAG GAGAC	Sense
SGLT_FLAG_R	ATCCTTGTAATCCAGGTCAATACGCTCCTCT TTGC	Antisense
PBAD_SGLT_R	TAATTAAGCTTTTAGGCAAATATGCA TGG	Antisense, <i>Hind</i> III
pPICZ_SGLT_F	TATTGAATTCAAATGGACAGTAGCACCTG	Sense, <i>EcoR</i> I
pPICZ α _SGLT_R	ATTATTGCGGCCGCGGCAAATATGCATGCC	Antisense, <i>Not</i> I

3.2.6. Plasmids

3.2.6.1. Original plasmids

Plasmid	Description	Reference
pET22b	Expression vector, T7- <i>lac</i> promoter, Signal sequence at N-terminal of gene, at C-terminal His tag, Amp ^R , origin of replication pBR322.	Novagen, San Diego, CA, USA
pBAD24	P _{BAD} promoter, His tag at C-terminal of gene, Amp ^R , pUC origin of replication.	Invitrogen, Carlsbad, CA, USA
pPICZB	<i>AOX1</i> promoter, His-tag at the C-terminal of gene, Zeo ^R ; <i>CoLE1</i> origin of replication.	Invitrogen, Carlsbad, CA, USA
pPICZ α A	<i>AOX1</i> promoter, α -factor secretion signal at the N-terminal of gene, His-tag at the C-terminal of gene, Zeo ^R ; <i>CoLE1</i> origin of replication.	Invitrogen, Carlsbad, CA, USA

3.2.6.2. Plasmid with insert

Plasmid	Description	Reference
DKFZp686N20230Q2	Plasmid containing full-length hSGLT1 gene	RZPD, Berlin, Germany
pET22b-hSGLT1	hSGLT1 gene cloned in pET22b	This study
pET22b-hSGLT1-Spacer	hSGLT1 gene cloned in pET22b with DNA sequence encoding for a 10 amino acids long spacer at the C-terminal of gene	This study
pET22b- Δ N12-377 hSGLT1	hSGLT1 gene cloned into pET22b after deletion of DNA sequence encoding amino acids 12-377	This study
pET22b- Δ N12-377 hSGLT1-Spacer	Clone pET22b- Δ N12-377 hSGLT1 with DNA sequence encoding for a 10 amino acids long spacer at the C-terminal of gene	This study
pET22b-Unc-F	Unc-F gene encodes β -subunit of <i>E. coli</i> ATPase under the control of bacteriophage T7 promoter	This study
pET22b-Unc-F-hSGLT1	Unc-F gene cloned in pET22b plasmid encoding full-length hSGLT1	This study
pET22b-Unc-F-hSGLT1-Spacer	Unc-F gene cloned in pET22b plasmid encoding full-length hSGLT1 with C-terminal spacer	This study
pET22b-Unc-F- Δ N12-377 hSGLT1	Unc-F gene cloned in pET22b plasmid encoding hSGLT1 gene shorten at N-terminal from 12-377 amino acids	This study
pET22b-hSGLT1-FLAG-Spacer	pET22b vector containing full-length hSGLT1 gene with C-terminal spacer and FLAG tag at position D ₅₇₄ .	This study
pBAD24-hSGLT1-FLAG-Spacer	pBAD24 vector containing full-length hSGLT1 gene with C-terminal spacer and FLAG tag at position D ₅₇₄ .	This study
pBAD24- Δ N12-377 hSGLT1-FLAG-Spacer	pBAD24 plasmid encoding hSGLT1 gene shorten at N-terminal from 12-377 amino acids and FLAG tag at position D ₅₇₄	This study
pPICZB-hSGLT1	<i>P. pastoris</i> plasmid pPICZB containing full-length hSGLT1 gene with FLAG tag at D ₅₇₄	This study
pPICZ α A-hSGLT1	<i>P. pastoris</i> plasmid pPICZ α A containing full-length hSGLT1 gene with FLAG tag at D ₅₇₄	This study

3.3. Work with *E.coli*

3.3.1. *E.coli* strains

Strain	Genotype	Source
C41 (DE3)	BL21 (DE3) derivative with uncharacterized mutations	Avidis
C43 (DE3)	BL21 (DE3) derivative with uncharacterized mutations	Avidis
C43 (DE3) Rosetta DH5 α	C43 (DE3) and Rosetta derivative	This study
Origami (DE3)	F ⁻ ϕ 80dlacZ Δ M15 Δ (lacZYA-argF)U169 deoR recA1endA1 hsdR17(r _k ⁻ , m _k ⁺) phoA supE44 λ -thi-1 Δ (ara-leu)7697 Δ lacX 74 Δ phoA PvuII phoR araD139ahpC galK rpsL F' [lac ⁺ lacI ^q pro] (DE3) gor522:: Tn 10trx (Kan ^R , Str ^R , Tet ^R)	Novagen
Rosetta TM (DE3) XL10-Gold	F ⁻ ompT hsdS _B (r _B ⁻ m _B ⁻) gal dem (DE3) pRARE (Cam ^R) Tet ^R Δ (mcrA)183 Δ (mcrCB-hsdSMR-mrr)173endA1 supE44 thi-1 recA1 gyrA96 relA1 lac Hte [F' proAB lacI ^q Z Δ M15 Tn10 (Tet ^R) Amy Cam ^R]	Novagen Stratagene
TOP10F ⁻	F' proAB, lacI ^q , lacZ Δ M15, Tn10 (Tet ^R) mcrA, Δ (mrr- hsdRMS-mcrBC), ϕ 80lacZ Δ M15, Δ lacX74, deoR, recA1, λ -araD139, Δ (ara-leu) 7697, galU, galK, rpsL, (str ^R), endA1, nupG	Invitrogen

3.3.2. Media for bacterial culture

LB-medium

1.0% tryptone
0.5% yeast extract
1.0% NaCl
pH 7.2

Terrific Broth

1.2% tryptone
2.4% yeast extract
0.4% glycerol
17 mM KH₂PO₄
72 mM K₂HPO₄

1.5% agar was added to the media for production of agar plates.

The following concentrations of the antibiotics were used if required:

Table 3.1 Antibiotic stock solutions and its working concentration.

Antibiotic	Stock solution	Working concentration
Ampicillin	100 mg/ml in water	100 μ g/ml
Chloramphenicol	30 mg/ml in ethanol	30 μ g/ml
Zeocin	100 mg/ml in water	100 μ g/ml
Tetracycline	5 mg/ml in ethanol	10 μ g/ml

3.3.3. General

E. coli were cultured at 37°C with LB medium or terrific broth. Bacteria transformed with an antibiotic resistance-conferring plasmid were selectively propagated by supplementing the LB medium with respective antibiotic (see Table 3.1). All solutions and supplements used for work with *E. coli* were autoclaved for 20 min at 121°C or filter-sterilized. Bacterial strains for long-term were stored at -70°C in LB medium supplemented with glycerol to a final concentration of 15 %.

3.3.4. Transformation of plasmid in *E. coli*

3.3.4.1. Preparation of competent cells by CaCl₂ method

LB medium (100 ml) was inoculated with an overnight culture of *E. coli* DH5α and grown at 37°C with shaking to an OD₆₀₀ of 0.4. This culture was transferred to sterile, disposable, ice-cold 50-ml plastic tubes and stored on ice for 10 minutes. After incubation, cells were centrifuged at 4,000 rpm for 15 min at 4°C. The pellet was resuspended in 50 ml ice-cold 100 mM MgCl₂, incubated for 30 min on ice, and centrifuged at 4°C. The cells were resuspended in 2 ml ice-cold 100 mM CaCl₂, incubated for 24 h at 4°C, supplemented with ice-cold 0.6 ml glycerol and 2.4 ml 100 mM CaCl₂ and stored in 200µl aliquots at -70°C.

3.3.4.2. Heat shock transformation of the plasmid

Treatment of competent bacterial cells with a brief heat shock enables transformation of DNA. Plasmid DNA or a plasmid ligation reaction (not more than 15ng or in a volume 2.5µL) was mixed with 50µl thawed competent bacteria and incubated for 30 min on ice. The bacteria were treated for 90s by heat shock of 42°C, placed on ice for 1-2 min, diluted with 950 µl LB medium and incubated for 1 h at 37°C with shaking. An aliquot of 50-200 µl or resuspended pellet was spread on LB/antibiotic agar plate and incubated overnight at 37°C to select for transformed bacteria. In case of ligation mixture, the transformed cells were pelleted by centrifugation at 13,000 rpm for 30 seconds, and the pellet was resuspended in 100µl of LB medium. The whole suspension was spread on the agar plate.

3.4. Work with *P. pastoris*

3.4.1. *P. pastoris* strains

Strain	Genotype	Phenotype
X-33	Wild-type	Mut ⁺
GS115	his4	His ⁻ , Mut ⁺
KM71H	arg4 aox1::ARG4	Mut ^S , Arg ⁺
GS115/Albumin	His4	Mut ^S
GS115/pPICZ/lacZ	his4	His ⁻ , Mut ⁺

3.4.2. Media for *P. pastoris* culture

Low Salt LB (Luria-Bertani) Medium

- 1.0 % tryptone
- 0.5% yeast extract
- 1.0% NaCl
- pH 7.0

Low salt LB medium is needed for use with Zeocin antibiotic.

Low salt LB agar plates were made by the addition of 1.5% agar before autoclaving.

Yeast Extract Peptone Dextrose Medium (YPD or YEPD)

- % yeast extract
- 2% peptone
- 2% dextrose (glucose)

Yeast Extract Peptone Dextrose Medium (YPD ± Zeocin)

- 1% yeast extract
- 2% peptone
- 2% dextrose (glucose)
- ± 2% agar
- ± 100 µg/ml Zeocin

Buffered Glycerol/ Methanol complex Medium (BMGY and BMMY)

- 1% yeast extract
- 2% peptone
- 100mM KH₂PO₄, pH 6.0
- 1.34% YNB
- 4× 10⁻⁵% biotin
- 1% glycerol or 1% methanol

Breaking Buffer

- 50 mM KH₂PO₄, pH 6.0
- Protease inhibitors cocktails
- 10% glycerol

3.4.3. General

P. pastoris was grown at 28-30°C in YPD medium. Cells transformed with pPICZB-hSGLT1 plasmid were selectively propagated by supplementing the YPD medium with Zeocin antibiotic (see Table 3.1). For protein expression pPICZB-hSGLT1 plasmid transformed cells were grown in BMGY medium supplemented with Zeocin. *P.pastoris* cells for long-term were stored at -70°C in YPD medium supplemented with glycerol to a final concentration of 15 %.

3.4.4. Electroporation of *P. pastoris* with plasmid pPICZB or pPICZB-hSGLT1

The purified DNA samples of pPICZB and pPICZB-hSGLT1 were linearized by *PmeI* digestion at 37°C for 3 h and the linearized plasmids DNA were purified by enzyme removal column.

YPD medium (100 ml) was inoculated in a 1-liter flask with 0.2 ml of overnight culture of *P. pastoris* strain GS115 and the cells were grown at 28°C overnight to an OD₆₀₀ of 2-4. Overnight grown culture was centrifuged at 1500 × g at 4°C for 5 min. The supernatant was removed and the pellet was resuspended with 25 ml of ice-cold sterile water. The resuspended cells were centrifuged again as above and the pellet was resuspended in 8 ml of ice-cold sterile 1 M sorbitol. The cells were centrifuged as above and then the pellet was resuspended with 1 ml of ice-cold sterile 1 M sorbitol. The suspension of competent cells was kept on ice and used the same day.

The suspension of competent cells (40 µl) and of linearized DNA (10 µl, 10 µg) were mixed and transferred to an ice-cold electroporation cuvette. The cuvette with the mixture of cells and DNA was incubated on ice for 5 min. The cells were pulsed at 1.5 kV, 50 µF and 200 Ω and 1 ml of ice-cold 1 M sorbitol was added to the cuvette. The cuvette contents were transferred to a sterile 15 ml tube and incubated at 30°C without shaking for 2 h. 200 µl of these cells were plated on YPD medium with 100, 500, and 1000 µg/ml Zeocin and incubated at 30°C for 2 days.

3.5. Recombinant DNA processing and manipulation

3.5.1. Buffers and solutions

TBE buffer (5X) (Working solution 0.5X)	Tris-base 54 g boric acid 27.5 g EDTA 20 ml of 0.5 M, pH 8.0 Final volume 1 Liter
TE	10mM Tris (pH 7.6), 1mM EDTA (pH8.0)
DNA loading buffer (6X)	0,25% (w/v) bromophenol blue 0,25% (w/v) xylene cyanol 30% (v/v) glycerol 50 mM EDTA
Ethidium bromide	1% (w/v) in water
DNA standard	SmartLadder™ Eurogentec GmbH, Germany

3.5.2. Restriction endonuclease digestion of DNA

For preparative purposes, 1-5 µg DNA was digested with 1-20 U of restriction enzyme in a volume of 10-50 µl of reaction buffer. Complete digestion was confirmed by agarose gel electrophoresis. For analytical purposes, 0.2-1 µg DNA were digested with 1-5 U enzyme in a volume of 10-20 µl of reaction buffer. In both cases digests were incubated for 3h at 37°C. Reaction buffers were supplied by the manufacturer. Enzymes were heat-inactivated as recommended by the supplier or removed by purification of the digested DNA by column chromatography.

3.5.3. Purification of the digested DNA

To inactivate and remove the proteins e.g. restriction enzymes, digested DNA was purified by using the QIAquick PCR purification kit (Qiagen) according to the manufacturer's instructions with slight modification. Buffers were provided in the kit and all centrifugation steps were carried out at 13,000 rpm at RT in a tabletop microcentrifuge. The 5 volume of the buffer PB and one volume of isopropanol were added to the DNA solution. The sample was then applied to QIAquick spin column (Qiagen) and centrifuged for 1 min in order to bind DNA to the column. For washing of DNA on the column, 0.75 ml of buffer PE was added to the column and spun down for 1 min. The flow-through was removed and the column was centrifuged for an additional 1 min to remove the residual ethanol. The column was then placed into a clean 1.5 ml tube and the DNA was eluted by the addition of 30-50 µl of buffer EB (10 mM Tris/HCl, pH 8.5) or dH₂O to the column followed by centrifuging for 1 min. If needed the DNA could be concentrated by precipitating with ethanol.

3.5.4. Ethanol precipitation of DNA

5 M NaCl solution was added to the DNA sample to a final concentration of 250 mM. Three volumes of ethanol (-20°C) were added to the solution and stored on ice for 30 min and then centrifuged at 13,000 rpm for 15 min at 4°C. The pellet was washed with one volume of ice-cold 70 % ethanol, recentrifuged for 5 min and dried at room temperature on desk. The DNA was dissolved in water or TE (pH 8) for 20 min at 37°C at an appropriate concentration.

3.5.5. Dephosphorylation of linearized plasmid DNA by CIP

In order to prevent self-ligation of vector ends in cloning strategies linearized plasmid DNA was treated with calf intestine alkaline phosphatase (CIP). CIP catalyzes the hydrolysis of 5'-phosphate residues to 5'-hydroxyl ends. Since T4 DNA ligase requires 5'-phosphate residues to catalyze new phosphodiester bonds, ligation is only possible between vector ends and inserts, but not between vector ends themselves. Dephosphorylation was carried out directly

following plasmid linearization. CIP was added to the digestion mixture at a concentration of 1 U per pmol linearized vector DNA. After 45 min incubation at 37°C, CIP and the restriction enzymes were removed as described previously.

3.5.6. Ligation of DNA fragments

Ligation was carried out using Rapid DNA ligation kit according to the manufacturer's instructions with slight modification. All the buffers were provided with the kit. The insert DNA was employed at a 2-5 molar excess relative to the linearized and dephosphorylated vector DNA. The vector DNA and insert mixture were diluted in dilution buffer to a final volume of 10µl. 10µl of ligation buffer was added in diluted DNA mixture. 5unit of T4 DNA ligase was added and mix thoroughly. The ligation reaction mixture was incubated 5-10 minutes at 15-25°C. The 5µl of ligation reaction mixture was used directly for transformation of the 200µl competent cells.

3.5.7. Miniprep: small-scale preparation of plasmid DNA

Plasmid DNA was purified from bacteria cultures by alkaline lysis of the bacterial cells by using QIAprep Spin miniprep kit according to the manufacture instructions. In brief, A small culture (10ml) of bacteria was grown in order to amplify *in vivo* the plasmid of interest. The bacteria were harvested by centrifugation at 13,000 rpm for 1 min at room temperature. This pellet was resuspended in 250µl buffer P1 (50 mM Tris·Cl pH 8.0, 10 mM EDTA, 100 µg/ml RNase A). 250µl lysis buffer P2 (0.2 N NaOH, 1 % SDS) was added in resuspended pellet followed by gently mixing and incubated for 5 minutes at room temperature. It causes denaturation of the DNA by NaOH and of the bacterial proteins by SDS. The alkaline mixture was neutralized by 350µl of buffer N3 (containing guanidine hydrochloride, 3M potassium acetate, pH 5.5) causing reannealing of plasmid DNA and precipitation of SDS. The white precipitate, containing Proteins, chromosomal DNA, SDS and cell debris was removed by centrifugation for 10 minutes at 13,000 rpm while the plasmid DNA was left in the solution. The supernatant was passed through the spin column by centrifugation at 13,000 rpm for 1 minute. After washing of the column with 0.75ml buffer PE, the column was additionally centrifuged for 1 minute to remove residual buffer. The DNA was eluted by adding 50µl water or TE and centrifugation of the column at 13,000 rpm for 1 min.

3.5.8. Large scale preparation of plasmid DNA

100 ml of bacterial culture was centrifuged at 4,000 rpm for 15 min at 4°C. The pellet was resuspended in 10 ml of P1 (50mM Tris.Cl, pH 8.0; 10mM EDTA; 100µg/ml Rnase A). Resuspended pellet was lysed with 10 ml P2 (200mM NaOH, 1% SDS) by incubating for 5

min at room temperature. The lysis was stopped by adding 10 ml ice-cold P3 (3M potassium acetate, pH 5.5) and the white precipitated mixture was poured into the barrel of QIAfilter cartridge and incubated for 10 min. After 10 minutes, the plunger was inserted into the QIAfilter cartridge and filtered the cell lysate into the 50ml tube. The lysate was loaded on an equilibrated anion exchange column that was subsequently washed twice with 30 ml of buffer QC (1.0M NaCl, 50mM MOPS, pH7.0; 15% isopropanol). The bound DNA was eluted with elution buffer QN (1.6M NaCl, 50mM MOPS, pH7.0; 15% isopropanol) by gravity flow. The eluted DNA was precipitated by adding 0.7 volumes isopropanol at room temperature and subsequent centrifugation at $\geq 15,000 \times g$ for 30 min at 4°C. The pellet was washed with 5 ml 70 % ethanol, re-centrifuged for 10 min, dried under vacuum and re-dissolved in 1ml of endothelial electroporation buffer or TE.

3.5.9. Quantification of DNA and RNA solutions

The concentration of nucleic acid solutions was determined by spectrophotometry. The ultraviolet (UV) absorption was measured at a wavelength of 260 nm (OD_{260}) using a quartz cuvette of 1 cm width. For double-stranded DNA an $OD_{260} = 1.0$ corresponds to approximately 50 μg DNA/ml. For RNA an $OD_{260} = 1.0$ corresponds to approximately 40 μg RNA/ml. In addition the OD_{260} was measured to estimate the purity of the nucleic acid sample. A ratio OD_{260}/OD_{280} of significantly less than 1.8-2.0 indicates protein contamination.

3.5.10. Agarose gel electrophoresis

Agarose gel electrophoresis was used for analytical and preparative purposes. The method is based on the migration of the negatively charged DNA towards the anode in an electric field. The fragments migrate through the gel matrix at rates inversely proportional to the logarithm (\log_{10}) of the number of base pairs. DNA bands were visualized within an agarose gel by staining with the intercalating fluorescent dye ethidium bromide and subsequent illumination under UV light. The length of a DNA fragment is determined by comparison of its mobility to that of DNA standards. For casting gel, 1-2 % (w/v) agarose was melted in 0.5xTBE electrophoresis buffer and supplemented with 0.5 $\mu\text{g}/\text{ml}$ ethidium bromide and cast in casting tray of desired size. The gel was placed in an electrophoresis tank and submerged in 0.5xTBE buffer. The DNA samples were mixed with DNA loading buffer and loaded into the gel wells. In addition 5 μl of a DNA standard was loaded in parallel with the samples. Horizontal electrophoresis was carried out at approximately 100 V. The stained gel was photographed under UV light.

3.5.11. DNA recovery from agarose gel

For preparative purposes DNA fragments of interest were cut out from stained agarose gels with a razor blade under UV illumination. The gel slices were solubilized and DNA was purified by using the QIAquick Gel extraction kit (Qiagen) according to the manufacturer's instructions.

Agarose gel slices were weighed (= 1 volume) and dissolved each slice in 3 volumes of solubilization buffer QG by incubation for 10 min at 50°C. 1 volume isopropanol was added and the solution was applied to a silica-gel QIAquick spin column. The column was centrifuged at 13,000 rpm for 1 min, washed with washing buffer PE and centrifuged again. The extra centrifugation was done to remove residual buffer. DNA was eluted by adding 30-50µl water or TE on the column and centrifugation of the column at 13,000 rpm for 1 min. All the buffers were provided by the manufacturer.

3.5.12. DNA sequencing

The sequence of specific target regions in recombinant plasmid DNA was determined by a commercial sequencing service (Agowa GmbH Berlin, Germany). The sequence data were verified on the basis of the corresponding fluorescence electropherogram and subjected to computer analysis.

3.5.13. DNA amplification of hSGLT1 gene by PCR for cloning into different expression systems

Primers for PCR amplification of SGLT1 cDNA were commercially synthesized (MWG Biotech, Ebersberg, Germany). They were designed corresponding to the DNA segment to be amplified, provided with restriction sites for endonuclease digestion. Pairs of primers were designed to have equivalent melting temperatures (T_m), calculated according to the formula¹ $T_m [^{\circ}C] = (A+T) \cdot 2 + (G+C) \cdot 4$. The annealing temperature for each PCR was typically estimated by experimentally. For preparative DNA amplification as part of cloning strategies, High fidelity DNA polymerase was used in preference to *Taq* DNA polymerase, due to its 3'→5' proofreading exonuclease activity which minimizes the risk of nucleotide misincorporation during elongation.

PCR reaction composition for DNA amplification was as follows:

Template DNA	20-50ng
Sense primer (forward)	100 pMoles
Antisense primer (reverse)	100 pMoles

¹ A, T, G, C: number of the 2'-deoxyribonucleosides adenosine (A), thymidine (T) guanosine (G) and cytidine (C) with in the primer sequence

dNTPs	200μM each
PCR reaction buffer	1x
DMSO	5-10% (Optional, to increase yield, specificity, consistency)
DNA polymerase	1-2.5 units
Final reaction volume	100μl (preparative PCR), 20-50μl (analytical PCR)

The PCR amplified products of hSGLT1 gene were analyzed by agarose gel electrophoresis, they were further proceeding for cloning into their respective vectors.

Thermal cycle parameters for PCR was as follows:

Lid temperature	105°C
Initial denaturation	94°C, 5 minutes
Denaturation	94°C, 30 seconds
Annealing	50-55°C (primer pair and template specific), 1minute
Elongation	72°C, 1 minute/kb
Cycles	30
Final elongation	72°C, 10 minutes

cDNA sequence encoding full length human SGLT1 was amplified by using plasmid DKFZp686N20230Q2 as a template and subcloned into the *EcoR*I and *Xho*I sites of the bacterial expression vector pET22b. Primers used for the amplification were SGLT1_F and SGLT1_R (see section 3.2.5).

For cloning into pBAD24 bacterial expression vector, pET22b-hSGLT1-FLAG-Spacer plasmid (see section 3.5.14.2 for detail) was used as a PCR template. The primers pPICZ_SGLT_F and PBAD_SGLT_R containing *EcoR*I and *Hind*III restriction sites respectively were used for PCR amplification.

For cloning hSGLT1 gene into eukaryotic expression system *Pichia pastoris*, pET22b-hSGLT1-FLAG-Spacer plasmid (see section 3.5.14.2 for detail) was used as a PCR template. hSGLT1-FLAG-Spacer gene product contains a FLAG epitop at position of 574 amino acid and a 10 amino acids spacer at the end of hSGLT1 gene. The primers used for PCR amplification were pPICZ_SGLT_F and pPICZ α _SGLT_R primer containing *EcoR*I and *Not*II restriction sites respectively

3.5.14. Addition or deletion mutagenesis in hSGLT1 gene

This method is a PCR-based site directed mutagenesis system that eliminates the necessity to subclone the amplified mutated DNA fragment. This procedure starts with a supercoiled, dsDNA vector with an insert of interest and two synthetic oligonucleotide primers containing the desired mutation. The oligonucleotide primers, each complementary to opposite strands of the vector, are extended during temperature cycling by *PfuUltra*® high-fidelity DNA polymerase. On incorporation of the oligonucleotide primers, a mutated plasmid is generated. After temperature cycling, the product is treated with *Dpn* I. *Dpn* I is used to digest the parental DNA template and select for the synthesized DNA containing mutations. Since DNA isolated from most *E. coli* strains is dam methylated, it is susceptible to *Dpn* I digestion, that

will cut only fully or hemimethylated 5'-G_m6ATG-3' DNA sequences². The nicked vector DNA incorporating the desired mutations is then transformed into the commercial XL10-Gold cells³. This method is very rapid and generates mutants with the efficiency greater than 80%.

The specific primer design consideration was applied which are as follows.

Both the primers must anneal to different strands of the plasmid.

Primers should be >22 bases in length

The mismatched portions should be at or near the 5' end of one or both of the primers with 15 or more bases of correct sequence on the 3' end.

For deletion, the primers should be designed in frame of the coding sequence of the gene. The forward primer and reverse primer should be designed at 3' and 5' end of the deletion sequence respectively. For addition of base pairs in the cDNA of hSGLT1 the additional base pairs should be incorporated at the 5' end of the primers.

One or both of the primers must be 5' phosphorylated. T4 polynucleotide kinase used for the 5' phosphorylation of an oligonucleotide primers.

The reaction composition of the phosphorylation reaction is as follows

Primer	1µl (100pmole)
Kinase buffer	0.5µl (1x)
T4 polynucleotide kinase	1µl (10 units)
Water	2.5µl

The reaction mixture was incubated for 1 hour. The 1.25µl of the reaction mixture was directly used for PCR.

The mutant strands synthesis reaction was setup for PCR according to the manufacturer's instructions. The PCR reaction composition and PCR cycling parameter were as follows:

Template DNA	30ng
Sense primer ⁴ (forward)	125ng
Antisense primer (reverse)	125ng
dNTPs	200µM each or 1µl (supplied with the kit)
PCR reaction buffer	1x
Quik solution reagent	3µl (supplied with the kit)
Water	added to a final volume of 50µl

Then 1µl of PfuUltra HF DNA polymerase was added and PCR was done with the following thermal cycling parameters.

Lid temperature	105°C
Initial denaturation	94°C, 2 minutes
Denaturation	94°C, 50 seconds
Annealing	60°C, 1 minute

² While plasmid DNA isolated from almost all the commonly used *E.coli* strains such as DH5α (dam⁺) is methylated and is suitable for mutagenesis, plasmid DNA isolated from the exceptional dam⁻ *E.coli* strains, including JM110 and SCS11, is not suitable.

³The DH5α chemical competent cells prepared in our lab are also worked well with this protocol.

⁴ The primers were design according to the mutagenic primer design rules, which were given in instruction manual.

Elongation	68°C, 1 miunte/kb
Cycles	18
Final elongation	68°C, 10 minutes

After the PCR the reaction mixture was cooled to $\leq 37^{\circ}\text{C}$ on ice. $1\mu\text{l}$ of *Dpn* I was added directly to reaction mixture and kept for 2 hours for digestion at 37°C . The PCR product was purified by PCR purification kit as described before. The $5\mu\text{l}$ of purified PCR product was ligated with rapid DNA ligation kit and transformed into DH5 α cells. The positive clone was confirmed by DNA sequencing.

3.5.14.1. Addition of 30 base pairs long spacer at the C-terminal of hSGLT1 gene

cDNA sequence encoding a 10 amino acids long spacer (VLYKSGGSPG) was introduced at the C-terminal of hSGLT1 gene. For the addition of spacer sequence, two primers (each containing 5 additional amino acids coding base pairs). The primers used for this mutation were Spacer_SGLT_His_F and Spacer_SGLT_His_R (see section 3.2.5) and designed as shown in Figure 3.1. The resultant plasmid was designated as pET22b-hSGLT1-Spacer.

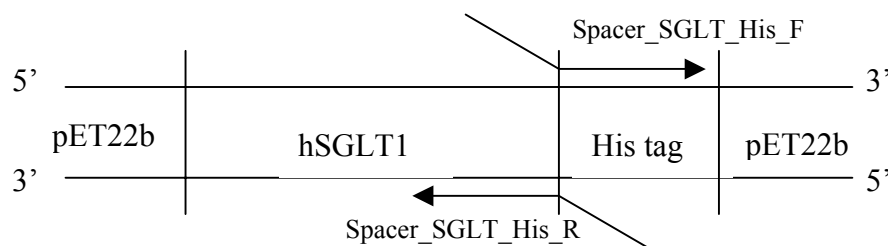


Figure 3.1 Positions of the mutation primers in pET22b-hSGLT1 plasmid. 15 base pairs were added to each primers. After Ligation 30 bps were incorporated between hSGLT1 gene and His tag.

3.5.14.2. Addition of FLAG tag in hSGLT-spacer gene

For better immunological detection and to provide ease in the purification process, the FLAG epitope was introduced in hSGLT1 by mutating the native hSGLT1 sequence $\text{D}_{574}\text{AEEEN}$ to $\text{D}_{574}\text{YKDDDDDK}$. In pET22b-hSGLT1-Spacer plasmid 21 base pairs encoding the FLAG tag were inserted at the position 574. During this mutation 15 base pairs encoding wildtype 5 amino acids (574-579) were deleted. The forward primer (SGLT1_FLAG_F) and reverse primer (SGLT1_FLAG_R) were designed similarly as shown in Figure 3.1. The resultant plasmid was designated as pET22b-hSGLT1-FLAG-Spacer.

3.5.14.3. Deletion of N-terminal half of hSGLT1 gene

To construct N-terminal truncated hSGLT1 gene, the base pairs 34 to 1131 (Amino acids 12-377) were deleted by deletion mutagenesis as described above. The primers $\Delta\text{N}12\text{-}377\text{_SGLT_F}$ and $\Delta\text{N}12\text{-}377\text{_SGLT_FR}$ were designed with a similar approach as describe in section 3.5.14.1 following the primer design rules as described in section 3.5.14.

pBAD24-hSGLT1-FLAG-Spacer	Yes	Yes	Yes	Yes	Yes	Conditions 7 and 8 in Rosetta, C43 and C43R cells
pBAD24-ΔN12-377 hSGLT1-FLAG-Spacer	Yes	Yes	Yes	Yes	Yes	Same

*Specification of different expression conditions;

1. LB medium, 1 mM IPTG, 37°C growing temperature.
2. LB medium, 1 mM IPTG, 37°C growing temperature with 45 min heat shock before induction of IPTG.
3. LB medium, 1 mM IPTG, 22°C growing temperature with 45 min heat shock before induction of IPTG.
4. LB medium, 0.5 mM IPTG, 16°C growing temperature with 45 min heat shock before induction of IPTG.
5. TB medium, 0.5 mM IPTG, 16°C growing temperature with 45 min heat shock before induction of IPTG.
6. TB medium with 1 M sorbitol, 0.5mM IPTG, 22°C growing temperature with 45 min heat shock before induction of IPTG.
7. LB medium, 0.2% L- (+) arabinose, 22°C growing temperature.
8. LB medium, 0.2% L- (+) arabinose, 22°C growing temperature with 45 min heat shock before Arabinose induction.

3.6.2. Growth condition of *P. pastoris* for hSGLT1 expression

In pilot experiments, single colonies of transformed cells were used to inoculate 2.5 ml of BMGY medium (1% (w/v) yeast extract, 2% (w/v) peptone, 100 mM potassium phosphate, pH 7.0, 1.34% (w/v) yeast nitrogen base, 4×10^{-5} % (w/v) biotin, and 1% (v/v) glycerol). After 16-20 h of incubation at 30°C, the cells were pelleted at $1000 \times g$ and were resuspended in BMMY medium (BMGY medium in which the glycerol was replaced by 1% (v/v) methanol) to induce protein expression. The positive colonies for recombinant protein expression were identified by Western blot analysis by using anti-FLAG antibody (Sigma). The clone with the highest protein yield was selected for medium-scale protein expression in 2-liters flasks. In all subsequent preparations, the cells were harvested at ~24 h of methanol induction.

3.6.3. hSGLT1 purification from *P. pastoris*

Membranes were prepared from *P. pastoris* cells as described below in the functional analysis of recombinant hSGLT1 section. Peripheral proteins and proteins adhering to the membrane were removed by washing with 4 M urea in breaking buffer containing protease inhibitor cocktail (Roche) at 4°C for 2 h and resulting membranes were centrifuged at $100,000 \times g$ at 4°C for 40 min. The stripped membranes were solubilized in buffer TG [20 mM Tris.Cl, pH 8/1 M NaCl/20% (v/v) glycerol] supplemented by 1.2% FosCholine-12 (Anatrace, Maumee, OH) and protease inhibitor cocktail, resulted membrane solution was shaken at 4°C, overnight. After removal of insoluble fraction by ultracentrifugation at $100,000 \times g$ for 40 min at 4°C, the clear supernatant was bound to the preequilibrated Protino Ni 2000 prepacked (Macherey-Nagel) polyhistidine-tag purification column at 4°C, unbound proteins were removed by washing with 3 column volume of buffer TG plus 0.2% FosCholine-12. Recombinant hSGLT1 was eluted with 9 ml of buffer TG plus 0.2% FosCholine-12

supplemented with 250 mM imidazole and protease inhibitor cocktail. The purified protein containing fractions were concentrated to 0.35 ml by ultrafiltration in Centricon YM100 devices (Millipore) and stored at -20°C for further use.

3.7. Protein analysis

3.7.1. Buffers and solutions

SDS sample buffer (2x)	100 mM Tris-HCl (pH 6.8) 20 % (v/v) glycerol 4 % (w/v) SDS 0.01 % (w/v) bromphenol blue 10% β -mercaptoethanol
acrylamide/bis-acrylamide	40% (w/v) acrylamide/bis-acrylamide ratio 37.5:1 (Amersco)
Stacking gel buffer	0.5 M Tris-HCl, pH 6.8
Resolving gel buffer	1.5 M Tris-HCl, pH 8.8
APS	10% (w/v) APS in water, aliquots were stored at -20°C
SDS	10% (w/v) SDS in water
Electrophoresis Buffer (10x)	30g Tris-base 142g glycine 10g SDS Water was up to 1 liter
Transfer buffer	5.82g (48mM) Tris-base 2.93g (39mM) glycine 200ml methanol Water was added up to 1 liter
TBST buffer	10mM Tris-base (pH 7.6) 150mM NaCl 0.05% (v/v) Tween 20
Blocking solution	5% blocking milk (BioRad) in TBST Phosphatase cocktail (1:100) 0.1% SDS
Coomassie staining solution	0.25% coomassie Brilliant Blue R-250 10%Acetic acid 40% methanol in water (filtered)
Coomassie destaining solution	10%Acetic acid 40% methanol in water

3.7.2. Measurement of protein concentration

3.7.2.1. Enhanced alkaline copper (Lowry) protein assay

The method is based on Peterson's modification of the micro-Lowery method (Peterson, 1977). An alkaline cupric tartrate reagent (Lowery reagent) complexes with the peptide bonds of proteins and becomes reduced to cuprous (Cu^+). The Cu^+ as well as the R groups of tyrosine, tryptophan, and cysteine residues then react with the Folin reagent. The reagent reacts by first producing an unstable product which is slowly reduce to become molybdenum/tungsten blue color complex. The absorbance is read at a suitable wavelength between 500 nm and 800 nm (preferably 750nm) for spectroscopic quantification of proteins in aqueous solution.

Lowry protein assay kit (Sigma) was used for protein quantification according to the manufacturer instructions. Using BSA stock solution (400 $\mu\text{g/ml}$), a set of protein standards with 0-300 $\mu\text{g/ml}$ was prepared. The protein samples were dilute to 1.0 ml with water. To each set of protein standards and samples, 1 ml of Lowry reagent was added and incubated for 20 minutes at room temperature. With rapid and immediate mixing, 0.5 ml of Folin & Ciocalteu's phenol reagent was added in each tube and allowed color to develop for 30 minutes. The absorbance was measured at the wavelength of 750 nm in a spectrophotometer. Based on the absorption values of the protein standards a calibration curve was calculated and used for determination of the protein concentrations in the samples. All protein standards and samples were prepared in duplicate.

3.7.3. SDS-PAGE

Table 3.2 Compostion of staking and resolving gel.

Components	Stacking gel 5% (5ml final vol.)	Resolving gel 10% (10ml final Vol)	Resolving gel 12% (10ml final vol.)
Water	3.2ml	4ml	3.3ml
Acrylamide mix	0.83 ml	3.3ml	4ml
1.5M Tris (pH8.8)		2.5ml	2.5ml
1.0M Tris (pH6.8)	0.63 ml		
10% SDS	0.05 ml	0.1ml	0.1 ml
10% ammonium persulphate	0.05 ml	0.1ml	0.1 ml
TEMED	0.005 ml	0.004ml	0.004 ml

Protein samples were resolved for analytical purposes by polyacrylamide gel electrophoresis (PAGE). The use of the anionic detergent sodium dodecyl sulfate (SDS) enables separation according to the molecular weight of the proteins. It binds to the polypeptides and confers a negative charge, which is in direct proportion to their size. The gel matrix is prepared by polymerization of acrylamide and *N,N'*-methylenebisacrylamide via free radicals. Initial radicals arise from chemical decay of ammonium persulfate (APS) catalyzed by *N,N,N',N'*-tetramethylethylenediamine (TEMED). The electrophoresis towards the anode is carried out

in a discontinuous buffer system that first concentrates SDS-protein complexes within a stacking gel before they migrate into the resolving gel. The size of proteins is determined by comparing their mobility with that of a protein standard.

The resolving gel solution was prepared, poured between two clean glass plates and overlaid with water or butanol. After polymerization, the top of the gel was washed with water and the residual water was removed by filter paper. Freshly prepared stacking gel solution was filled and allowed to polymerize. The plastic comb was inserted in poured stacking gel to prepare the wells for sample loading. After polymerization comb was removed and the wells were washed with water to remove un polymerized acrylamide. Subsequently the gel was placed in a vertical electrophoresis apparatus filled with 1x electrophoresis buffer. SDS-PAGE protein samples were prepared by mixing protein samples with 2x SDS sample buffer in the ratio of 1:1, if not already prepared with 1x SDS sample buffer. The SDS-PAGE protein samples and a protein standard were denatured at 95°C for 5 min and loaded onto the gel. Electrophoresis was carried out at 200 V. The resolving gel was subsequently subjected to western blot analysis or gel staining.

3.7.4. Coomassie staining of the polyacrylamide gels

Coomassie Brilliant Blue is an aminotriarylmethane dye that forms strong covalent complexes with proteins, most probably by a combination of van der Waals forces and electrostatic interactions with NH_3^+ groups. The uptake of dye is approximately proportional to the amount of protein.

The polyacrylamide gel was immersed in at least 5 volumes of the coomassie staining solution and placed on a slowly rotating platform for 15-30 minutes at room temperature. The gel was destained in coomassie destaining solution on a slowly rotating platforms, changing the destaining solution three to four times. The rapid destaining can also be achieved by keeping the staining gel in hot water (80°C). The remaining background was removed by leaving the gel overnight in water.

3.7.5. Western blot analysis

Western blotting consists of the transfer of electrophoretically separated proteins from a SDS-PAGE gel to a nitrocellulose membrane by electroblotting. The membrane-immobilized target protein is identified by an appropriate primary antibody and a horseradish peroxidase (HRP)-conjugated secondary antibody directed against the primary antibody. Detection of the antigen-antibody-antibody complex occurs by HRP-mediated oxidation of the chemiluminescent substrate luminol, a cyclic diacylhydrazide. The reaction product exhibits an excited state which decays to ground state via a light emitting pathway, and is detectable by exposure of the membrane to an autoradiography film.

After SDS-PAGE, the gel, nitrocellulose membrane pads and electrode papers were equilibrated with pre chilled transfer buffer. The gel cassette was placed with the gray side down on a clean surface. The fiber pad, electroblotting papers (7papers on each side), gel and nitrocellulose membrane were arranged in the cassette.

The firmly closed cassette was put into the blotting module and then placed into the electroblotting buffer tank with ice cooling unit. The proteins were transferred to the membrane towards the anode at 200 mA for 1 h at 4°C in ice-cooled transfer buffer with continuous stirring. Non-specific binding sites on the blotted membrane were blocked by shaking in blocking solution for 2 h at room temperature. After blocking, the membrane was washed thrice with TBST for 5 minutes each wash. The washed membrane was sealed in polybag along with the primary antibody and incubated at 4°C for over night with an end-to-end shaking. The membrane was washed thrice for minutes each washing and incubated with the secondary antibody in blocking solution for 45 minutes. The membrane was washed thrice for 5 minutes each washing. The freshly prepared chemiluminescent substrate working solution was added to the surface of the membrane (approx. 0.2 ml/cm²) and incubated for 4 min at room temperature. The membrane was wrapped in plastic foil and exposed in the darkroom for 10 s - 30 min to an autoradiographic film that was subsequently developed in dark room conditions.

3.8. Functional analysis of recombinant hSGLT1

Sugar uptake assays were carried out in membranes prepared from *Pichia* GS115 cells harboring pPICZB-hSGLT1 plasmid and with purified recombinant hSGLT1 reconstituted into liposomes.

3.8.1. Membrane preparations for transport studies

Cells cultured in BMMY medium were harvested at O.D₆₀₀ of 4-6/ml by centrifugation at 3000 × g at 4°C for 10 min, washed once with ice-cold breaking buffer (50 mM sodium phosphate, pH 7.4, 10% glycerol) and resuspended in breaking buffer supplemented with protease inhibitor cocktail. An equal volume of acid- washed chilled glass beads (0.5 mm diameter) was added to the suspension, and cells were disrupted by vigorous vortexing ten times for 1 min, with intervening 1 min incubations on ice. Unbroken cells were removed by centrifugation at 2000 × g at 4°C for 5 min. Membranes were pelleted at 100,000 × g at 4°C for 30 min and resuspended in membrane suspension buffer (100 mM Mannitol, 20 mM HEPES- Tris, pH 7.4) with protease inhibitor cocktail. Aliquots were snap-frozen and stored at -80°C. The protein concentration of the membrane preparation was determined by using a micro-BCA kit.

3.8.2. Reconstitution of recombinant hSGLT1

Proteoliposomes were made using Triton X-100 destabilized liposomes (Jung et al., 1998; Heiermann et al., 1999; Rigaud and Daniel, 2003). Liposomes were composed of 90% (w/v) asolectin soy lecithin and 10% (w/v) cholesterol. 10 mg cholesterol and 90 mg asolectin soy lecithin were dissolved in 5 ml of chloroform in a beaker. The solvent was evaporated under a stream of argon to obtain a thin layer of dry lipids. Last traces of solvent were removed under vacuum in a desiccator overnight. Before each reconstitution the lipids were suspended in 5 ml of 100 mM potassium phosphate, pH 7.5/2 mM β -mercaptoethanol to yield a lipid concentration of 20 mg/ml and subsequently sonicated in argon atmosphere in a tip probe sonicator (until the suspension became slightly clear), and resulting liposomes were stored in liquid nitrogen. Triton X-100 was added at concentrations corresponding to the onset and or total solubilization of lipids as determined by turbidity measurements (Rigaud et al., 1995). Detergent-destabilized liposomes were mixed with purified protein in a 400:1 (w/w) and incubated at room temperature under gentle agitation for 10 min. Detergent was removed by adding Bio-Beads SM-2 activated according to (Holloway, 1973) at a wet weight beads: detergent ratio of 6:1. After 1 h of incubation at room temperature, fresh Bio-Beads were added, and incubation was continued for an additional hour. After the third addition of Bio-Beads, incubation was continued overnight at 4°C. Bio-Beads were removed by filtration on glass silk. Proteoliposomes were concentrated by centrifugation at $300,000 \times g$ for 45 min and stored in liquid nitrogen. Proteoliposomes pellet for sugar uptake assay were resuspended in 100 mM potassium phosphate, pH 7.5/2 mM β -mercaptoethanol for final protein concentration of 0.1 $\mu\text{g/ml}$.

3.8.3. Transport assay of hSGLT1 in membranes and in proteoliposomes

Sugar uptake by right-side-out membrane vesicles was performed as described for *E. coli* right-side-out membrane vesicles (Jung et al., 1998; Turk et al., 2000). Proteoliposomes (preloaded with 100 mM potassium phosphate, pH 7.5/2 mM β -mercaptoethanol) were subjected to three sonication/freeze/thaw cycles before uptake assays at 22°C. Uptake was initiated by mixing 10 μl of proteoliposomes with 10 μl of transport buffer 2X (200 mM choline.Cl, 50 mM NaCl, 100 mM mannitol, 20 mM Tris, 20 mM HEPES, 300 mM KCl, 6 mM MgSO_4 , 2 mM CaCl_2) with methyl α -D- [^{14}C] glucopyranoside ([^{14}C] α -MDG). Each reaction was stopped by with 1 ml of ice-cold stop solution (10 mM Tris, 10 mM HEPES, 100 mM mannitol, 150 mM KCl, 50 mM choline.Cl, 50 mM NaCl, 3 mM MgSO_4 , 1 mM CaCl_2 , 0.2 mM phlorizin), applied centrally to a 0.22 μm nitrocellulose filter GSWP (Millipore) over vacuum and washed with 3 ml of ice-cold stop solution, and the filter was assayed by scintillation counting. All experiments were performed at least in triplicate, and errors indicate the SE of the mean values.

3.9. Chemical synthesis of photoaffinity probes

TIPDG, BzG, 3-AP and 6-AG were synthesized according to schemes given in Figure 3.2, Figure 3.3, Figure 3.4 and Figure 3.5.

3.9.1. [(2'-Iodo-4'-(3''-trifluoromethyldiaziriny) phenoxy)]-D-glucopyranoside (TIPDG)

3.9.1.1. 4-Methoxytrifluoroacetophenone (1)

The titled compound in (Figure 3.2) was synthesized as previously reported (Delfino et al., 1993; Hatanaka et al., 1994) in 95% yield.

3.9.1.2. 3-Iodo-4-methoxytrifluoroacetophenone (2)

A mixture of 10 g (0.5 mol) of 1, 21.6 g (1.0 mol) of HgO, 5 ml of concentrated H₂SO₄, and 12.7 g (0.5 mol) of iodine in 250 ml of CCl₄ was heated to reflux with vigorous stirring for 4 h. The reaction mixture was cooled to room temperature, and then filtered through a pad of celite. The filtrate was washed with 2 N aqueous sodium thiosulfate solution and brine, and dried over Na₂SO₄. The residue obtained after evaporation was purified by column chromatography (hexane: EA = 9:1) to give 13.87 g (85%) of 2 as a white solid; mp 52-54°C. ¹H NMR (CDCl₃, 400MHz): δ = 3.98 (s, 3H), 6.89 (d, 1H, *J* = 8.8Hz), 8.04 (d, 1H, *J* = 8.8Hz), 8.47 (s, 1H). ¹³C NMR (CDCl₃, 100MHz): δ = 56.9, 86.5, 110.3, 116.6, 124.3, 132.7, 141.7, 163.6, 177.9.

3.9.1.3. 4-Hydroxy-3-iodo-trifluoroacetophenone (3)

O-Demethylation of 2 was carried out as follows. A mixture of 6.70 g (20 mmol) of 2 and 2.6 g (62 mmol) of LiCl in 50 ml of DMF was heated at reflux under argon for 2 h. The reaction mixture was cooled to room temperature, poured into water (200 ml) and acidified with 10% HCl. The product was extracted with Et₂O. The ethereal layer was washed with brine twice, dried over MgSO₄, and the residue obtained after evaporation of solvent was purified by column chromatography (CH₂Cl₂) affording 5.59 g (88%) of 3 as a white solid; mp 87-88°C. ¹H NMR (CDCl₃, 400MHz): δ = 6.13 (s, 1H), 7.09 (d, 1H, *J* = 8.8Hz), 7.98 (d, 1H, *J* = 8.6Hz), 8.40 (d, 1H, *J* = 0.4Hz). ¹³C NMR (CDCl₃, 100MHz): δ = 86.3, 115.3, 118.0, 124.6, 125.9, 132.9, 141.2, 160.8, 178.4. DEI-MS 316 (M⁺); HRMS calcd for (C₈H₄F₃IO₂)⁺ 315.9208, found 315.9208.

3.9.1.4. [(2'-Iodo-4'-trifluoroacetyl) phenoxy]-2,3,4,6-tetra-O-acetyl-D- glucopyranoside (5)

To a solution of α-D-acetobromoglucose 4, 4.0 g (9.73 mmol) in 80 ml of dry benzene-nitro methane 1:1, 3.07 g (9.71 mmol) of compound 3, 2.45 g (9.73 mmol) mercuric cyanide, and 3.0 g molecular sieves (4Å) were added. The resulting suspension was stirred for 12 h at 50°C.

The solvent was evaporated in vacuum and the residue was purified by column chromatography (EA: P.E = 3:1) to yield 4.71 g (75%) compound 5. ^1H NMR (CDCl_3 , 400MHz): δ = 2.01, 2.03, 2.07, 2.09 (s, 3H, H-Ac), 4.01-4.16 (m, 1H, H-5), 4.20-4.28 (m, 2H, H-6), 4.88 (dd, 1H, $J_{1,2}$ = 4.5Hz, H-1), 5.07 (t, 1H, J = 11.7Hz, H-4), 5.18-5.33 (m, 1H, H-2), 5.53 (t, 1H, $J_{3,4}$ = 11.7Hz, H-3), 7.03 (d, 1H, J = 10.75Hz, Ar-H), 7.92-7.96 (m, 1H, Ar-H), 8.41 (s, 1H, Ar-H). ^{13}C NMR(CDCl_3 , 100MHz): δ = 21.05, 21.16, 21.17, 21.23, 62.40, 67.43, 68.87, 70.27, 71.46, 95.73, 115.36, 118.25, 124.39, 132.84, 141.81, 161.71, 169.92, 170.41, 170.49, 171.19, 177.57, 177.70, 178.05, 178.83. FAB-MS 646.09 (M-H) $^+$, 670.04 (M+Na) $^+$, HRMS calcd for $(\text{C}_{22}\text{H}_{23}\text{O}_{11}\text{F}_3\text{NaI})^+$ 670.0134, found 670.0122.

3.9.1.5. [(2'-Iodo-4'-trifluoroacetyloxime) phenoxy]-2,3,4,6-tetra-O-acetyl-D-glucopyranoside (6)

A solution of 5, 4.0 g (6.18 mmol) and hydroxylamine hydrochloride 1.27 g (18.28 mmol) in 10 ml absolute ethanol and 30 ml dry pyridine was stirred at 60°C for 8 h. After evaporation of the solvent, the residue was partitioned between water and ether. The organic layer was washed with 1 N HCl and dried over MgSO_4 . After evaporation of the solvent, the crude oxime was purified by column chromatography on silica gel (CH_2Cl_2 : MeOH = 10:1) to leave 3.68 g (90%) of a colorless syrupy product 6. ^1H NMR (CDCl_3 , 400MHz): δ = 2.01, 2.04, 2.06, 2.09 (s, 3H, H-Ac), 4.09-4.15 (m, 1H, H-5), 4.22-4.30 (m, 2H, 2H-6), 4.88 (dd, 1H, $J_{1,2}$ = 4.5Hz, H-1), 5.08 (t, 1H, J = 11.7Hz, H-4), 5.20-5.34 (m, 1H, H-2), 5.54 (t, 1H, $J_{3,4}$ = 11.7Hz, H-3), 7.04 (d, 1H, J = 10.75Hz, Ar-H), 7.92-7.96 (m, 1H, ArH), 8.36 (s, 1H, NOH), 8.41 (s, 1H, ArH). ^{13}C NMR (CDCl_3 , 100MHz): δ = 21.06, 21.15, 21.18, 21.24, 62.33, 67.36, 68.89, 70.33, 71.49, 95.73, 115.38, 118.25, 124.40, 132.84, 141.41, 141.83, 161.71, 169.92, 170.49, 177.58, 177.70, 178.15, 178.83. FAB-MS 661.96 (M+H) $^+$, 683.94 (M+Na) $^+$, HRMS calcd for $(\text{C}_{22}\text{H}_{24}\text{NO}_{11}\text{F}_3\text{I})^+$ 662.0347, found 662.0356, calcd for $(\text{C}_{22}\text{H}_{23}\text{NO}_{11}\text{F}_3\text{NaI})^+$ 684.0165, found 684.0197.

3.9.1.6. [(2'-Iodo-4'-(3''-trifluoromethyldiaziridiny) phenoxy]-2,3,4,6-tetra-O-acetyl-D-glucopyranoside (7)

To a solution of oxime 6, 3.5 g (5.28 mmol), triethylamine 1.44 g (10.54 mmol) and (*N,N*-dimethylamino) pyridine 25 mg (0.02 mmol) in 20 ml CH_2Cl_2 at 0°C, was added *p*-toluenesulfonyl chloride 1.0 g (5.28 mmol) portion wise with stirring. After the addition, the reaction mixture was stirred at room temperature for 45 min. The mixture was washed with water, and the organic phase was dried over MgSO_4 . After evaporation of the solvent, the crude oxime tosylate was dissolved in 20 ml dry CH_2Cl_2 , and the solution is cooled to -78 °C in a sealed tube. Liquid ammonia 3 ml was added and the mixture was stirred at room temperature for 16 h in a sealed tube. The excess ammonia was allowed to evaporate at room temperature. The residue was partitioned between water and CH_2Cl_2 , and the organic layer was dried over MgSO_4 . After evaporation of the solvent, the residual syrupy product was purified by column chromatography on neutral alumina (CH_2Cl_2) to give 2.27 g (65%) of a

pale yellow syrupy compound 7. $^1\text{H NMR}$ (CDCl_3 , 400MHz): $\delta = 2.00, 2.01, 2.06, 2.08$ (s, 3H, H-Ac), 4.00- 4.28 (m, 5H, H-5, H-6, NH), 4.78 (dd, 1H, $J_{1,2} = 4.4\text{Hz}$, H-1), 5.02 (t, 1H, $J = 11.6\text{Hz}$, H-4), 5.12-5.27 (m, 1H, H-2), 5.43 (d, 1H, $J_{3,4} = 11.7\text{Hz}$, H-3), 7.02 (d, 1H, $J = 10.75$, Ar-H), 7.90-7.96 (m, 1H, Ar-H), 8.41 (s, 1H, Ar-H).

FAB-MS 659.73 (M^+), 661.06 ($\text{M}+\text{H}^+$), 683.08 ($\text{M}+\text{Na}^+$), HRMS calcd for $(\text{C}_{22}\text{H}_{24}\text{N}_2\text{O}_{10}\text{F}_3\text{I})^+$ 661.3408, found 661.0506, calcd for $(\text{C}_{22}\text{H}_{24}\text{N}_2\text{O}_{10}\text{F}_3\text{NaI})^+$ 683.3226, found 683.0297

3.9.1.7. [(2'-Iodo-4'-(3''-trifluoromethyldiaziriny) phenoxy)-2,3,4,6-tetra-O-acetyl-D-glucopyranoside (8)

To a vigorously stirred solution of 7, 1.0 g (1.51 mmol) and triethylamine 0.3 g (3.0 mmol) in 10 ml MeOH was added portionwise I_2 total 0.39 g (1.54 mmol). After being stirred for 30 min at room temperature, the dark brown reaction mixture was partitioned between Et_2O and saturated aqueous citric acid. The Et_2O phase was washed with solutions of citric acid, sodium hydrogen sulfite and finally with water. The organic layer was dried over MgSO_4 and concentrated in vacuo to give syrupy residue, which was purified by column chromatography on silica (CH_2Cl_2) to give 0.9 g (91%) yellow color syrupy compound 8. $^1\text{H NMR}$ (CDCl_3 , 400MHz): $\delta = 2.00, 2.01, 2.06, 2.08$ (s, 3H, H-Ac), 4.00-4.10 (m, 1H, H-5), 4.18-4.24 (m, 2H, H-6), 4.76 (dd, 1H, $J_{1,2} = 4.4\text{Hz}$, H-1), 5.02 (t, 1H, $J = 11.6\text{Hz}$, H-4), 5.12-5.26 (m, 1H, H-2), 5.40 (d, 1H, $J_{3,4} = 11.7\text{Hz}$, H-3), 7.00 (d, 1H, $J = 10.75$, Ar-H), 7.90-7.96 (m, 1H, Ar-H), 8.40 (s, 1H, Ar-H).

FAB-MS 658.00 (M^+), 681.04 ($\text{M}+\text{Na}^+$), HRMS calcd for $(\text{C}_{22}\text{H}_{22}\text{O}_{10}\text{N}_2\text{F}_3\text{NaI})^+$ 681.0168, found 681.0159.

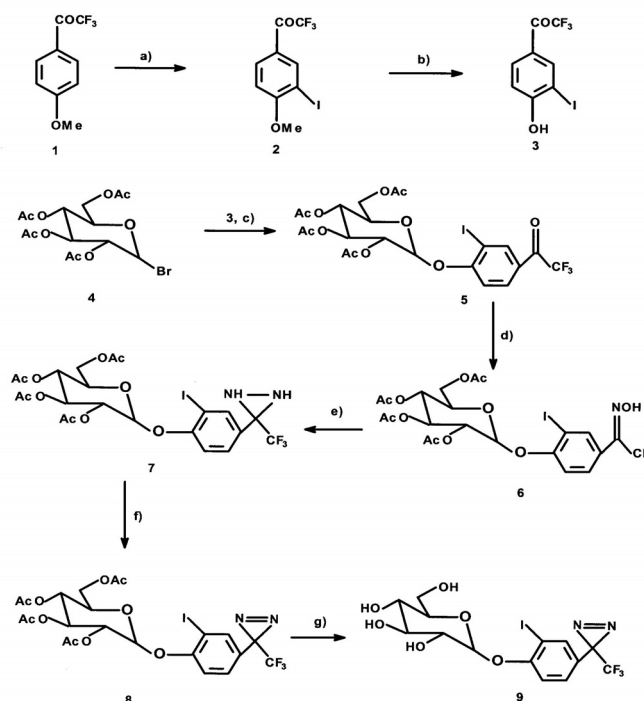


Figure 3.2 Reaction scheme for the synthesis of TIPDG 9. The reagents were (a) I_2 , HgO , conc. H_2SO_4 , CCl_4 ; (b) LiCl , DMF; 3,4-hydroxy-3-iodo-trifluoroacetophenone; (c) $\text{Hg}(\text{CN})_2$, nitro methane, benzene; (d) $\text{NH}_2\text{OH}\cdot\text{HCl}$, EtOH, pyridine; (e) tosyl chloride, DMAP, Et_3N , DCM, NH_3 ; (f) I_2 , Et_3N , MeOH; (g) NaOMe .

3.9.1.8. [(2'-Iodo-4'-(3''-trifluoromethyldiazirinyloxy)phenoxy]-D-glucopyranoside (9)

Compound 8, 0.5 g (0.75 mmol) was deacylated by stirring with 10 ml dry MeOH containing 0.9 g (22.5 mmol) NaOH for 2 h at room temperature. The solution was neutralized with ion exchange resin (Amberlite IR 120, H⁺), the solvent was evaporated in vacuo and the residue was purified on a silica column (CHCl₃: MeOH = 9:1) to yield 0.36 g (98%) 9, λ_{\max} (ME) = 358 nm ($\epsilon = 290 \text{ M}^{-1} \cdot \text{cm}^{-1}$). ¹H NMR (CD₃OD, 400MHz): $\delta = 3.25$ (dd, 1H, $J = 7.7\text{Hz}$, H-2), 3.30-3.39 (m, 3H, H-3, H-4, H-5), 3.70-3.82 (dd, 1H, $J = 6.0\text{Hz}$, H-6), 3.88-3.91 (dd, 1H, $J = 1.6\text{Hz}$, H-6), 4.27 (d, 1H, $J = 7.8\text{Hz}$, H-1), 7.06 (d, 1H, $J = 10.8$, Ar-H), 7.94-7.98 (m, 1H, Ar-H), 8.41 (s, 1H, Ar-H).

¹³C NMR (CD₃OD, 100MHz): $\delta = 71.51, 71.56, 75.15, 78.03, 78.15, 103.0, 117.37, 120.52, 126.92, 134.82, 171.20, 176.67, 178.07, 179.05, 179.93$. FAB-MS 489.98 (M)⁺, 490.99 (M+H)⁺, HRMS calcd for (C₁₄H₁₄N₂O₆F₃I)⁺ 489.9846, found 489.9846, calcd for (C₁₄H₁₅N₂O₆F₃I)⁺ 490.9925, found 490.9927.

3.9.2. [(4'-Benzoyloxy)phenoxy]-D-glucopyranoside (BzG)

3.9.2.1. [4'-Benzoyloxy]-2,3,4,6-tetra-O-acetyl-D-glucopyranoside (11)

A solution of α -D-Acetobromoglucose 4, 5.0 g (12.16 mmol) in 50 ml of benzene and in 50 ml of nitro methane was mixed with 4-hydroxybenzophenone 10, 2.41 g (12.16 mmol), mercuric cyanide 3.07 g (12.16 mmol) and 3.9 g of molecular sieves (4Å) and the resulting mixture was stirred at 60°C for 15 h. The reaction mixture was partitioned in between water and Et₂O and the resulting organic phase was washed with brine and dried over MgSO₄. After evaporation of the solvent in vacuo, the resulting residue was purified by column chromatography on silica (EA: PE = 1:1) to yield 4.36 g (68%) white solid compound 11. ¹H NMR (CDCl₃, 400MHz): $\delta = 2.01, 2.02, 2.06, 2.07$ (s, 3H, H-Ac), 4.08-4.11 (m, 1H, H-5), 4.21-4.26 (m, 2H, H-6), 4.88 (dd, 1H, $J_{1,2} = 4.5\text{Hz}$, H-1), 5.06 (t, 1H, $J = 11.7\text{Hz}$, H-4), 5.20-5.28 (m, 1H, H-2), 5.53 (t, 1H, $J_{3,4} = 9.4\text{Hz}$, H-3), 6.80 (dd, 2H, $J = 8.42$ and 2.45Hz , Ar-H), 7.43-7.47 (m, 2H, Ar-H), 7.52-7.56 (m, 1H, Ar-H), 7.70-7.75 (m, 4H, Ar-H).

¹³C NMR (CDCl₃, 100MHz): $\delta = 21.08, 21.16, 21.18, 21.22, 67.34, 68.89, 70.36, 71.51, 95.67, 115.51, 128.42, 129.55, 132.27, 133.23, 138.26, 161.15, 169.99, 170.50, 170.58, 171.30, 196.61$.

3.9.2.2. [(4'-Benzoyloxy)phenoxy]-D-glucopyranoside (12)

Deacetylation of compound 11 was carried out as follows. A mixture of 2.0 g (3.78 mmol) of 11 and 4.53 g (151.2 mmol) NaOH in 20 ml dry methanol was stirred at room temperature for 5 h. After completion of reaction the resulting reaction mixture was neutralized with ion exchange resin (Amberlite IR 120, H⁺), the solvent was evaporated in vacuo and crude product was purified by column chromatography on silica (CHCl₃: MeOH = 3:1) to yield 1.22 g (90%) white solid compound 12; mp 163 °C; λ_{\max} (ME) = 293 nm ($\epsilon = 290 \text{ M}^{-1} \cdot \text{cm}^{-1}$). ¹H

NMR (CD₃OD, 400MHz): δ = 3.22 (dd, 1H, J = 7.6Hz, H-2), 3.27-3.38 (m, 3H, H-3, H-4, H-5), 3.68-3.71 (dd, 1H, J = 5.9Hz, H-6), 3.87-3.90 (dd, 1H, J = 1.6Hz, H-6), 4.27 (d, 1H, J = 7.8Hz, H-1), 7.51 (t, 2H, J = 7.8Hz, Ar-H), 7.62 (tt, 1H, J = 1.7 and 6.4Hz, Ar-H), 7.69 (d, 2H, J = 8.1Hz, Ar-H), 7.83 (m, 4H, Ar-H).

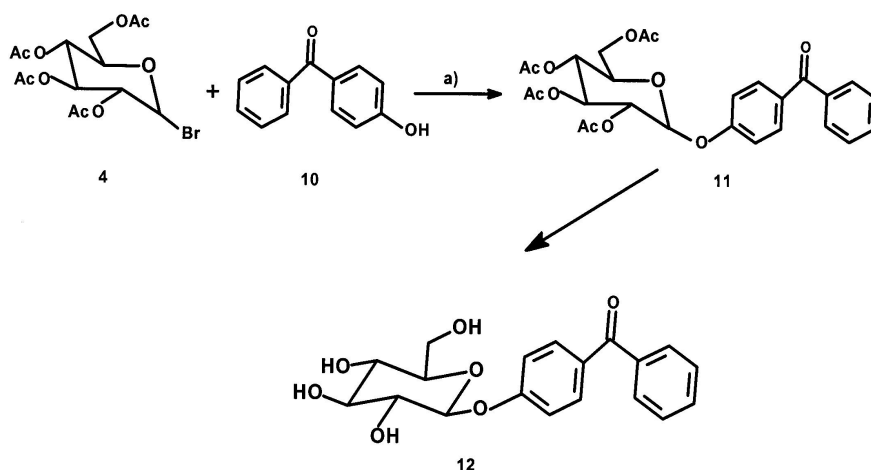


Figure 3.3 Synthesis of BzG 12. The reagents were (a) Hg(CN)₂, nitro methane, benzene; (b) NaOMe.

3.9.3. 3-Azidophlorizin (3-AP)

3.9.3.1. 3-Nitrophlorizin (14)

472 mg Phlorizin 13 was dissolved in 10 ml of glacial acetic acid. The temperature of the solution was brought to 15°C. 75 μ l of nitric acid (specific gravity 1.4) was added dropwise to the solution under vigorous stirring. At the end of the reaction, the color of the solution turned to red-brown. The solution was then poured onto 20 g ice. The green precipitates were collected and dried under vacuum. For further purification, the dry precipitates were dissolved in tetrahydrofuran. The solution was passed through a neutral aluminum oxide column. The yellow solution was then concentrated and a small amount of petroleum ether 30-60°C was added until the solution became slightly turbid. After some time crystals developed. Melting point 217-218°C.

3.9.3.2. 3-Aminophlorizin (15)

482 mg 3-Nitrophlorizin 14 was dissolved in 5 ml ethanol and mixed with 150 mg palladium/carbon (10% Pd). Hydrogen gas was introduced into the solution gently for a period of 1 h at room temperature. The catalyst was then removed by filtration. The ethanolic solution was diluted with 10 ml of deoxygenated water and frozen immediately. Solid 3-Aminophlorizin was obtained by freeze-drying. The yield of reduction product was almost 100%. Melting point 91-93°C. During the whole procedure the reaction mixture was protected from light by aluminum foil.

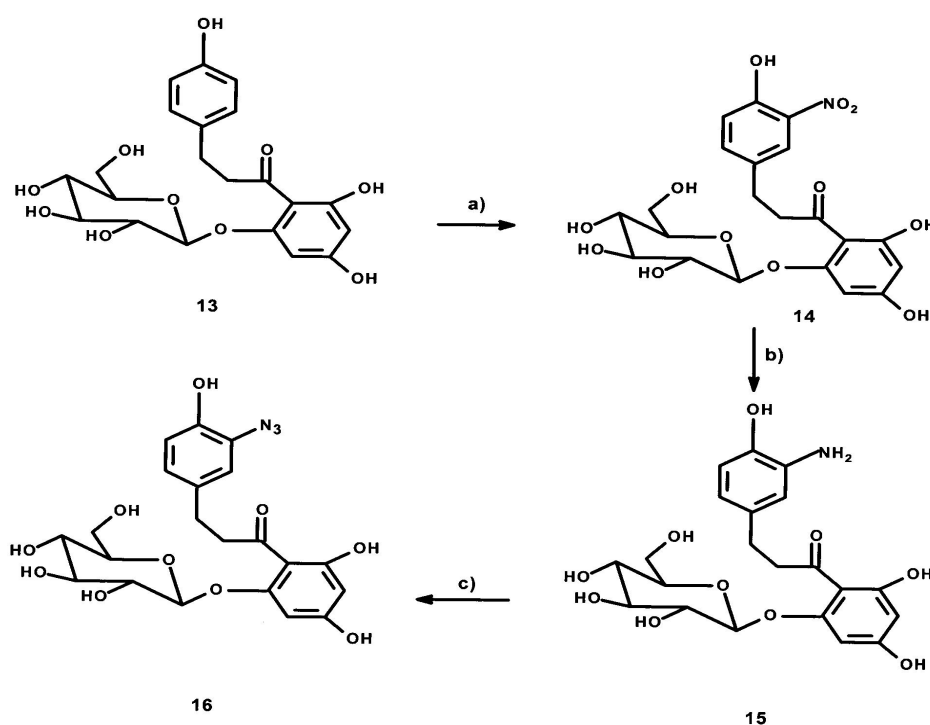


Figure 3.4 Reaction scheme for the synthesis of 3-AP. The reagents were (a) HNO_3 , CH_3COOH ; (b) H_2 , Pd/C, EtOH; (c) NaNO_2 , NaN_3 .

3.9.3.3. 3-Azidophlorizin (16)

45 mg of 3-Aminophlorizin were dissolved in 3 ml of 0.5 N ice-cold hydrochloric acid. The solution was cooled down to -5°C . To this solution 0.5 ml 0.2 M cold sodium nitrite was added. The reaction was allowed to proceed at -5°C for 10 min. A deep green color developed. Subsequently, 0.5 ml of 0.2 M sodium acetate was added. The solution changed its color rapidly to red brown while bubbling occurred because of nitrogen release. A gel-like precipitate was obtained by centrifugation (low speed). The dry precipitate was then dissolved in an excess of THF. The deep brown solution was decolorized by passing through a short silica gel column. After part of THF had been evaporated, a few drops of water were added to obtain 3-Azidophlorizin precipitate. Melting point 85°C (decomposed).

3.9.4. n-Methyl-6C- (Azimethyl)-D- glucopyranoside (6-AG)

3.9.4.1. Methyl-2,3,4-tri-O-benzyl-7-deoxy-DL-glycero-D-glucohepta-1,5- pyranoside (18)

Compound 17, 11.5 g (25 mmol) (Lehmann and Thieme, 1986) dissolved in 200 ml dry ether was added at room temperature over a period of 45 min to a stirred solution of methylmagnesium iodide prepared from 5.4 g (0.18 mol) magnesium turnings and 24.8 g (0.18 mol) methyl iodide in 310 ml dry ether. The mixture was stirred for 1 h at room temperature and poured on 400 g ice, and saturated aqueous NH_4Cl was added until

precipitated magnesium salts dissolve. The organic phase was separated and the aqueous layer was extracted three times with 150 ml ether. The combined ether extracts were washed with water, dried with MgSO_4 , evaporated in vacuo to yield 11.5 g (97%) as syrup. The crude product was used without further purification in next step.

3.9.4.2. Methyl-2,3,4-tri-O-benzyl-7-deoxy-D-glucohepto-1,5-pyranoside-6-ulose (19)

Compound 18, 11.5 g (24 mmol), 14.0 g (69 mmol) DCC, and 1.0 g anhydrous phosphoric acid were dissolved in 170 ml anhydrous dimethyl sulfoxide and the mixture was stirred for 19 h at room temperature. The suspension was added slowly with stirring to an ice-cold solution of 9.5 g (0.11 mol) oxalic acid in 20 ml methanol within 15 min; the mixture was stirred for 30 min and diluted with 350 ml saturated aqueous NaCl. After stirring for a further 30 min, the precipitated solid was filtered and stirred two times with 250 ml ether and filtered again. The combined ether extracts were neutralized with saturated aqueous NaHCO_3 , washed with water, dried with MgSO_4 , and evaporated in vacuo. The syrupy crude product was dissolved in boiling ethyl acetate (40 ml) and after addition of 40 ml petroleum ether it was crystallized at -20°C to yield 5.5 g (48%) 19, melting point 97°C .

^1H NMR (CDCl_3 , 500MHz): δ = 2.16 (s, 3H, H-7), 3.39 (s, 3H, OCH_3), 3.54 (dd, 1H, H-2, $J_{2,3} = 9.6\text{Hz}$), 3.62 (t, 1H, H-4, $J_{4,5} = 9.9\text{Hz}$), 4.01 (t, 1H, H-3, $J_{3,4} = 9.5\text{Hz}$), 4.12 (d, 1H, H-5), 4.61 (d, 1H, H-1, $J_{1,2} = 3.5\text{Hz}$), 4.60-5.00 (m, 6H, H-Bn), 7.72-7.36 (m, 15H, H-Ph).

^{13}C NMR (CDCl_3 , 125.8MHz): δ = 27.85, 55.55, 74.22, 73.46, 74.84, 75.79, 78.59, 79.57, 81.77, 98.53, 127.58-128.43, 137.84, 137.96, 138.55, 204.36.

3.9.4.3. Methyl- 7- deoxy-D-glucohepta- 1, 5- pyranoside-6- ulose (20)

Compound 19, 5.8 g (12 mmol) dissolved in 200 ml methanol-ethyl acetate was debenzylated in the presence of 3.0 g palladium (10% C) by catalytic hydrogenation for 5 h with shaking using a hydrogen pressure of 3 bar at room temperature. The suspension was filtered from the catalyst and evaporated in vacuo to yield 2.5 g (100%) 20 as syrup.

For further characterization 0.86 g (4.2 mmol) 17 was per-O-acetylated by stirring with 30 ml pyridine-acetic anhydride (2:1) for 15 h at room temperature. The mixture was poured on 250 g ice, stirred for 30 min, and extracted three times with 50 ml dichloromethane. The combined organic extracts were washed with water, dried with MgSO_4 , and concentrated in vacuo. The resulting syrup was purified on silica gel column to yield 0.97 g (67%) acetylated compound 21.

^1H NMR (CDCl_3 , 500MHz): δ = 2.01, 2.02, 2.09 (s, 3H, H-Ac), 2.26 (s, 3H, H-7), 3.45 (s, 3H, OCH_3), 4.09 (d, 1H, H-5), 4.89 (dd, 1H, H-2, $J_{2,3} = 10.2\text{Hz}$), 5.03 (d, 1H, H-1, $J_{1,2} = 3.6\text{Hz}$), 5.10 (t, 1H, H-4, $J_{4,5} = 10.3\text{Hz}$), 5.50 (t, 1H, H-3, $J_{3,4} = 9.8\text{Hz}$).

^{13}C NMR (CDCl_3 , 125.8MHz): δ = 20.51- 20.63, 25.82, 55.85, 68.93, 69.47, 70.72, 73.32, 97.03, 169.64, 169.79, 170.09, 203.65.

3.9.4.4. n-Methyl-6C-(Azimethyl)-D-glucopyranoside (22)

A stream of dry NH_3 was introduced into a solution of 2.5 g (12 mmol) 20 in 100 ml dry methanol at -30°C until the volume increased about 20%. Then 2.0 g (17 mmol) hydroxyl-O-sulfonic acid was added in small portions over a time period of 1 h to the vigorously stirred mixture. The suspension was stirred for 3 h at -30°C , allowed to attain room temperature overnight, filtered, and concentrated in vacuum. A solution of the residue in 100 ml dry methanol containing 20 ml Et_3N was cooled to 0°C and iodine was added until the red color persisted. The solution was then concentrated and the residue was purified on a silica gel column to give 1.6 g (61%) pure compound 22. λ_{max} (Methanol) = 335 nm ($\epsilon = 52 \text{ M}^{-1} \cdot \text{cm}^{-1}$). For further characterization of compound 22, 0.2 g of it was per-O-acetylated as described for compound 20, to yield 0.16 g (76%) compound 23.

^1H NMR (CDCl_3 , 500MHz): $\delta = 1.08$ (s, 3H, H-7), 2.02, 2.07, 2.15 (s, 3H, H-Ac), 3.02 (d, 1H, H-5), 3.39 (s, 3H, OCH_3), 4.82 (dd, 1H, H-2, $J_{2,3} = 10.2\text{Hz}$), 4.96 (d, 1H, H-1, $J_{1,2} = 3.6\text{Hz}$), 5.03 (t, 1H, H-4, $J_{4,5} = 10.3\text{Hz}$), 5.37 (t, 1H, H-3, $J_{3,4} = 10.1\text{Hz}$).

^{13}C NMR (CDCl_3 , 125.8MHz): $\delta = 15.15, 20.47\text{--}20.83, 25.09, 55.33, 68.58, 69.52, 70.48, 71.19, 96.56, 169.54, 169.72, 169.90$.

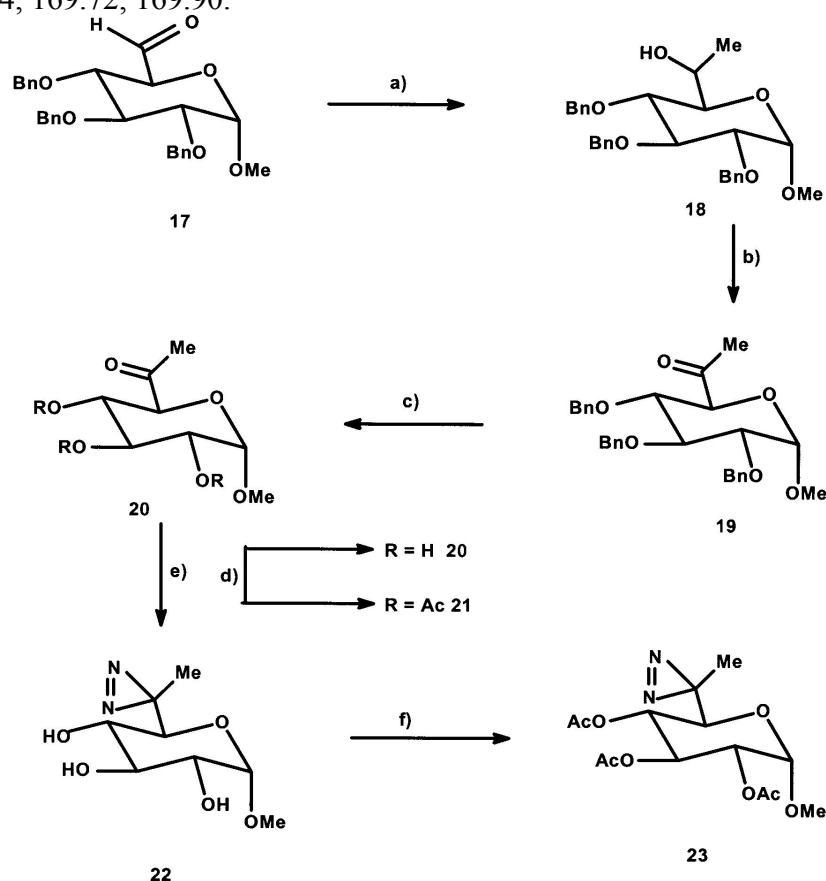


Figure 3.5 Synthesis of 6-AG. The reagents were (a) MeMgI, H_2O ; (b) Me_2SO , *N,N'*-dicyclohexylcarbodiimide; (c) H_2 , Pd/C, EtOH; (d) Ac_2O , pyridine; (e) NH_3 , hydroxylamine-O-sulfonic acid, I_2 ; (f) Ac_2O , pyridine.

3.10. Photoaffinity labeling of loop 13

Truncated loop 13 protein used in this study was a gift from Mobeen Raja. Before using these photoprobes as a label for truncated loop 13 we performed transport assays of these probes with rabbit small intestine brush border membrane vesicles.

3.10.1. Isolation of small intestine brush border membrane vesicles (BBMV)

Rabbit small intestines were obtained immediately after sacrifice of the animals. Brush border membrane vesicles (BBMV) from rabbit small intestine epithelial scratching were prepared by the magnesium precipitation method of Booth and Kenny (Booth and Kenny, 1974). Final BBMV were suspended at a concentration of 16 mg protein/ml in mannitol-Hepes-Tris (MHT) buffer (100 mmol/l mannitol, 20 mmol/l Hepes-Tris, pH 7.4, and protease inhibitor: Aprotinin 20 µg/ml, leupeptin 20 µg/ml, pepstatin 5 µg/ml, and chymostatin 5 µg/ml). The purity of the preparation was routinely determined by assaying the marker enzyme alkaline phosphatase (E.C.3.1.3.1), which was enriched 8 to 10 fold. BBMV were stored at -70°C until use and diluted to the concentration of 5 mg protein/ml with MHT buffer for transport studies.

3.10.2. Transport measurements

Uptake of radioactive substrate was determined at 22°C with the rapid filtration technique as described initially by Hopfer (Hopfer et al., 1973). The uptake was initiated by adding 20 µl BBMV suspension (100 µg protein) to 50 µl incubation media to give 100 mmol/l mannitol, 20 mmol/l Hepes-Tris (pH 7.4), 100 mmol/l NaSCN or KSCN, 0.1 mmol/l substrate 5µCi D-³H] glucose, and the indicated inhibitor concentrations. The incubation was terminated after 5 s by adding 1 ml ice-cold stop solution (100 mmol/l NaCl, 100 mmol/l mannitol, 20 mmol/l Hepes-Tris and 0.2 mmol/l phlorizin, pH 7.4) followed by rapid filtration of the suspension through prewetted 0.45 µm nitrocellulose filters. After rinsing with 3.5 ml ice-cold stop solution the wet filters were dissolved in 7 ml scintillation cocktail and counted for radioactivity in a liquid scintillation counter.

Substrate uptakes presented are mean values ± S.E from at least three independent experiments, each performed in duplicate or triplicate. For statistical comparisons, Student's t-test was used.

3.10.3. Photoaffinity labeling of truncated loop 13 protein with TIPDG or BzG

The photolabeling experiments were carried out in 200 µl PBS buffer (140 mM NaCl, 2.7 mM KCl, 10 mM Na₂HPO₄, 1.8 mM KH₂PO₄, pH 7.4) containing 200 µg truncated loop 13

protein and 1 mM TIPDG or with 0.5 mM BzG. The mixture was preincubated at room temperature in the dark for 5 min. After incubation, photolysis was carried out in a Rayonet photochemical reactor RPR-100, fitted with 16, 3500Å lamps at 22°C for 5 min for TIPDG and for BzG an Oriel photochemical reactor, fitted with 200 W medium pressure Hg lamp at 25°C for 30 min. As a control, the photoprobe was first exposed to UV light and then added to the protein. No labeling was observed in the absence of UV light. We also performed photoaffinity labeling of truncated loop 13 with 1 mM TIPDG in the presence of 100 µM arbutin and with 0.5 mM BzG in the presence of 15 µM phlorizin under the same conditions that were employed in the other photolabeling experiments. After photoaffinity labeling the protein was precipitated with chloroform methanol (v/v 2:1). The protein pellet was solubilized with 0.1% TFA in 50% acetonitrile for MALDI-TOF mass spectrometry analysis.

Mass spectra were acquired in the positive ion, linear mode on a Voyager DE-PRO MALDI (PE- Biosystems, Shelton, USA). After mixing the solubilized protein with sinapinic acid matrix (saturated sinapinic acid solution in 0.1% TFA in 50% acetonitrile), samples were deposited on a MALDI plate and dried at room temperature.

3.10.4. Photoaffinity labeling of truncated loop 13 protein with 3-AP

Photoaffinity labeling was performed with the photolabile phlorizin analogue 3-Azidophlorizin. The photolabeling experiments were carried out in 200 µl PBS buffer (pH 7.3) containing 200 µg truncated loop 13 protein and 1 mM 3-Azidophlorizin. The mixture was preincubated at room temperature in the dark for 5 min. After incubation, photolysis was carried out in a Rayonet photochemical reactor RPR-100, fitted with sixteen, 2800Å lamps at 22° C for 10 min. As a control, the photoprobe was first exposed to UV light and then added to the protein. No labeling was observed in the absence of UV light. After photoaffinity labeling the protein was precipitated with chloroform methanol (v/v 2:1). A small part of the protein pellet was solubilized with 0.1% TFA in 50% acetonitrile for MALDI-TOF mass spectrometry analysis and the rest of the protein pellet was dissolved in sample buffer for SDS-PAGE. Proteins were separated by SDS-PAGE using NuPAGE 4-12% Bis-Tris gels (Invitrogen). Gels were stained with Coomassie Brilliant Blue G-250 (Neuhoff et al., 1985). Bands of interest were excised from gel with a clean razor blade, sliced into 1 mm³ cubes and incubated over night at room temperature with 200 µl of 50 mM NH₄HCO₃, pH 8.5, 50% acetonitrile, then dehydrated with 200 µl acetonitrile and dried in a centrifugal evaporator. Gel pieces were rehydrated with a small volume of digestion solution (50 mM NH₄HCO₃, 5 mM CaCl₂, and 12.5 ng/µl of trypsin) at 4° C for 30 min. Trypsin was used at an enzyme: substrate ratio of ~ 1:100 by weight. Digestion was allowed to proceed overnight at 37° C. Peptides were extracted from the gel pieces with 100 µl of 20 mM NH₄HCO₃ followed by 2 extractions of water: acetonitrile (1:1) plus 1% trifluoroacetic acid and finally, 1 extraction with 100 µl of acetonitrile. All extracts were combined in a fresh tube, flash frozen and dried in a centrifugal

evaporator. Dried extracts were stored at -20° C until analyzed. Mass spectra were acquired in the positive ion, linear mode on a Voyager DE-PRO MALDI (PE-Biosystems, Shelton, USA). After mixing the solubilized protein with 2,5-dihydroxybenzoic acid matrix (saturated DHB solution in 0.1% TFA in 50% acetonitrile) for intact truncated loop 13 protein, and for acquisition of mass spectrometric peptide map of the trypsin digested protein, 0.5 µl aliquots of the generated cleavage products were dispensed onto the sample support, followed by 0.5 µl of CHCA matrix solution (solution of α -Cyno-4-hydroxycinnamic acid in 0.1% TFA in 50% acetonitrile). Samples were deposited on a MALDI plate and dried at room temperature prior to collecting the spectra.

4. Results

4.1. *E. coli* as an expression host

4.1.1. Construction of different clones of hSGLT1 in pET22b vector

The full-length cDNA sequence of human sodium/D-glucose cotransporter 1 (hSGLT1) was amplified by PCR. Agarose gel electrophoresis shows the amplification of 2.0 Kbp fragments (Figure 4.1A) as expected, which corresponds to the gene size of hSGLT1. In order to further ensure that amplified gene product is hSGLT1 gene we performed its digestion with *Bam*H1 because hSGLT1 gene contains only one *Bam*H1 restriction site. Therefore, after *Bam*H1 digestion it would reveal 2 DNA fragments if the PCR amplified product was correct. The predicted size of 2 DNA fragments is 1576 and 419 bp (which is in total 1995 bp), respectively. Analysis of the digestion mixture revealed that 2 DNA fragments were precisely produced by *Bam*H1 digestion (Figure 4.1B).

The cDNA sequence encoding full-length hSGLT1 was cloned into pET22b *E. coli* expression vector by using *Eco*R1 and *Xho*1 restriction enzymes sites. The plasmid was transformed into *E. coli* DH5 α strain for further replication. The restriction digestion of this clone with *Eco*R1 and *Xho*1 obtained the evidence for the successful construction of pET22b-hSGLT1 plasmid.

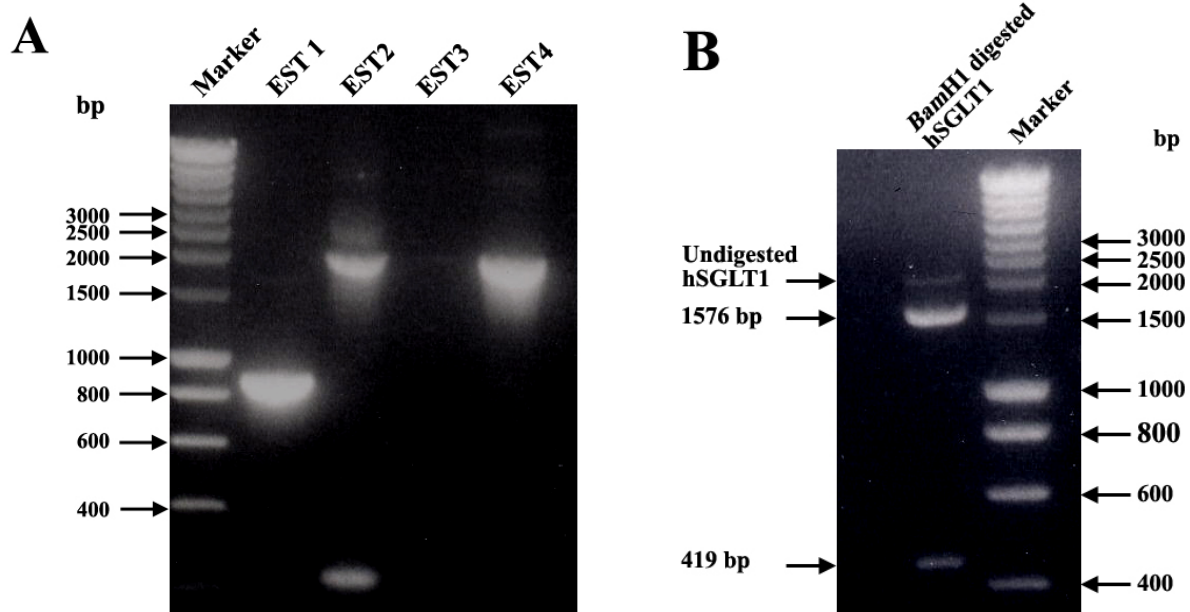


Figure 4.1 Different steps for the construction of pET22b-hSGLT1 clone. (A) PCR amplification of hSGLT1 gene by using *Eco*R1 and *Xho*1 restriction sites containing primers from EST clones. Only EST4 clone contains full-length hSGLT1 gene. (B) Agarose gel of *Bam*H1 digested hSGLT1 gene resulted in 2 DNA fragments of 1576 and 419 bp (total 1995 bp).

In addition to the evidence mentioned above, the construct was also sequenced by using appropriate sequencing primer. The full sequence of the construct revealed that the cloning

process was successful. Other constructs of hSGLT1 in pET22b expression vector were made with help of the same strategy by using their respective set of primers and restriction enzymes. Some-times it is difficult to express full-length transporter but the expression of small parts as functional domains of the transporters can be favored by using suitable hosts. Domains are known as the regions along a single polypeptide chain that can act as independent units. To that extent, they can be excised from the chain, still be shown to fold correctly, and often exhibit biological activity (Kachalsky et al., 1995; Li de La Sierra et al., 2000). So we tried to express the last seven domain of hSGLT (with 11 amino acids N-terminal part) in pET22b expression vector. Sequence encoding Δ N12-377hSGLT1 was amplified by QuikChange Site-Directed Mutagenesis method by using Δ N12-377SGLT sense and Δ N12-377SGLT antisense primers. pET22b- Δ N12-377 hSGLT1 clone was confirmed by DNA sequencing. The same clones as mentioned in the pET22b series were also prepared using the pBAD24 vector.

4.1.2. Construction of pET22b-Unc-F and pET22b-Unc-F-hSGLT1 clones

Unc-F gene encodes the subunit β of F_0 membrane sector of *E. coli* ATP synthase (Walker et al., 1982). Fusion of Unc-F gene at the N-terminal of gene of interest resulted in a polycistronic gene, which encodes two different proteins. Over-expression of β -subunit of the *E. coli* ATP synthase induces a massive proliferation of membranes in *E. coli* C43 (DE3) strain, which helps in the proper insertion of membrane proteins (Arechaga et al., 2000), sometimes this means help in the expression of eukaryotic membrane proteins. To test this idea for the expression of hSGLT1 protein, we constructed pET22b-Unc-F (*control*) and pET22b-Unc-F-hSGLT1 clones by the ligation of *Xba*I digested purified Unc-F gene fragment (511 bp) with similarly treated dephosphorylated pET22b and pET22b-hSGLT1 expression vectors. The resulting expression plasmids pET22b-Unc-F and pET22b-Unc-F-hSGLT1 were transformed into DH5 α cells for replication and for DNA isolation. It is a single enzyme ligation so the Unc-F gene can ligate into pET22b and pET22b-hSGLT1 vector into two ways, right orientation or reverse orientation. For the identification of clones containing Unc-F gene in the right orientation we performed colony PCR of these clones with primers: forward T7 promoter and reverse UncF. Clones with right orientation of Unc-F gene only shows amplification of Unc-F fragment (Figure 4.2).

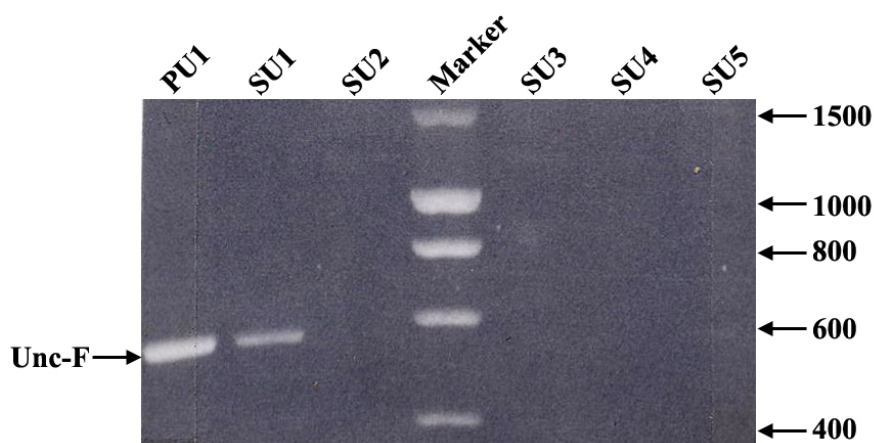


Figure 4.2 Agarose gel of PCR amplified Unc-F gene product from the clones pET22b-Unc-F and pET22b-Unc-F-hSGLT1 for the identification of positive clones with right orientation of Unc-F gene. Lane PU1 and SU1 indicate the clone containing Unc-F gene in correct orientation.

4.1.3. hSGLT1 expression in *E.coli*

Since *E. coli* is the first choice for heterologous expression of any foreign gene, heterologous expression of hSGLT1 was tried in *E. coli*. For the expression of hSGLT1 each clone was transformed into following *E. coli* strains (Rosetta, C41, C43, and C43Rosetta) except pET22b-Unc-F-hSGLT1 clone, which was transformed, into C43 and C43Rosetta cells. For the analytical purpose each clone was grown in 10 ml culture volume in different expression conditions (mentioned in the section 3.6.1 of Material and Methods). When O.D₆₀₀ of culture reached between 0.4-0.6, protein expression was induced by IPTG (in case of pET22b vector) and by L- (+) arabinose (pBAD24 vector). 1 ml culture was withdrawn before and after 4 h of protein induction and protein expression was probed by Western blot analysis by using anti-His tag, anti-SGLT1 and anti-FLAG tag antibodies but none of the clones tested positive for hSGLT1 expression (Table 4.1).

Table 4.1 Expression of hSGLT1 in different clones of *E. coli*

Clone	<i>E. coli</i> strain	Outcome
pET22b-hSGLT1	R, C41, C43 and C43R*	Expression not observed
pET22b-hSGLT1-Spacer	Same	Same
pET22b-ΔN12-377 hSGLT1	Same	Same
pET22b-ΔN12-377 hSGLT1-Spacer	Same	Same
pET22b-Unc-F-hSGLT1	C43 and C43R	Same
pET22b-Unc-F-hSGLT1-Spacer	Same	Same
pET22b-Unc-F-ΔN12-377 hSGLT1	Same	Same
pET22b-hSGLT1-FLAG-Spacer	R, C41, C43 and C43R	Same
pBAD24-hSGLT1-FLAG-Spacer	R, C41, C43 and C43R	Same
pBAD24-ΔN12-377 hSGLT1-FLAG-Spacer	R, C41, C43 and C43R	Same

R, Rosetta; C41, C41 (DE3); C43, C43 (DE3); C43R, C43 (DE3) Rosetta. Conditions for expression are described in Material and Methods.

However in all Western blot probed by anti- His tag antibody a specific band around 72 kDa (expected molecular weight region of hSGLT1) appears but this band is also present in control as well as in uninduced samples.

The rationale for preparing the various plasmids is briefly summarised in the following paragraph. First we constructed full-length hSGLT1 clone in pET22b vector (pET22b-hSGLT1 series), in which the sequence encoding His tag was just after C-terminal of hSGLT1 gene but in this case we could not see any expression of hSGLT1. Thus we were thinking about highly charged His tag might interfere with the proper insertion of newly synthesized protein into the membrane, which would result in degradation of protein. In order to test this possibility we constructed a second series of clones in pET22b vector (pET22b-hSGLT1-spacer series), in which we added a 10 amino acids long spacer between hSGLT1 gene and the His tag, but also in this case protein expression results were negative.

Because bacterial cotransporter posses significantly shorter N-terminal hydrophilic extensions than those in eukaryotes (Turk and Wright, 1997), we deleted the first seven helices (pET22b- Δ N12-377hSGLT1 series) but also in vain. Taking into consideration a possible advantage associated with co-expression of outer membrane protein Unc-F with our gene of interest, we constructed a new series of expression plasmid in pET22b vector (pET22b-Unc-F-hSGLT1). Results of hSGLT1 expression in this type of clones were also negative.

4.1.4. β -subunit of *E.coli* ATPase expression in pET22b-Unc-F and pET22b-Unc-F-hSGLT1 plasmids

We tested pET22b-Unc-F and pET22b-Unc-F-hSGLT1 plasmids for the expression of β -subunit of *E. coli* ATPase in C43 and C43Rosetta strains (Unc-F is toxic for other strains of *E. coli*). In this case we could not detect expression of hSGLT1 but SDS-PAGE analysis of uninduced and induced samples from pET22b-Unc-F and pET22b-Unc-F-hSGLT1 indicates quite interesting and unique band pattern (Figure 4.3). pET22b-Unc-F clone indicates very good expression of the β -subunit of *E. coli* ATPase around 20 kDa in the induced sample (*lane 3*) while as expected there was no protein band detected in the uninduced sample (*lane 2*) at this molecular weight. To our surprise this protein band was completely absent in case of pET22b-Unc-F-hSGLT1 clone, uninduced (*lane 4*) and induced (*lane 5*). The most interesting thing with these results is that we constructed a polycistronic gene in which protein translation is independent from each other but in one case we are getting expression of β -subunit of *E. coli* ATPase but when we fused the Unc-F gene with hSGLT1 gene the expression of β -subunit of *E. coli* ATPase was completely abolished. These results lets assume that mRNA of hSGLT1 might be unstable in *E. coli* and that therefore when expressed simultaneously also the mRNA of the Unc-F gene is destroyed.

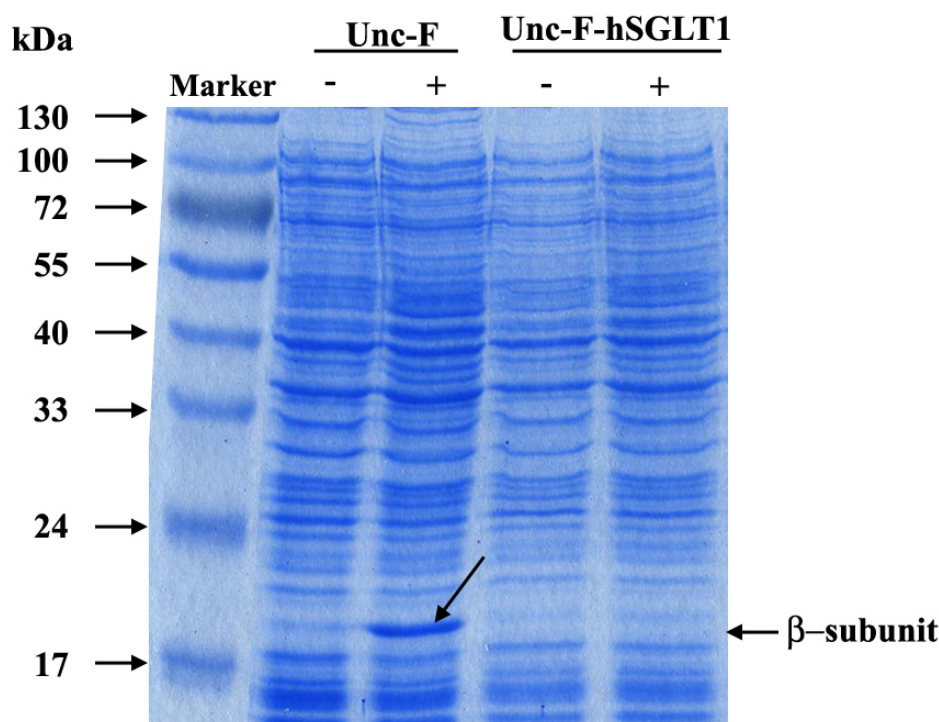


Figure 4.3 Coomassie- stained SDS-PAGE gel for the expression of β - subunit of *E. coli* ATPase in pET22b-Unc-F and pET22b-Unc-F-hSGLT1 plasmids. M, marker protein; PU0, pET22b-Unc-F uninduced; PU1, pET22b-Unc-F induced by 0.5 mM IPTG after 4 h of induction (position of arrow is indicating expression of β - subunit of *E. coli* ATPase around 20 kDa); SU0, pET22b-Unc-F-hSGLT1 uninduced; SU1, pET22b-Unc-F-hSGLT1 induce by 0.5 mM IPTG after 4 h of induction.

4.1.5. Messenger RNA stability of hSGLT1 in *E. coli*

In order to further shed light on mRNA stability of hSGLT1 and its possible implication in heterologous expression of hSGLT1 in *E. coli*, we performed computational analysis of hSGLT1 mRNA by RNAdraw V1.1B program, which predicts secondary structure and minimum energy (Figure 4.4). Calculated secondary structure of hSGLT1 mRNA shows energy of -541.99 kCal at 37°C with 323 CG pairs, 225 AU pairs and 96 GU pairs. Computational analysis revealed that hSGLT1 mRNA sequence contains 5 potential RNase E sites at nucleotide sequence 576, 600, 1488, 1500, and 1558 (Table 4.2). RNase E is an endoribonuclease, which degrades mRNA from 5'- to 3' direction (Mackie, 1998). RNase E is known to cleave mRNA substrates in single stranded regions that are preceded or followed by a stable stem-loop structure (Carpousis et al., 1994; Lin-Chao and Cohen, 1991; Melefors and von Gabain, 1988). Moreover, the stem-loop structures adjacent to the cleavages site do not affect the specificity of cleavages but can influence the rate of cleavage indirectly (McDowall et al., 1995).

While originally suggested that an RNase E cleavages site encompasses a 10 nucleotide region (ACAGA/UAUUUG) (Tomcsanyi and Apirion, 1985), subsequent analysis of many more sites indicate that RNase E prefers single-stranded regions that are typically, but not always A-U rich (Coburn and Mackie, 1999). Additionally, it is known that RNase E is a 5'-

end-dependent endoribonuclease (Mackie, 1998) that prefer substrates with monophosphorylated 5' ends to triphosphorylated termini (Lin-Chao and Cohen, 1991). The predicted RNase E sites in the mRNA of hSGLT1 are thus at positions 1488, 1500, and 1558 (see Table 4.2) and the discussion section.

Table 4.2 Predicted RNase E sites in the mRNA of hSGLT1

Cleavage site	Nucleotide sequence	Stem-loop structure adjacent to cleavage site
576	ACAAUUACAG	Absent
600	GUGAUUUACA	Absent
1488	GGGAUUUCAC	Present
1500	UAUGAUUACU	Present
1558	GAUUAUCUGU	Present

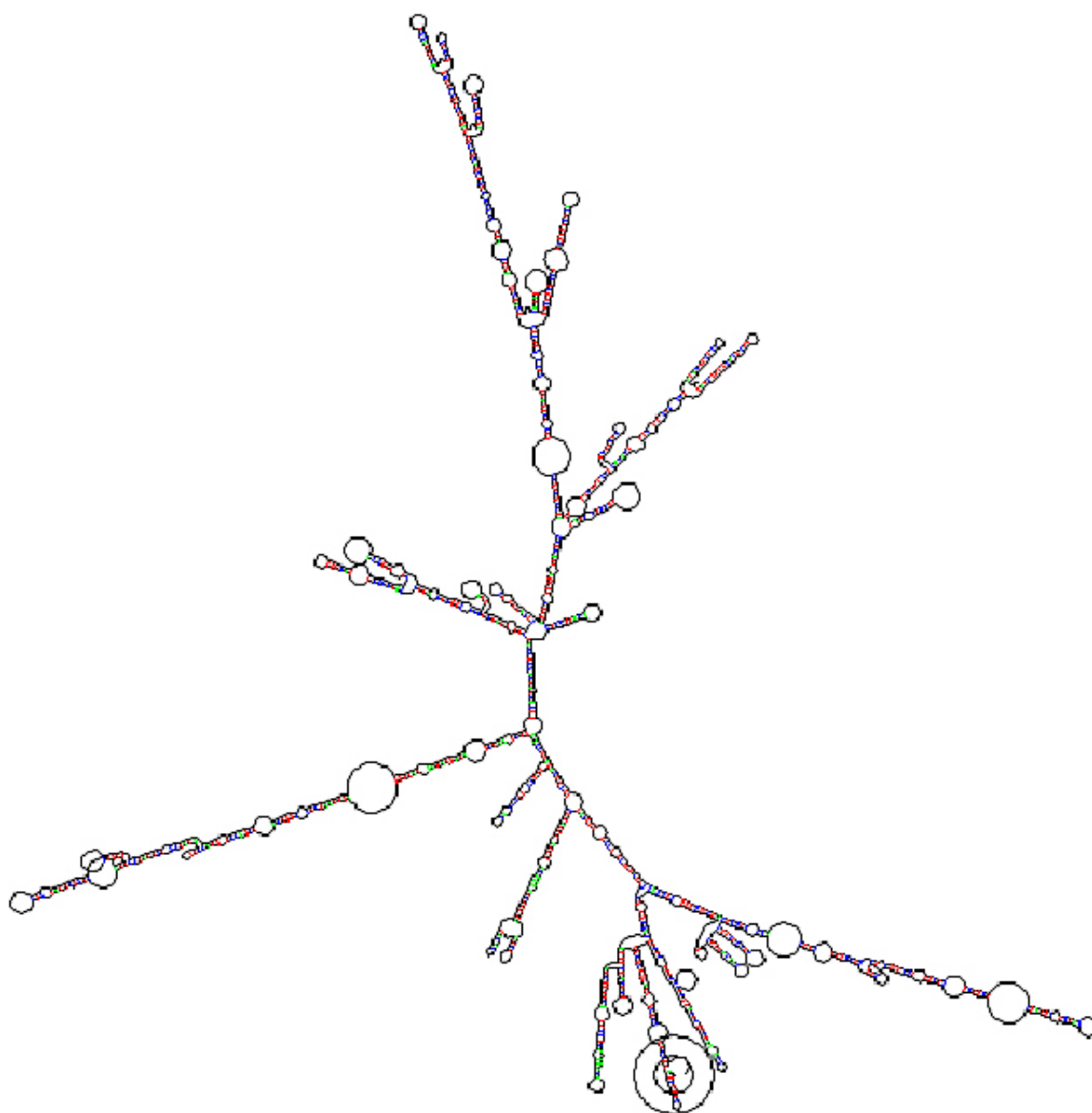


Figure 4.4 Secondary structure of hSGLT1 mRNA as calculated by RNAdraw V1.1B program.

4.2. *Pichia pastoris* as an expression host

4.2.1. Construction of expression plasmid pPICZB-hSGLT1

hSGLT1 gene was PCR amplified using an EST clone (DKFZp686N20230Q2) as a template. The cDNA coding for the human sodium/glucose cotransporter hSGLT1 was cloned into the plasmid pPICZB that uses the *AOX* promoter, which is able to drive over-expression of the hSGLT1 gene in *P. pastoris*. hSGLT1 was cloned into pPICZB vector under '*AOX*' promoter. *Eco*R1 and *Not*I restriction sites were introduced upstream and downstream of the hSGLT1 gene by PCR and the *Eco*R1 and *Not*I containing gene fragment was cloned into the respective sites of the pPICZB vector (Figure 4.5). To facilitate immunological detection and protein purification, the FLAG epitope and 6His tag were attached to the C-terminus of the hSGLT1. In order to resolve the potential effect of 6 His tag on the proper targeting of hSGLT1 in the membrane we placed a 10 amino acids long spacer (VLYKSGGSPG) between the His tag and the hSGLT1 gene sequence. In the resulting expression vector pPICZB-hSGLT1 the hSGLT1 gene was under the transcriptional control of the *AOX1* promoter, which is inducible by methanol (Figure 4.5). For further propagation and growth this plasmid was transformed into TOP10F⁻ *E. coli* strain and five colonies were grown in 10 ml low salt LB with 100 µg/ml Zeocin and 10 µg/ml Tetracycline for 12 h at 37°C for plasmid isolation, which was used for the identification of positive clones by *Eco*R1 and *Not*I restriction digestion (Figure 4.6) and by DNA sequencing.



Figure 4.5 hSGLT1 expression construct. cDNA sequence encoding full-length hSGLT1 cloned into pPICZB vector in *Eco*R1 and *Not*I restriction sites in the multiple cloning site (MCS), for the expression of hSGLT1.

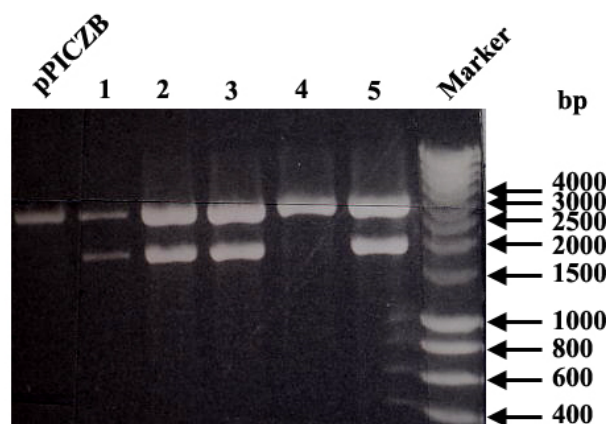


Figure 4.6 *Eco*R1 and *Not*I restriction digestion for the identification of positive colony of pPICZB-hSGLT1 clone. Lane pPICZB E/N, pPICZB vector digested by *Eco*R1 and *Not*I restriction enzymes; Lane1-5, colonies of pPICZB-hSGLT1 clone digested by *Eco*R1 and *Not*I restriction enzymes. Only positive colonies (1, 2, 3, and 5) yield fragments of 2000 bp after *Eco*R1 and *Not*I restriction digestion.

4.2.2. Identification of positive clones of hSGLT1 showing protein expression

Recombinant derivatives of plasmid pPICZB linearized by digestion with *Pme*I typically integrate at the *AOX* locus as a single copy, but multiple copy integration occurs with a frequency of 1 to 10%. Resistance to higher levels of Zeocin correlates with higher copy number for the integrated plasmid, which usually (Romanos et al., 1998) but not always (Clare et al., 1991) correlates with higher levels of expression of the recombinant protein of interest. In our case clones selected on 1000 µg/ml Zeocin concentration give the highest yield of hSGLT1 as judged by Western blot analysis by anti-FLAG antibody (Figure 4.7), so for further expression we used the clone of this plate.

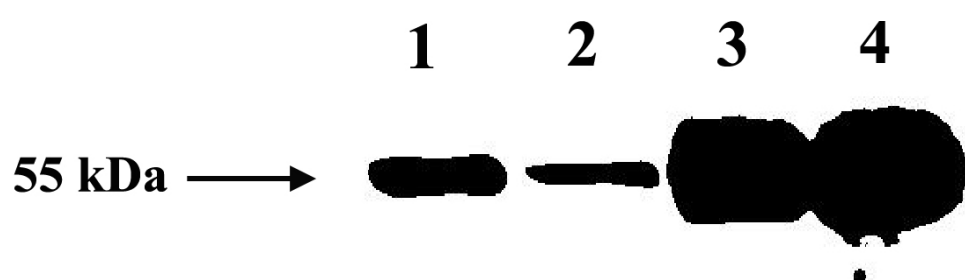


Figure 4.7 Western blot analysis by anti-FLAG antibody for the identification of positive clones for hSGLT1 expression. Clones 1 and 2 were selected from 500 µg/ml Zeocin plate whereas 3 and 4 were selected from 1000 µg/ml Zeocin plate. Clones 1, 2, 3, and 4 show expression of hSGLT1. Clones from 1000 µg/ml Zeocin plate shows highest expression of hSGLT1.

4.2.3. Optimization of feeding and induction in the shake flask cultures

For expression of proteins using the *AOX1* promoter it is important to keep the methanol level within a relatively narrow range. In bioreactors this can be achieved by different control methods (Cereghino and Cregg, 2000). For expression in shake flasks Guarna (Guarna et al., 1997) introduced a technique for on-line monitoring of methanol concentration. This still requires significant technical effort. Our aim was to empirically optimize a feeding protocol for our host strain (GS115, methanol using genotype), which works without any measuring devices and is, therefore, suitable for optimization. So far most expression protocols for shake flask scale are based on the recommendations by Invitrogen Corporation, USA, where 0.5% methanol (v/v) are added to start induction and the rest addition of 0.5% (v/v) methanol occurs after 24 h.

To determine the optimum course of methanol feeding we varied the amount of methanol added to the culture. We decided to add methanol twice a day instead of 24 h to minimize concentration shifts in the medium. The medium used was BMMY. Our results shows that after 24 h of induction a methanol feed of 1% twice a day led to a 2 times higher protein expression than a methanol feed of 0.5% (v/v) twice a day as judged by Western blot by anti-

FLAG antibody (Figure 4.8). So far induction with 1% (v/v) methanol and feeding with 1% (v/v) methanol twice a day gave optimal results in our expression system.

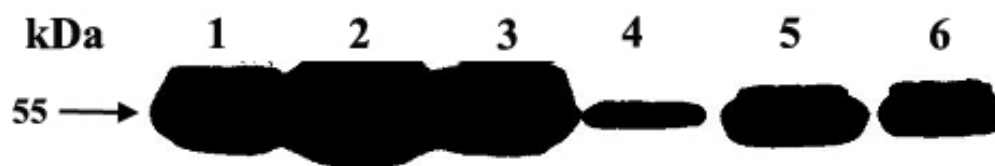


Figure 4.8 Western blot analysis by anti-FLAG antibody for the optimization of feeding and induction in shake flasks. Clones from 1000 $\mu\text{g/ml}$ Zeocin plate were grown in the same condition but induced in different conditions. 1, 2, 3 induced and feed with 1% methanol twice in 24 h. 4, 5, 6 same clones (1, 2, 3) induced and feed with 0.5% methanol once in 24 h.

4.2.4. Purification of hSGLT1 from *Pichia pastoris*

The clone with the highest protein yield was grown in BMGY medium supplemented by 100 $\mu\text{g/ml}$ Zeocin for 30-36 h at 28°C for O.D₆₀₀ of 2-4/ml and then transferred to methanol containing medium (BMMY with 100 $\mu\text{g/ml}$ Zeocin) to induce protein expression for 24 h. After expression, cells were disrupted in breaking buffer containing protease inhibitor cocktail with vigorous vortexing with acid washed chilled 0.5 mm glass beads. The cell pellet obtained by high-speed ultra centrifugation was washed with 4 M urea to remove peripheral membrane proteins. The stripped membranes were solublized in 1.2% FosCholine-12 in TG buffer at 4°C overnight and the solublized material was removed by high-speed centrifugation. The clear supernatant was applied to a preequilibrated Protino Ni-resin column for the purification of hSGLT1 by using buffer TG with 250 mM imidazole. The obtained protein was more than 95% pure as judged from Coomassie stained SDS gels (Figure 4.9A). Western blot analysis of different steps of hSGLT1 purification by anti-FLAG antibody (Figure 4.9B, lane I, L1, P1, and S4) reveal some proteolytic degradation of the recombinant transporter (protein bands around 30 kDa range), even though all purification steps were carried out at 0-4°C. These degradation products were completely absent in purified hSGLT1 (Figure 4.9B, lane hSGLT1).

Purified hSGLT1 migrates on SDS-PAGE at an apparent mass of 55 kDa (Figure 4.9A, lane hSGLT1), which corresponds to that of the nonglycosylated transporter (Firmges et al., 2001; Panayotova-Heiermann et al., 1997; Quick and Wright, 2002) and is recognized by anti-FLAG antibody (Figure 4.9B) and by anti-hSGLT1 and anti-His tag antibodies. The 1-liter culture of *P. pastoris* gives 3 mg of purified protein.

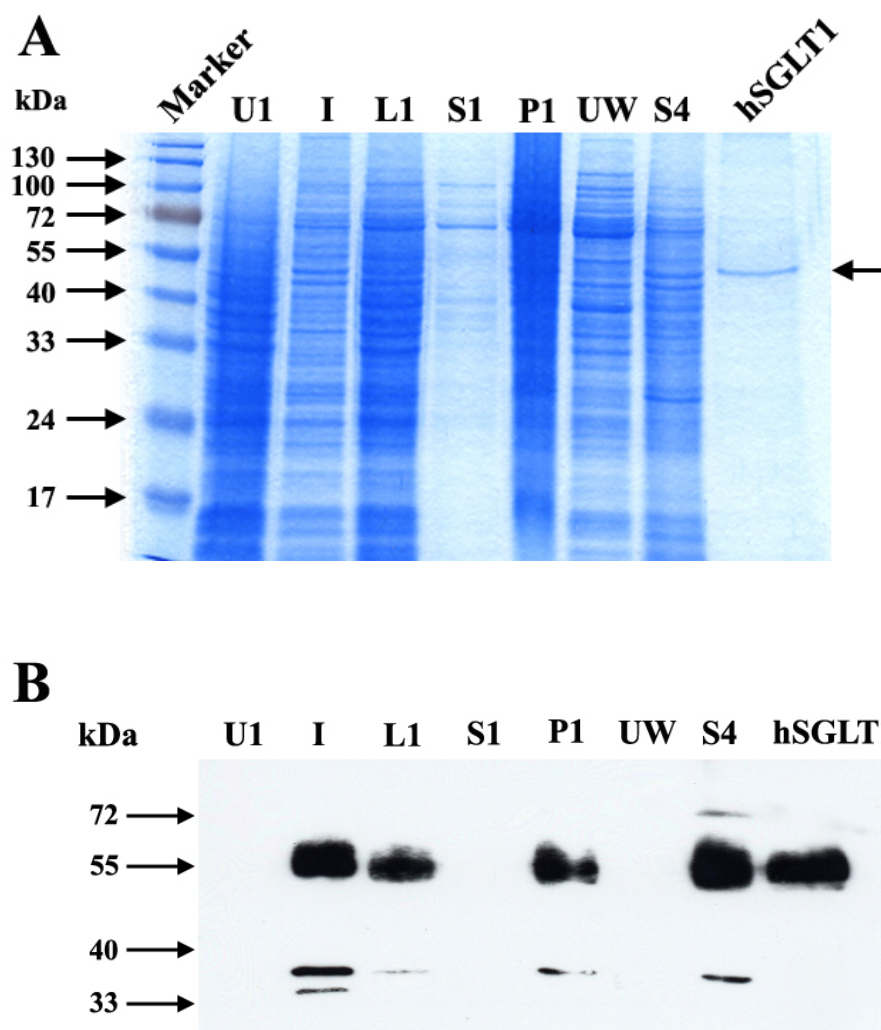


Figure 4.9 Coomassie- stained SDS-PAGE gel and immunoblot of it with anti-FLAG antibody during different stages of hSGLT1 purification. (A) M, protein marker; U1, uninduced sample; I, induced sample after induction of 1% methanol; L, whole cell lysate after lysis of *Pichia pastoris* cells expressing hSGLT1; S1, supernatant; P1, pellet after high-speed centrifugation; UW, washing obtained after 4 M urea wash to pellet P1; S4, supernatant obtained after solubilization of urea wash pellet in 1.2% FosCholine-12; and hSGLT1, Protino column purified hSGLT1 which shows an apparent molecular mass of 55 kDa (marked by arrow). (B) Western blot of above mentioned SDS-PAGE gel with anti-FLAG antibody.

4.2.5. Functional analysis of recombinant hSGLT1 in right-side-out membrane vesicles

Functionality of hSGLT1 was confirmed by determining sugar uptake (50 μ M α -MDG) by right-side-out vesicles of *P. pastoris* GS115 producing hSGLT1, shown in Figure 4.10, when stimulated by sodium a rate of 273 ± 11 nmol \times mg of membrane protein⁻¹ \times min⁻¹ is observed. The uptake is almost completely blocked by phlorizin (29 ± 4 nmol \times mg of membrane protein⁻¹ \times min⁻¹). For the control vesicles, there was no significant difference in sugar uptake in the presence or absence of Na⁺ (33 ± 3 nmol \times mg of membrane protein⁻¹ \times min⁻¹), transport was also not affected by the addition of phlorizin.

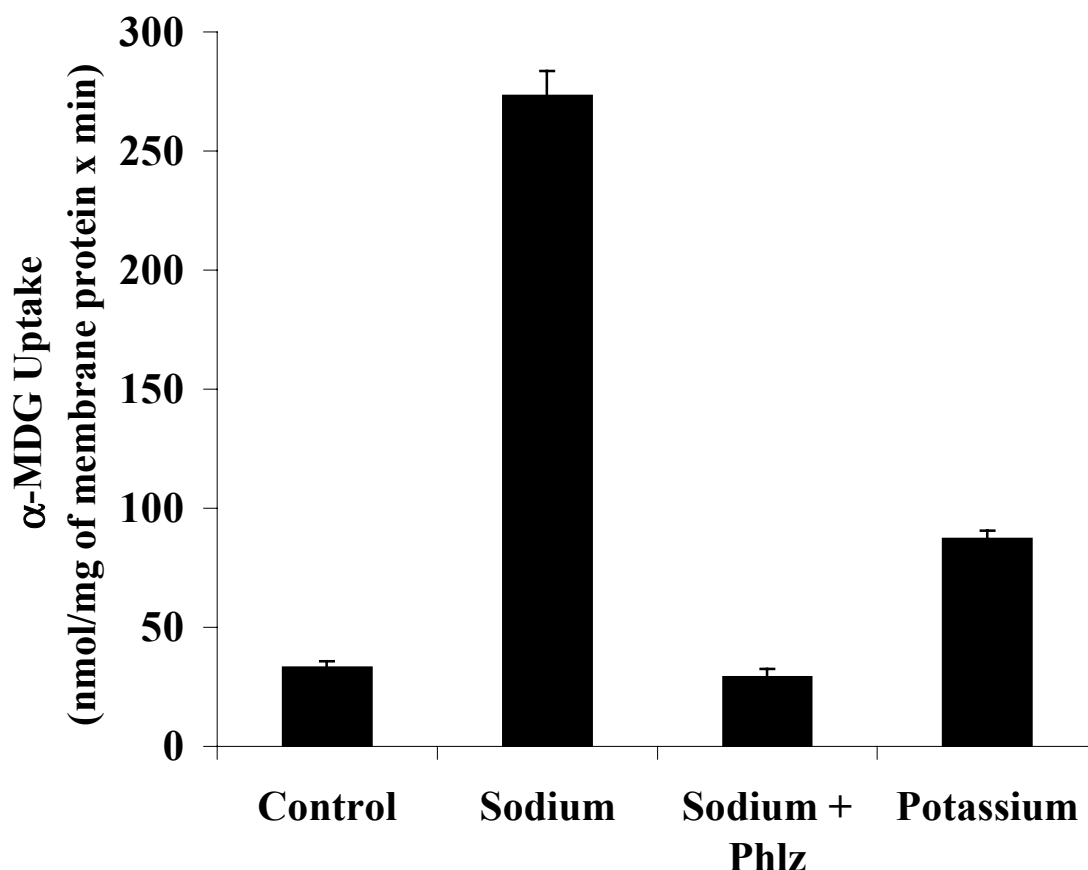


Figure 4.10 Sugar uptake by right-side-out vesicles of *P. pastoris* expressing hSGLT1. 50 μ M α -MDG uptake by right-side-out vesicles of *P. pastoris* GS115 producing hSGLT1 is stimulated by sodium (Na^+ , 100 mM) and inhibited by phlorizin (Phlz, 10 μ M). No sodium-dependent, phlorizin-sensitive uptakes were observed with vesicles of GS115 harboring plasmid pPICZB as a control. For the control vesicles, there was no significant difference in sugar uptake in the presence or absence of Na^+ (33 ± 3 nmol \times mg of membrane protein $^{-1}$ \times min $^{-1}$), transport was also not affected by the addition of phlorizin.

4.2.6. Functional analysis of recombinant hSGLT1 in prteoliposomes

For reconstitution of purified hSGLT1, performed liposomes made of 90% (w/v) asolectin soy lecithin and 10% (w/v) cholesterol were titrated with Triton X-100 and solubilization was followed by turbidity measurements. The detergent concentration was adjusted to the onset or total solubilization of lipid. After mixing of the detergent-destabilized liposomes with the purified transporter, detergent was removed by addition of Bio-Beads SM-2 in three steps, first two steps at room temperature and third step at 4°C overnight.

The time course of 10 μ M α -MDG uptake into the proteoliposomes in the presence and absence 100 mM Na^+ , and in the presence of 100 μ M phlorizin is shown in Figure 4.11. In the presence of 100 mM Na^+ , sugar transport peaked within 30 min at 313 ± 13 nmol α -MDG per mg of recombinant hSGLT1 before falling to the concentration equilibrium of about 60 nmol α -MDG per mg of recombinant hSGLT1 in more than 5 h time. The time course of α -MDG uptake in proteoliposomes demonstrated a classical overshoot (Kinne, 1976; Lucke et al., 1978) in the presence of Na^+ , indicating that sugar was concentrated within the

proteoliposomes and that uptake was energised by the Na^+ electrochemical gradient via secondary active cotransport. The overshoot is absent if there is no sodium gradient across the membrane. These findings indicate a coupling of sodium flux to glucose flux.

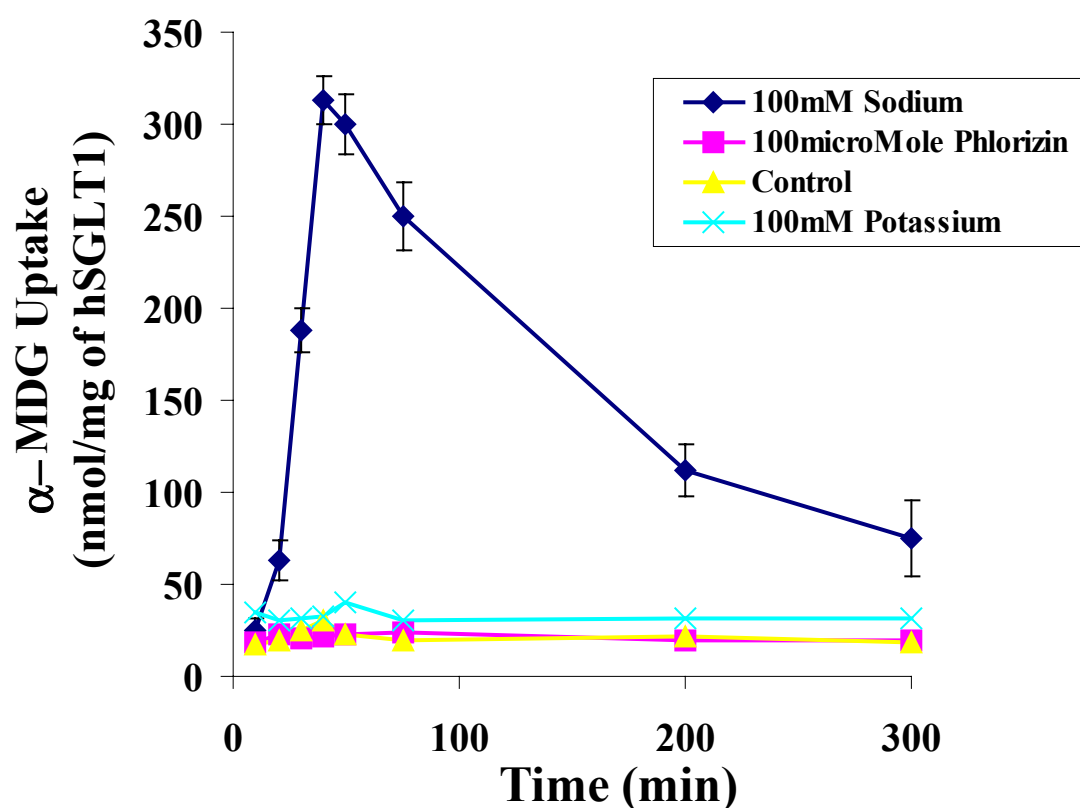


Figure 4.11 Time course of sugar uptake into proteoliposomes containing purified recombinant hSGLT1. The time course of $10 \mu\text{M}$ α -MDG in the presence of 100 mM sodium (\blacklozenge) shows a 35 fold of increase in the initial rate of sugar uptake before reaching concentration equilibrium in 5 h. After addition of $100 \mu\text{M}$ phlorizin (\blacksquare) or removal of Na^+ (\times), the initial rate was identical to control liposomes (\blacktriangle) and sugar accumulation above the equilibrium was not observed.

In order to further check the functionality of purified recombinant hSGLT1, we performed sugar uptake in the proteoliposomes composed of hSGLT1 asolectin soy lecithin and cholesterol. Proteoliposomes take-up $1874 \pm 65 \text{ nmol} \times \text{mg}^{-1} \text{hSGLT1} \times \text{min}^{-1}$ (Figure 4.12) as compared to $125 \pm 24 \text{ nmol} \times \text{mg}^{-1} \text{hSGLT1} \times \text{min}^{-1}$ by liposomes alone. Sodium-dependent α -MDG uptake was completely blocked by $10 \mu\text{M}$ phlorizin (Figure 4.12).

Phlorizin is a potent high-affinity competitive inhibitor of sugar transport by SGLT1 in native tissue, brush border membrane vesicles, *Xenopus* oocytes, and reconstituted in proteoliposomes (Diedrich, 1966; Diez-Sampedro et al., 2001; Ikeda et al., 1989; Quick and Wright, 2002; Schultz and Curran, 1970) with a half-maximum inhibition constant ($K_i^{\text{Phlorizin}}$) in the micromolar range. In our study, $10 \mu\text{M}$ phlorizin inhibited the initial rate of α -MDG transport in membrane vesicles by 89% (Figure 4.10), whereas the same concentration of phlorizin in proteoliposomes inhibits uptake by 86% (Figure 4.12).

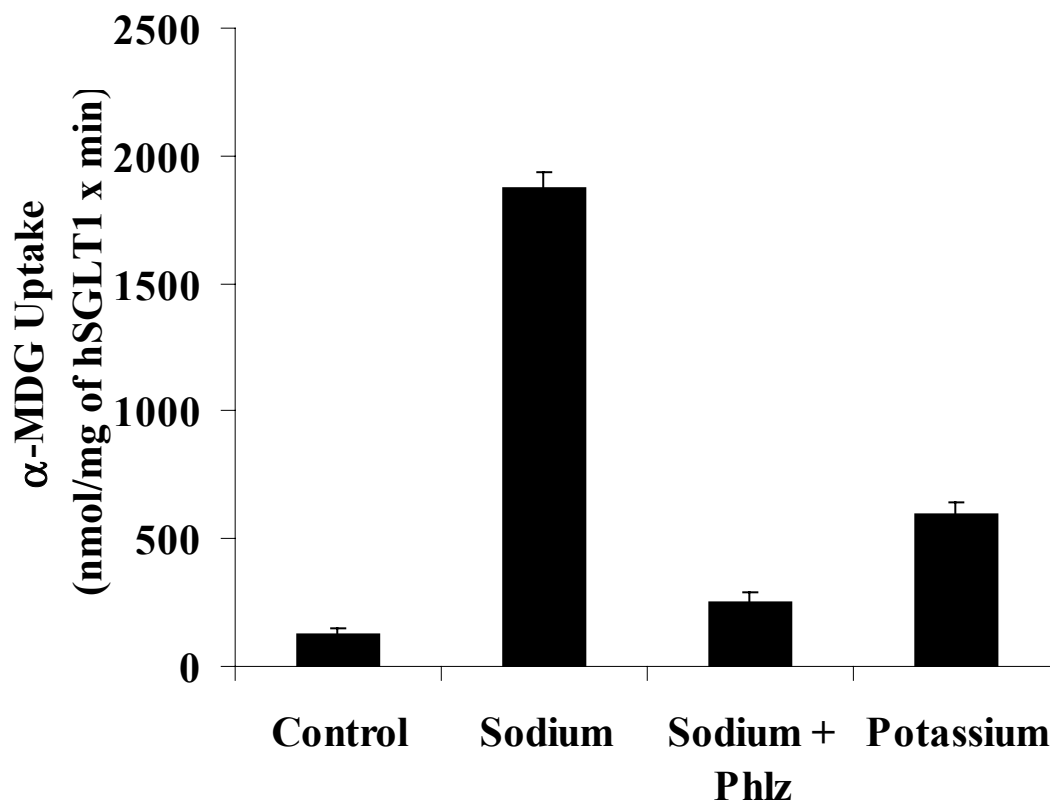


Figure 4.12 Sugar uptake kinetics of proteoliposomes containing purified recombinant hSGLT1. 50 μ M α -MDG uptake by proteoliposomes made of purified hSGLT1 transport 1874 ± 65 nmol \times mg of hSGLT1⁻¹ \times min⁻¹ in a sodium-dependent manner (when 100 mM Na⁺ was replaced by 100 mM K⁺ transport slows down to 598 ± 3 nmol \times mg of hSGLT1⁻¹ \times min⁻¹) and 10 μ M phlorizin inhibited sugar transport upto 251 ± 39 nmol \times mg of hSGLT1⁻¹ \times min⁻¹), whereas liposomes (control) transported only 125 ± 24 nmol \times mg of hSGLT1⁻¹ \times min⁻¹.

The sugar selectivity of recombinant hSGLT1 in proteoliposomes was measured by determining the uptake of 100 μ M α -MDG in the presence of 10 mM D-Glucose (D-Glc), D-Galactose (D-Gal), 2-Deoxy-D-Glucose (2Doglc), Mannose (Man), Allose (All), L- Glucose (L-Glc), and 100 μ M phlorizin (Phlz) in the presence of 100 mM Na⁺. High-affinity substrates of hSGLT1 D-Glc and D-Gal inhibited Na⁺-dependent α -MDG by 70% and 72%, while low affinity substrates 2Doglc, Man, All, and L-Glc inhibited sugar uptake 44%, 18%, 15%, and 2% respectively and in the presence of 100 μ M phlorizin the Na⁺-dependent sugar uptake was reduced to 84% of original value (Figure 4.13, Table 4.3). hSGLT1 in proteoliposomes exhibits substrate specificity in the following order, Phlz \gg α -MDG \approx D-Glc \approx D-Gal \gg 2Doglc $>$ Man $>$ All $>$ L-Glc.

Recombinant reconstituted hSGLT1 shows stereospecificity as it preferred D-Glu over L-Glu, D-Glu inhibited 75% α -MDG uptake L-Glu, inhibited only 2%. Furthermore, the sugar selectivity of the reconstituted recombinant hSGLT1 appears to be similar to that reported for transporter in different systems (Diez-Sampedro et al., 2000; Firnges et al., 2001; Kinne, 1976; Quick and Wright, 2002). The equatorial orientation of the OH-group at the positions C-2 and C-3 of the D-glucose seems to be important for its recognition by hSGLT1 since in

the presence of mannose, 2-Deoxy-D-glucose and allose the significant inhibitory effect on α -MDG uptake was observed. The importance of the equatorial OH-group orientation at the C-2 and C-3 was also reported for the renal SGLT1 (Burckhardt and Kinne, 1992). The 78% inhibition of α -MDG uptake in the presence of D-galactose indicates that the orientation of OH-group at C-4 (equatorial in D-glucose and axial in D-galactose) is not that important for the recognition by cotransporter because D-Glu and D-Gal inhibited sugar uptake by transporter upto equal extent (Table 4.3), Phlz inhibited 84% of α -MDG uptake in proteoliposomes.

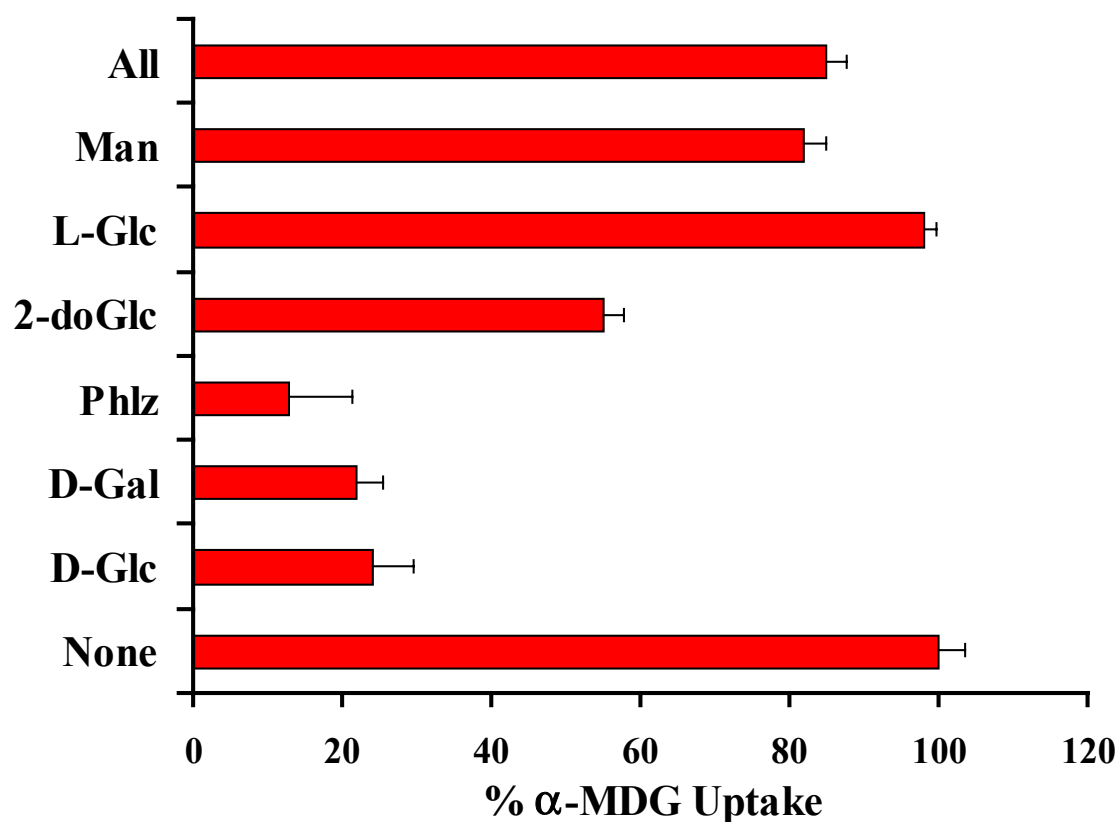


Figure 4.13 Sugar uptake kinetics of proteoliposomes containing purified recombinant hSGLT1. Uptake of 100 μ M α -MDG is inhibited by high-affinity substrates or inhibitors of hSGLT1 (10 mM D-glucose, D-Glc; 10 mM D-galactose, D-Gal; 100 μ M phlorizin, Phlz) but not by low-affinity substrates (e.g., 10 mM 2-deoxy-D-glucose, 2Doglc; 10 mM mannose, Man; 10 mM allose, All; 10 mM L- glucose, L-Glc).

Table 4.3 Effect of various substrates and inhibitors on the uptake of 100 μ M α -MDG as shown in Figure 4.13.

Substrate/ Inhibitor	Concentration used	% of α -MDG uptake inhibition
None	100 μ M	0
D- Glu	10 mM	75
D- Gal	10 mM	78
2- Doglc	10 mM	44
Man	10 mM	18
All	10 mM	15
L- Glu	10 mM	2
Phlz	100 μ M	84

For the determination of sugar uptake kinetics parameters, 1 min α -MDG uptake assays were performed by varying α -MDG concentration from 0.01 to 25 mM. A half-saturation constant (K_m^{sugar}) of 0.4 ± 0.05 mM/L and a maximum velocity (V_{max}) of 3.4 ± 0.34 $\mu\text{mol} \times \text{mg hSGLT1}^{-1} \times \text{min}^{-1}$ was observed (Figure 4.14). The carrier catalytic turnover number (King et al., 1993; Napoli et al., 1995), an index of number of sugar molecules transported per transporter was calculated by dividing the sugar transport V_{max} by the total number of transporter present in the proteoliposomes. Catalytic turnover of hSGLT1 based on the V_{max} of 3.4 $\mu\text{mol} \times \text{mg hSGLT1}^{-1} \times \text{min}^{-1}$ is 6 s^{-1} (Table 4.4), which is in good agreement with that obtained in previous studies (Quick and Wright, 2002) and other Na^+ -dependent transporter [e.g., the Na^+ /glucose transporter of *Vibrio parahaemolyticus* (vSGLT) (Turk et al., 2000), and the Na^+ / proline transporter of *Escherichia coli* (PutP) (Jung et al., 1998)].

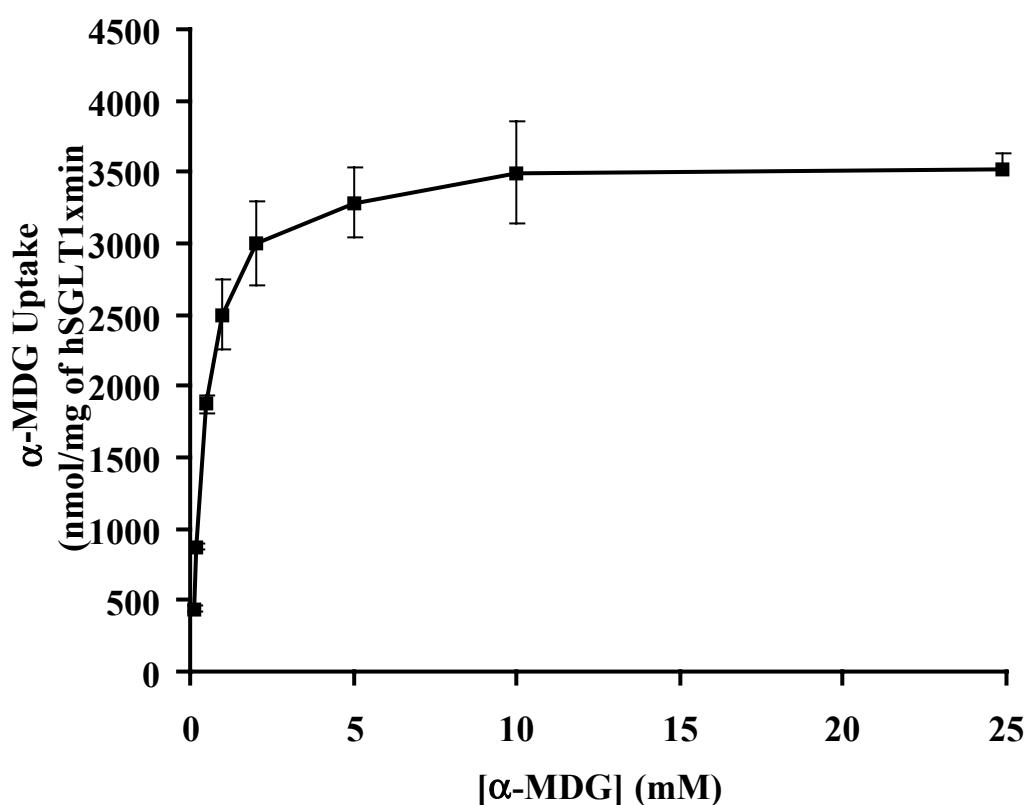


Figure 4.14 Sugar uptake kinetics of proteoliposomes containing purified recombinant hSGLT1. Concentration dependence of the initial-rate sugar uptake shows a half-saturation constant (K_m^{sugar}) of 0.4 ± 0.05 mM/L and maximum velocity (V_{max}) of 3.4 ± 0.34 $\mu\text{mol} \times \text{mg hSGLT1}^{-1} \times \text{min}^{-1}$.

Table 4.4 Kinetics of hSGLT1 in different systems.

Kinetic parameters	Xenopus oocytes*	Proteoliposomes*	Proteoliposomes This study
	hSGLT1	hSGLT1 Δ N-GFP	hSGLT1
K_m^{sugar} , mM/L	0.41 ± 0.03	0.38 ± 0.1	0.4 ± 0.05
Turnover number, s^{-1}	50	4	6

*Reported values in previous studies(Quick and Wright, 2002).

4.3. Synthesis and Characterization of different photoaffinity probes

In order to study the functional domains of SGLT1 photoaffinity labels were synthesized. They were derived from phlorizin a non-transported inhibitor, from arbutin, a transported inhibitor of SGLT1 and a D-glucose based label. The aim of these studies is to obtain information about the important contact points within the transporter at different depth and in various conformations.

In the following section we describe the synthesis, photochemical properties, stability, effects of these probes on SGLT1 mediated glucose uptake in natural membranes and photoaffinity labeling of an isolated recombinant functional domain of SGLT1. In the future above labels will be employed for the photoaffinity labeling of whole recombinant hSGLT1.

4.3.1. Synthesis of labels BzG and 3-AP for the identification of phlorizin interaction sites

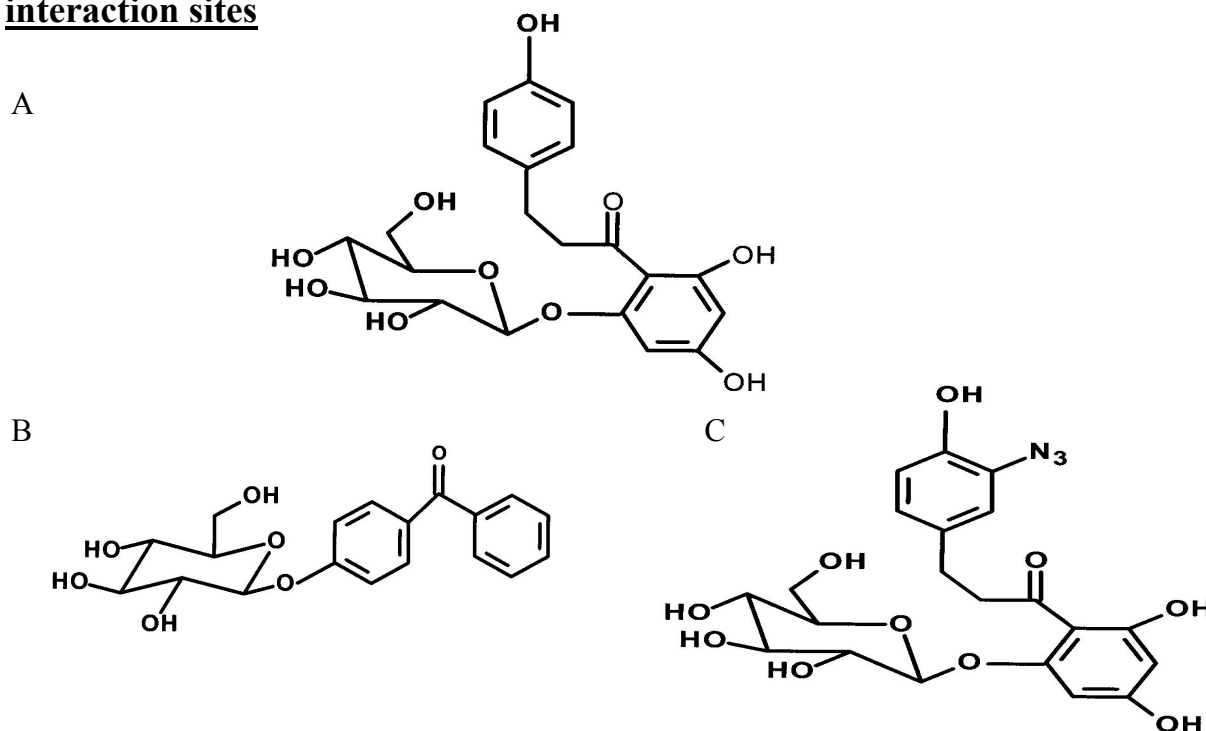


Figure 4.15 Chemical structure of photoaffinity probes and their sibling. (A) Phlorizin highest-affinity inhibitor of sugar uptake by SGLT1, (B) [(4'-Benzoyl) phenoxy]-D- glucopyranoside (BzG), (C) 3-Azidophlorizin (3-AP).

BzG and 3-AP were synthesized to identify phlorizin interactions sites in the cotransporter. The scheme for BzG synthesis (compound 12) is given in Figure 3.3. Compound 11 was obtained by the reaction of α -D-acetobromoglucose 4 with 4-hydroxybenzophenone 10 in the presence of mercuric cyanide, which was further deacetylated to give final compound 12 in 98% yield.

The synthesis scheme for 3-AP (compound 16) was shown in Figure 3.4. 3-Nitrophlorizin (compound 14) was obtained by simple nitration of phlorizin, which was subsequently

reduced to 3-aminophlorizin (compound 15). The transformation of 3-aminophlorizin into 3-azidophlorizin by reacting it in the cold with dilute hydrochloric acid and sodium nitrite followed by addition of sodium azide to the diazotated phlorizin represents a classical reaction in organic chemistry. The infrared absorption at 2170 cm^{-1} of the final product is characteristic for the azido group.

4.3.2. Synthesis of label TIPDG for the identification of arbutin interaction sites

In order to get information about arbutin binding sites in cotransporter we have synthesized TIPDG. The reaction scheme for the synthesis of TIPDG 9 is presented in Figure 3.2. The coupling of α -D-acetobromoglucose 4 with 4-hydroxy-3-iodo-trifluoroacetophenone 3 gave the corresponding keto compound 5, in 75% yield. Keto compound 5 on reaction with hydroxylamine hydrochloride gave oxime 6, which was finally converted into aceto TIPDG 8 by the reaction of oxime 6 with triethylamine, DMAP, *P*-toluenesulfonyl chloride, and NH_3 and oxidation of diaziridine 7 with iodine. TIPDG 9 was obtained after deacetylation of compound 8.

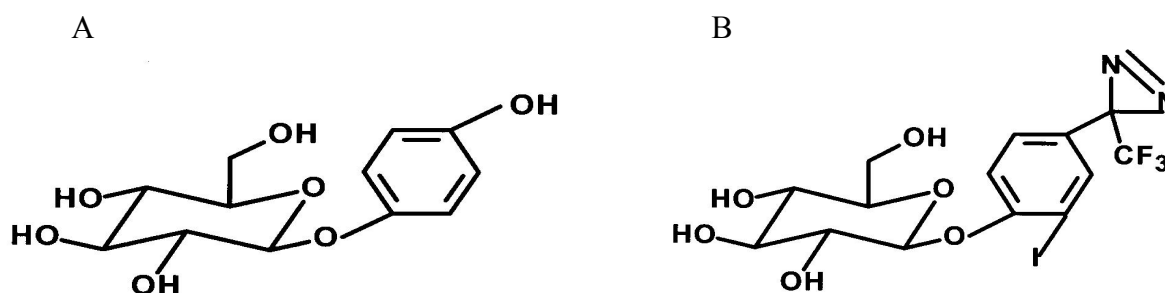


Figure 4.16 Chemical structure of photoaffinity probe and its sibling. (A) Arbutin, a high-affinity sibling of TIPDG transported by SGLT1, (B) [(2'-Iodo-4'-(3''-trifluoromethyldiazirinyloxy) phenoxy)]-D-glucopyranoside (TIPDG).

4.3.3. Synthesis of label 6-AG for the identification of D-glucose interaction sites

D-Glucose is a high-affinity transported substrate of SGLT1, in order to identify its binding sites in cotransporter we have synthesized 6-AG photoprobe. The synthesis of 6-AG (compound 22) is depicted in Figure 3.5. The direct conversion of the debenzylated aldehyde 17 into the diazirine as described (Lehmann and Thieme, 1986) gave only unsatisfactory results. Therefore the aldehyde 17 was converted into the corresponding methyl ketone 19 by reacting with methylmagnesium iodide followed by oxidation of the formed secondary alcohol. The less-reactive keto compound 19 could be easily converted into the diazirine

group with the NH_3 , Hydroxylamine-O-sulfonic acid reagent and subsequent oxidation of the intermediate diaziridine with iodine (Church et al., 1972; Church and Weiss, 1970).

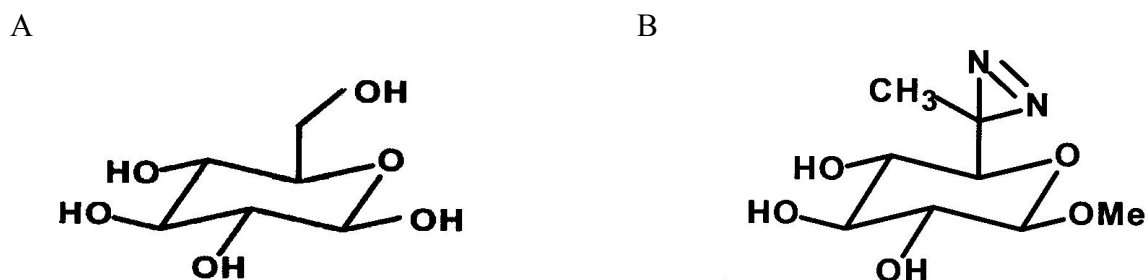


Figure 4.17 Chemical structure of photoaffinity probe and its sibling. (A) D-glucose transported ligand by SGLT1, (B) n-Methyl-6C-(Azimethyl)-D- glucopyranoside (6-AG).

4.3.4. Photochemical properties and stability of TIPDG, BzG, 3-AP and 6-AG

Consistent with the spectral properties of other 3-(trifluoromethyl)-3-phenyldiazirine (Brunner et al., 1980; Delfino et al., 1993; Fang et al., 1998; Hatanaka et al., 1994; Nassal, 1984; Platz et al., 1991), the TIPDG described here shows a characteristic absorption maximum at 358 nm ($\epsilon = 290 \text{ M}^{-1} \cdot \text{cm}^{-1}$). This is depicted in Figure 4.18 for TIPDG 9 photolysis studies. When a 0.5 mM solution of 9 in methanol was irradiated in a Rayonet photochemical reactor RPR-100 fitted with 16, 3500Å lamps at 22°C, the diazirine absorption band at 358 nm decreased with a half-life of 20.1 s following apparent first-order kinetics. Upon photolysis, the solution turned slightly orange (absorbance maximum at around 460 nm), a result of the well documented partial rearrangement of the diazirine to the diazo isomer.

There have been reports on the reduction of photoactivable reagents containing azido groups (Bayley and Knowles, 1978) or 2-diazo-3, 3,3-trifluoropropionyloxy groups (Takagaki et al., 1983) by commonly used reducing agents like dithiothreitol, 2-mercaptoethanol and reduced glutathione. To check the stability of TIPDG in the presence of these reducing agents, a methanolic solution of TIPDG was treated with 2- mercaptoethanol and dithiothreitol at an equimolar concentration or in the presence of a 5-fold excess of these reagents at 25°C. The reaction was followed spectrophotometrically wherein no change was observed up to 1 h. The diazirine moiety of TIPDG is also stable under hydrogenation with 10% Pd on carbon, which leads to a non-iodinated TIPDG derivative.

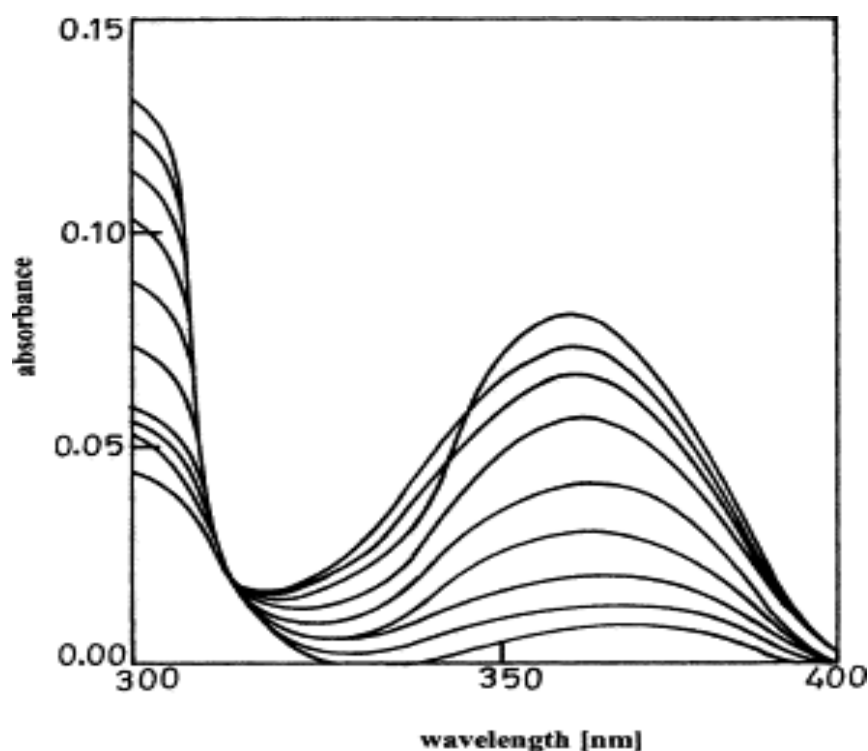


Figure 4.18 UV spectra of the reaction products from photolysis of TIPDG 9. A solution (0.5 mM) in methanol was irradiated for different times (0, 5, 10, 15, 20, 25, 30, 35, 40, and 45 s). The spectra show the decay of the characteristic diazirine absorption with a maximum at 358 nm. The half-life of decomposition was calculated from a logarithmic plot of the absorbance data against the irradiation time. The half-life $t_{1/2}$ was 20.1 s.

BzG shows absorption maximum at 293 nm ($\epsilon = 22500 \text{ M}^{-1} \cdot \text{cm}^{-1}$) and reveals other characteristic features of benzophenone photochemistry (Dorman and Prestwich, 1994; Dorman and Prestwich, 2000). The half-life of photolysis of BzG was determined by irradiating a 0.5 mM solution in isopropanol in an Oriel photochemical reactor fitted with 200 W medium pressure Hg lamp at 25°C. The characteristic absorption band of benzophenone in BzG at 293 nm disappeared with an approximate half-life of 25.4 min following first order reaction kinetics.

3-AP exhibits photochemical properties similar to other aryl azide compounds. The absorption maxima of azide group of 3-AP are at 211 nm ($\epsilon = 28150 \text{ M}^{-1} \cdot \text{cm}^{-1}$), 258 nm ($\epsilon = 6700 \text{ M}^{-1} \cdot \text{cm}^{-1}$), and 288 nm ($\epsilon = 16800 \text{ M}^{-1} \cdot \text{cm}^{-1}$). Half-life of decomposition of this compound was not determined.

The absorption maximum of the diazirine group of 6-AG is at 330 nm ($\epsilon = 45 \text{ M}^{-1} \cdot \text{cm}^{-1}$). On irradiation with long wavelength UV light (λ_{max} around 350 nm) in a Rayonet photochemical reactor, the 6-AG decompose with a half-life of 1.3 min.

4.3.5. Inhibition of glucose uptake in rabbit small intestine BBMVs by BzG and 3-AP

To determine the affinity of BzG towards the SGLT1 cotransporter we measured its inhibitory potential on sodium-dependent D-glucose uptake into rabbit intestinal BBMVs according to the method of Dixon. The effect of BzG on Na^+ -dependent glucose uptake in small intestine

BBMV is shown in Figure 4.19. BzG clearly acts as a fully competitive inhibitor. The apparent K_i value $12 \pm 2 \mu\text{M}$ is only slightly higher than the previously reported K_i value of $8 \pm 1.2 \mu\text{M}$ (Evers et al., 1978; Gibbs et al., 1982) phlorizin.

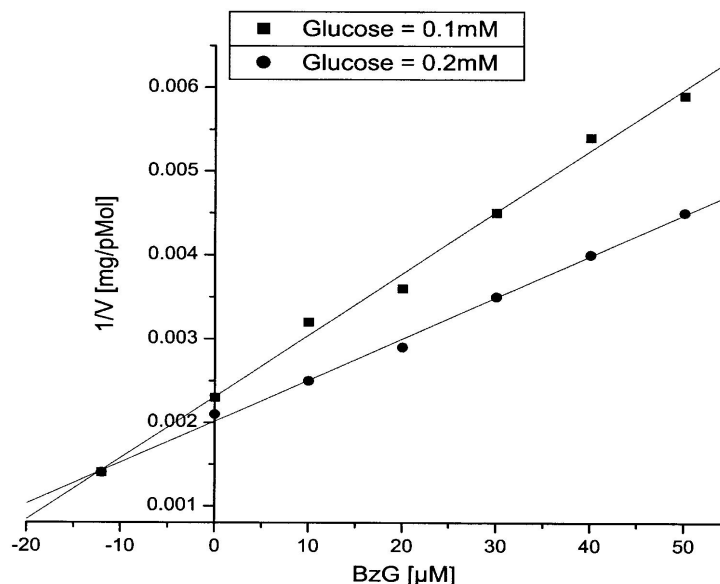


Figure 4.19 Inhibitory effects of 0, 10, 20, 30, 40, and 50 μM BzG on 5 s sodium-dependent D-glucose uptake into rabbit small intestine BBMV measured at two substrate concentrations, 0.1 mM (squares) and 0.2 mM (circles) D-glucose according to the method of Dixon. Representative experiments are shown. An inhibition constant (K_i) of $12 \pm 2 \mu\text{M}$ was calculated from three independent experiments.

The affinity of 3-AP for the SGLT1 cotransporter was measured according to method of Dixon. 3-AP strictly act as a high affinity inhibitor of sugar uptake by Na^+/D -glucose cotransporter with a K_i value of $8.6 \pm 1.6 \mu\text{M}$. The calculated K_i value for 3-AP is exactly similar to its parent compound phlorizin (K_i of $8 \pm 1.2 \mu\text{M}$). 3-AP exhibits all characteristics features similar to phlorizin so we used this compound for the identification of phlorizin-binding sites in truncated loop 13 protein which is predicted to be region involved in inhibitor binding (Novakova et al., 2001; Xia et al., 2003).

4.3.6. Inhibition of glucose uptake in rabbit small intestine BBMV by TIPDG

As shown in Figure 4.20 TIPDG exhibits a fully competitive inhibition with respect to D-glucose with a K_i of $22 \pm 5 \mu\text{M}$, this affinity is almost identical to the one of its parent compound arbutin ($25 \pm 6 \mu\text{M}$). The modification of the phenyl ring OH group into a trifluoromethyl diazirine group and the mono iodination of its phenyl ring thus did not significantly alter the affinity to the transporter.

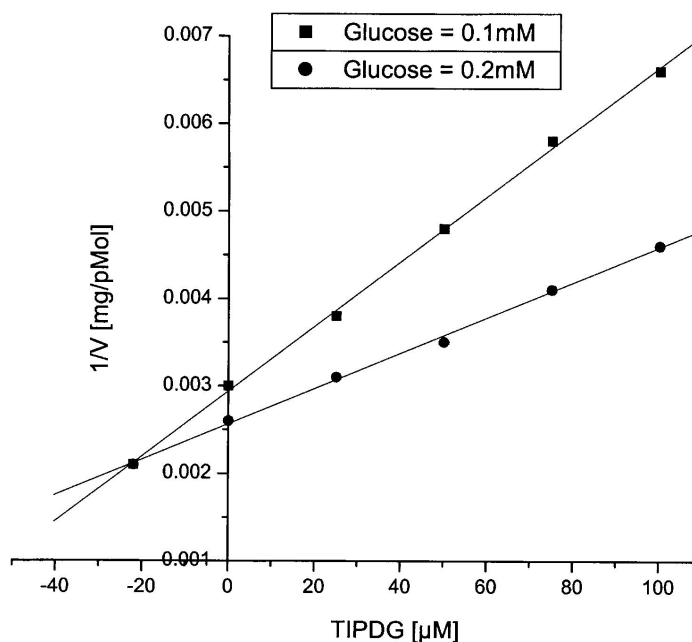


Figure 4.20 Inhibitory effects of 0, 25, 50, 75, and 100 μM TIPDG on 5 s sodium-dependent D-glucose uptake into rabbit small intestine BBMV measured at two substrate concentrations, 0.1 mM (squares) and 0.2 mM (circles) D-glucose according to the method of Dixon. Representative experiments are shown. From three independent experiments a K_i value of $22 \pm 5 \mu\text{M}$ for TIPDG was calculated.

4.3.7. Inhibition of glucose uptake in rabbit small intestine BBMV by 6-AG

The affinity of 6-AG for the SGLT1 cotransporter was also evaluated by measuring its inhibitory potential on sodium-dependent D-glucose uptake into rabbit small intestine BBMV according to method of Dixon. As shown in Figure 4.21, 6-AG exhibits a fully competitive inhibition characteristic with respect to D-glucose with a K_i of $40 \pm 5 \mu\text{M}$. Compared to the inhibitory effect of D-glucose (K_i of 1 mM) the modification of the molecule with the photolabile diazirine group and methyl group at position C-6 of the D-glucose moiety drastically increase the affinity for the transporter. These results indicate that presence of alkyl and diazirine group (hydrophobic interaction) increase the affinity of 6-AG 25 fold as compared to its parent compound.

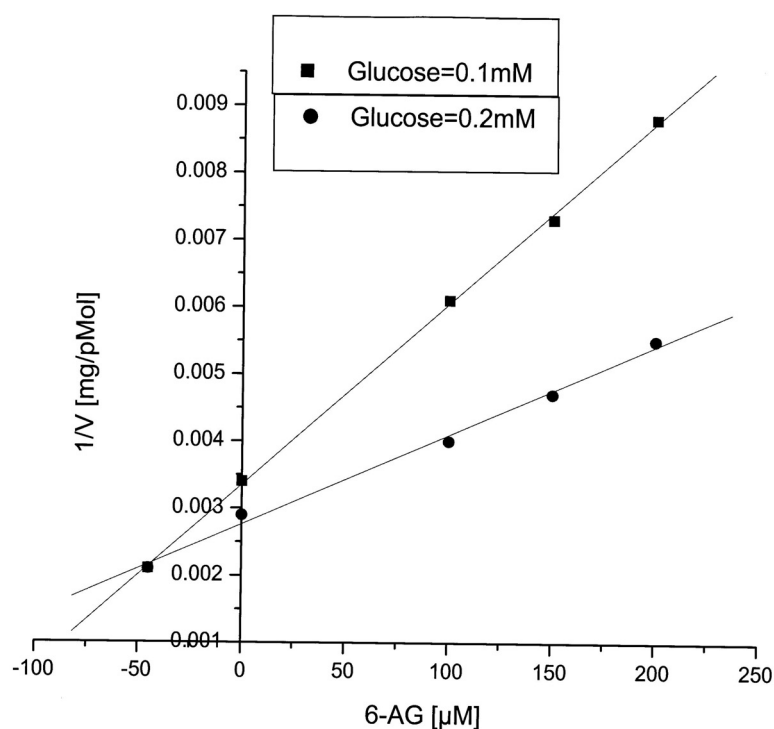


Figure 4.21 Inhibitory effect of 0, 100, 150, and 200 μM 6-AG on 5-s D-glucose uptake into rabbit small intestine BBMV measured at two substrate concentrations, 0.1 mM (squares) and 0.2 mM (circles) D-glucose according to the method of Dixon. Representative experiments are shown. From three independent experiments K_i value of $40 \pm 5 \mu\text{M}$ for 6-AG was calculated.

Table 4.5 Photochemical and biochemical properties of different photoaffinity probes.

Photoaffinity probe	Sibling	λ_{max} nm ($\epsilon = \text{M}^{-1} \cdot \text{cm}^{-1}$)	Half-life of photolysis ($t_{1/2}$)	Inhibition constant (K_i) photoaffinity probe	Inhibition constant (K_i) of sibling
TIPDG	Arbutin ^S	358(290) ^a	20.1 s	$22 \pm 5 \mu\text{M}$	$25 \pm 6 \mu\text{M}$
BzG	Phlorizin ^I	293(22500) ^b	25.4 min	$12 \pm 2 \mu\text{M}$	$8 \pm 1.2 \mu\text{M}$
3-AP	Phlorizin	211(28150) ^c 258(6700) ^c 288(16800) ^c	ND ^d	$8.6 \pm 1.6 \mu\text{M}$	$8 \pm 1.2 \mu\text{M}$
6-AG	D-Glucose ^S	330 (45) ^a	1.3 min	$40 \pm 5 \mu\text{M}$	1 mM

^S Substrate

^I Inhibitor

^a Methanol

^b Isopropanol

^c Ethanol

^d not determined

4.4. Photoaffinity labeling of truncated loop 13 with TIPDG, BzG, and 3-AP

According to studies employing site-directed mutagenesis (Novakova et al., 2001) and molecular recognition atomic force microscopy (Wielert-Badt et al., 2002), the extra-membranous loop 13 of SGLT1 appears to be involved in substrate and inhibitor recognition of SGLT1 (Panayotova-Heiermann et al., 1997; Panayotova-Heiermann et al., 1996; Xia et al., 2003). We therefore used this functional domain of SGLT1 (a model system loop 13 in its truncated form that has amino acids sequence 564-638 of SGLT1) for the identification of substrates and inhibitor sites.

4.4.1. Photoaffinity labeling of truncated loop 13 with TIPDG and BzG

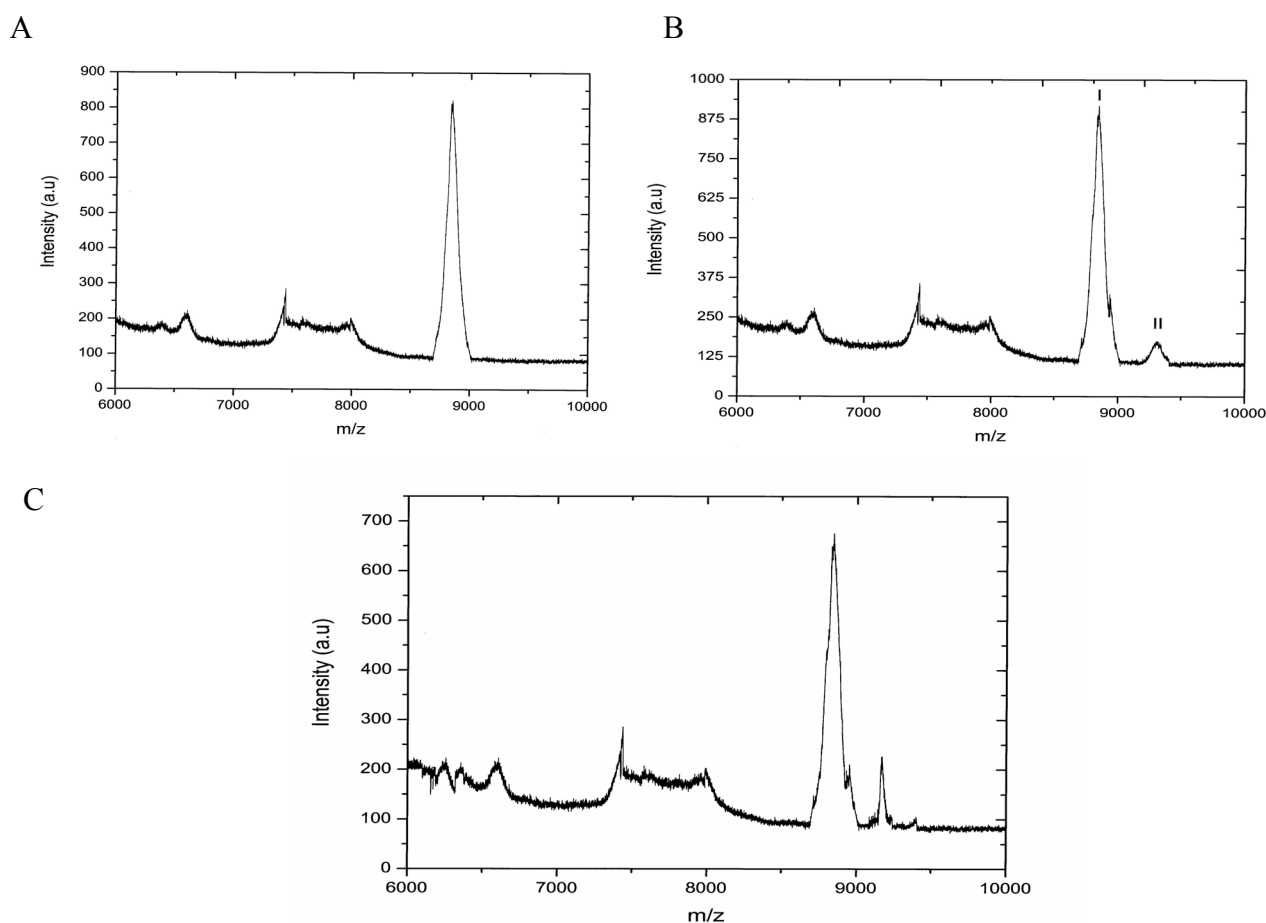


Figure 4.22 MALDI-mass spectrometry of photoaffinity labeled truncated loop 13. (A) Truncated loop 13 before labeling, (B) Photoaffinity labeling with TIPDG and (C) Photoaffinity labeling with BzG. Truncated loop 13 protein (200 μ g) was incubated with 1 mM TIPDG or with 0.5 mM BzG in 200 μ l of PBS buffer for 5 min in the dark at room temperature followed by irradiation at 350 nm for 5 min (TIPDG) and 30 min (BzG). After separation from noncovalently bound TIPDG or BzG by chloroform/methanol extraction, protein was dissolved in SA matrix at a concentration of 50 pmol/ μ l and subjected to MALDI- mass spectrometry, (A) peak I, truncated loop 13 protein; (B) peak I, truncated loop 13 protein; peak II, truncated loop 13 protein cross-linked with TIPDG; (C) peak I, truncated loop 13 protein; peak II, truncated loop 13 protein labeled with BzG.

Photoincorporation of TIPDG into truncated loop 13 proteins was complete within 1 min of light exposure under our condition. Figure 4.22A shows the expected mass peak at m/z 8825.6. Figure 4.22B demonstrates that after photoaffinity labeling with TIPDG two peaks of m/z 8825.6 and 9287.5 can be observed. Peak I corresponds to truncated loop 13 protein and peak II to the photolabeled truncated loop 13 protein (9287.5). The mass difference between peak I and peak II (Figure 4.22B) corresponds to the mass of photolysed TIPDG (461.9).

MALDI-mass spectra of photolabeled loop 13 proteins with BzG are shown in Figure 4.22C. Two intense ion signals at m/z 8825.6 and at m/z 9187.2 are observed. The ion signal at m/z 9187.2 was absent in the MALDI-mass spectrum of control truncated loop 13 protein Figure 4.22A. The mass increment of 361.6 amu suggests a simple carbon bond insertion of the photoaffinity label BzG into the protein (Figure 4.22C, *peak II*).

4.4.2. Photoaffinity labeling of truncated loop 13 with 3- Azidophlorizin

The reaction product of photolabeling of the truncated loop 13 with 3-azidophlorizin was also analysed by MALDI-mass spectrometry. Figure 4.23A shows the expected mass peak for loop 13 at m/z 8825.60 and in Figure 4.23B the product after photoaffinity labeling of the loop with 3-azidophlorizin is depicted. Peak I corresponds to truncated loop 13 (8825.60) and peak II to the photolabeled truncated loop 13 protein (9275.10). The mass difference between peak I and peak II (Figure 4.23B) corresponds to the mass of photolysed 3-azidophlorizin (449.5).

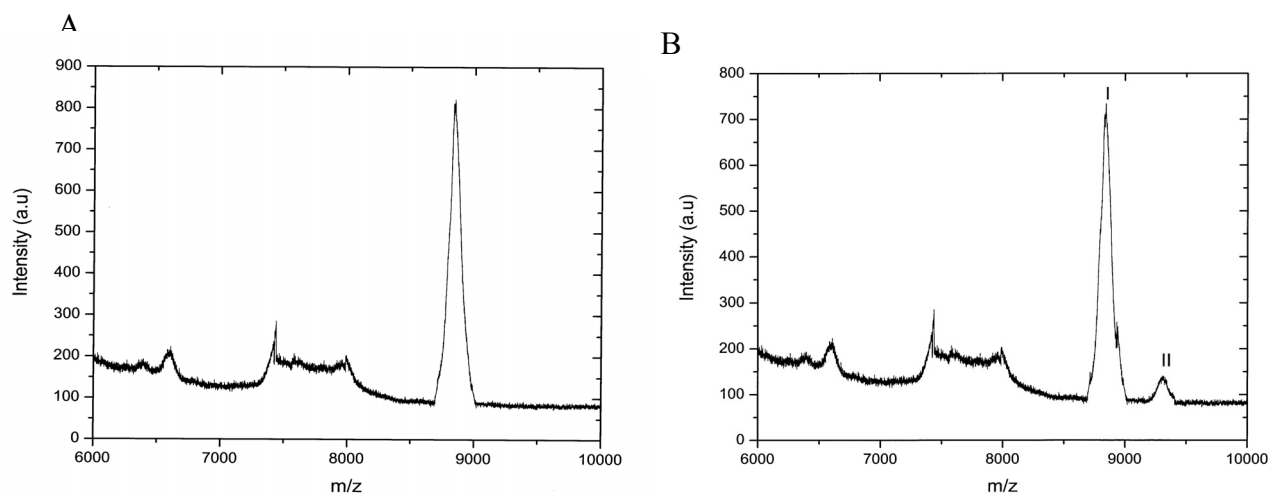
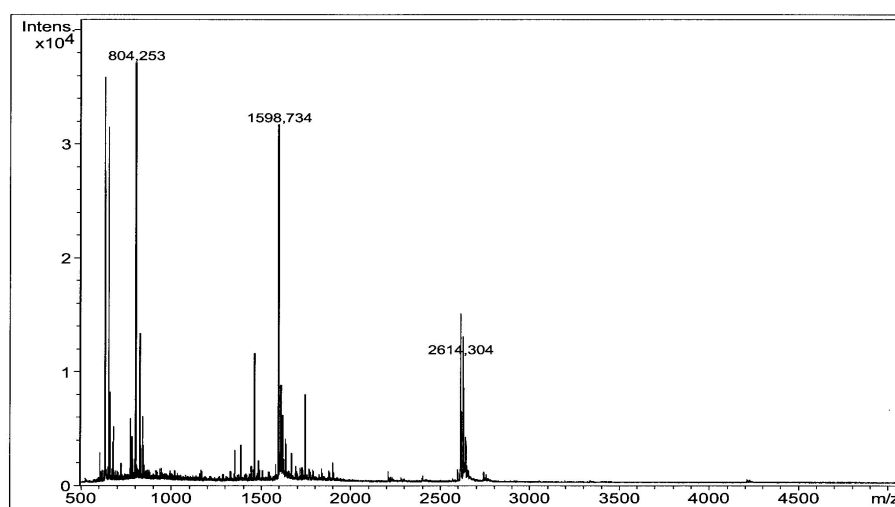


Figure 4.23 MALDI-mass spectrometry of photoaffinity labeled truncated loop 13. Protein (200 μ g) was incubated with 1 mM 3-azidophlorizin in 200 μ l of PBS buffer for 5 min in the dark at room temperature followed by irradiation at 280 nm for 10 min. After separation from noncovalently bound 3-azidophlorizin by chloroform/ methanol extraction, protein was dissolved in DHB matrix at a concentration of 50 pmol/ μ l and subjected to MALDI-mass spectrometry, (A) Control experiment; peak I, truncated loop 13, (B) Products after photolabeling; peak I, truncated loop 13; peak II, truncated loop 13 cross-linked with 3-azidophlorizin.

4.4.3. Identification of the ligand contact points

As a next step in identification of the ligand contact points, the photolabeled-truncated loop 13 was digested in gel with trypsin. After extraction of the peptides from the gel, the resulting mixture was analyzed by MALDI-TOF mode with unlabeled-truncated loop 13 as a reference (Table 4.6). The only additional peak observed in the labeled probe was at m/z 624.52 (Figure 4.24B). This can be explained as an adduct peak to m/z 175.11 (corresponding to Arg-602) with a difference of 449.41. The latter is equal to the mass of photolysed 3-azidophlorizin. All other peaks appear also in the control as shown in Figure 4.24A.

A



B

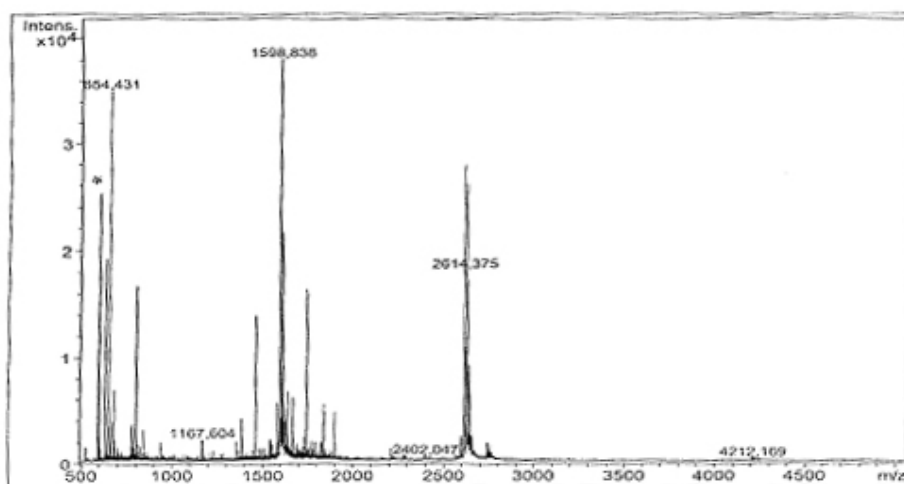


Figure 4.24 MALDI-mass spectrum of in-gel trypsin cleaved truncated loop 13. 200 μ g of truncated loop 13 was photolabeled with 3-azidophlorizin, proteins were separated on SDS-PAGE and protein bands of interest were excised, destained and digested in gel with trypsin. The peptides were extracted from the gel pieces with acetonitrile. Subsequently 0.5 μ l aliquots of the generated cleavage products were dispensed onto the sample support, followed by 0.5 μ l of CHCA matrix solution and the MALDI-mass spectra were recorded. (A) Truncated loop 13 before photoaffinity labeling, (B) truncated loop 13 after photoaffinity labeling with 3-azidophlorizin. (*) peak indicates the mass shift due to modification of Arg-602 with 3-azidophlorizin.

Table 4.6 Theoretical and measured masses of photolabeled truncated loop 13 digested with trypsin as shown in Figure 4.24.

Fragment	Amino acids	Sequence	Theoretical mass (M+H) ⁺ monoisotopic	Measured mass (M+H) ⁺	Additional peaks
1	1-3	PER	401.21	ND ^a	
2	4-6	NSK	348.18	ND	
3	7-9	EER	433.20	ND	
4	10-33	IDL DAGEEDIQEAPEEATDTEVPK	2614.18	2614.37	
5	34	K	147.11	147.27	
6	35	K	147.11	147.27	
7	36	K	147.11	147.27	
8	37-40	GFFR	526.27	526.11	
9	41	R (602)	175.11	175.35	624.52 ^b
10	42-53	AYDLFCGLDQDK	1387.61	1387.63	
11	54-56	GPK	301.18	ND	
12	57-59	MTK	379.20	380.85	
13	60-66	EEEEAMK	807.35	807.26	
14	67-68	LK	260.19	ND	
15	69-77	LTD TSEHPL	1012.49	ND	

^a not determined.

^b Denominates a peptide plus label

We also performed photoaffinity labeling of truncated loop 13 with 1 mM 3-AP in the presence of 15 μ M phlorizin under the same conditions that were employed in the other photolabeling experiments. MALDI- mass spectrum of photolabeled truncated loop 13 did not show any additional peak in intact truncated loop 13 and also no additional peak was present in the Trypsin digested samples.

In order to further strengthen our results that labeling of residue Arg (602) is specific and it is not an artifact, we chemically modified the guanidino moiety of arginine with phenylglyoxal treatment. Photoaffinity labeling of arginine-modified protein with 3-AP did not resulting any additional peak in the MALDI- mass spectrum of trypsin digested photolabeled protein.

Taking these evidences into consideration we can claim that the ortho position of ring B of phlorizin labeled amino acid Arg-602 of truncated loop 13, which thus forms part of a phlorizin-binding site.

5. Discussion

Integral membrane proteins such as channels and transporters are essential for all living organisms as they mediate the passage of ions and molecules across the membrane. The understanding of how membrane proteins work in health and disease has been restricted hitherto largely due to lack of purified protein. Most membrane proteins are present in very low concentrations in their native tissue, and their over-expression is a prerequisite for purification. The use of eukaryotic expression system has illuminated mechanistic features of human membrane proteins, but these are unsuitable for their large-scale purification (Fleming, 2000; Tate, 2001). In addition, genetic disorders of membrane proteins are frequently caused by improper trafficking in cells, and it is not known whether missorted proteins retain their catalytic activity.

The first crystal structures of membrane proteins were obtained with proteins isolated from naturally abundant sources, and recombinant proteins still represent minority of the membrane proteins that have been crystallized to date. In the case of soluble proteins, over 90% have been crystallized using recombinant protein, which is in contrast to the 21 recombinant of 50 total structures for membrane proteins (Loll, 2003). Only three mammalian membrane proteins to date have had crystal structures determined using recombinant protein: prostaglandin H₂ synthase-2 (COX-2), produced in insect cells (Barnett et al., 1994; Kurumbail et al., 1996), monoamine-oxidase B, produced in yeast (Binda et al., 2002) and fatty acid amide hydrolase, produced in bacteria (Bracey et al., 2002). All three proteins are monotopic membrane proteins and therefore have little hydrophobic surface. It should also be noted that the only GPCR crystallized to date, bovine rhodopsin, was obtained from natural source, from bovine retina where it is found in large amounts. These statistics reflect the fact that active recombinant membrane proteins are difficult to obtain.

It is not surprising that heterologous production of membrane proteins poses big challenges. Unlike their cytoplasmic counterparts, membrane proteins have a longer way to the fully functional form. Once their synthesis begins, the complicated secretory machinery is engaged in order to achieve proper targeting and insertion into the membrane. The majority of proteins synthesized in many cells are cytoplasmic proteins; such cells have no sufficient capacity to handle large amounts of newly synthesized membrane proteins. Therefore, when produced in a heterologous system, membrane proteins can “saturate” the secretory pathway of cell, leading to protein aggregation inside different cell compartments.

Therefore, the choice of expression system is a crucial step towards obtaining large amounts of transporter in its active form. Devising a successful strategy for its subsequent purification is nonetheless important. For the expression of hSGLT1, various animal heterologous expression systems have been widely used but major disadvantages associated with these systems are that modified protein are frequently not trafficked properly to plasma membrane

(Lam et al., 1999; Lostao et al., 1995; Martin et al., 1997; Martin et al., 1996) and that it is costly to produce sufficient amounts of protein for structural studies. Recently functional expression of hSGLT1 Δ N-GFP was reported in *E. coli* (Quick and Wright, 2002), but hSGLT1 expression in *E. coli* was not reproducible in our lab as reported in the results section.

5.1. *E. coli* as an expression host

Among the many systems available for heterologous protein production, the Gram-negative bacterium *E. coli* remains one of the most attractive because of its ability to grow rapidly and at high density on inexpensive substrates, its well-characterized genetics and the availability of an increasingly large number of cloning vectors and mutant host strains. Taking advantages of *E. coli* expression system into consideration, first we attempted expression of hSGLT1 in this system. For the expression of hSGLT1, we used two types of vectors, pET22b (T7 promoter based) and pBAD24 (P_{BAD} promoter), both having some advantages and disadvantages. We constructed different clones of hSGLT1 in pET22b and pBAD24 and tested hSGLT1 expression in different *E. coli* strains and at different conditions (Table 4.1) but we were not able to express hSGLT1 in *E. coli*.

5.1.1. Probable reasons for not getting hSGLT1 expression in *E. coli*

There are some probable reasons for not getting expression of hSGLT1 in *E. coli*.

5.1.1.1. Codon usage

E. coli and indeed all cells, use a specific subset of the 61 available amino acid codons for the production of most mRNA (Zhang et al., 1991). So-called major codons are those, which occur, in highly expressed genes, whereas the minor or rare codons tend to be in genes expressed at low level. The hSGLT1 gene was directly amplified from human genome and cloned into different expression vectors in *E. coli*, therefore, the codons of this gene are not optimized for *E. coli* expression host. Codon degeneracy analysis shows that the hSGLT1 gene contains 23% codons, which cannot be translated efficiently, due to the low frequency of the corresponding tRNAs in *E. coli*. Therefore, a special host strain Rosetta (DE3) was used for the expression of hSGLT1 in prokaryote. Rosetta host strains are BL21 derivatives, designed to enhance the expression of eukaryotic proteins that contain codons rarely used in *E. coli*. These strains supply tRNA genes for AGG (Arg), AGA (Arg), AUA (Val), CUA (Leu), CCC (Pro), GGA (Gly) on a Col-E1 compatible chloroamphenicol-resistant plasmid. Thus, the Rosetta strains provide for “universal” translation, which is otherwise limited by the codon usage of *E. coli*. Transcription of the tRNAs genes is driven by their native promoters. The use of this strain did not solve the problem of expression. Thus, codon usage does not

appear to be a hurdle for the expression of hSGLT1. This signifies the importance of some other factors, which are responsible for the expression of human membrane proteins in *E. coli*.

5.1.1.2. Signal sequences

Signal sequences or signal peptides are a well-characterized but heterogeneous group of cleavable N-terminal peptide extensions that direct the newly synthesized proteins to specific subcellular compartments. In *E. coli* ~20 aa signal peptides direct secretion of proteins to the periplasma and outer membrane (Arkowitz and Bassilana, 1994; Driessen, 1994; Driessen et al., 2001). In eukaryotes, signal peptides are more variable in length and direct secretion to the endoplasmic reticulum lumen and the general secretory pathway (Sakaguchi, 1997). There are however, distinctions between the prokaryotic and eukaryotic systems; most notable are differences in the amino acid sequences of the signal peptide itself (Nielsen et al., 1997). In addition there are differences in the process of secretion: i.e., the function of the signal recognition particle (SRP), a more highly evolved secretion apparatus, and the use of different chaperones (Pohlschroder et al., 1997). If *E. coli* signal sequences were not working for hSGLT1 protein we should get hSGLT1 expression either in the form of aggregated protein in inclusion bodies, or in degraded forms, but our results indicate that this was not the case since we could not detect any sign of protein expression in the *E. coli* expression system. We also attempted expression of hSGLT1 at different conditions by changing the protein inducer and temperature from 37 to 16°C to change folding and degradation, but in all cases no expression was observed. Therefore in our experiments it seems that some phenomena other than those mentioned above could be the real cause for not getting expression of hSGLT1 in *E. coli*.

5.1.1.3. Degradation of hSGLT1 mRNA in *E. coli*

As already shown by the results obtained by SDS-PAGE analysis of β - subunit of *E. coli* ATPase expression in pET22b-Unc-F and pET22b-Unc-F-hSGLT1 plasmids (Figure 4.3), the expression of this protein was completely abolished when simultaneous expression of both the β -subunit and hSGLT1 was attempted. Subsequent computational analysis of the mRNA sequence of hSGLT1 revealed that it contains 5 potential RNase E sites at position 576, 600, 1488, 1500, and 1558 (Table 4.2). The position 576 (ACAAUUACAG) and 600 (GUGAUUUACA) contains the preferred nucleotide sequence (Figure 5.1) for degradation by RNase E but they are lacking a stem-loop structure adjacent to the cleavage site. RNase E prefers AU rich nucleotide sequences with adjacent secondary structure (stem-loop) for degradation. So these two sites may not be all that prone for RNase E degradation. The three predicted RNase E sites at position 1488 (GGGAUUUCAC), 1500 (UAUGAUUACU), and 1558 (GAUUAUCUGU) (Table 4.2) contain extended stem loop structures adjacent to these sites (Figure 5.2), so these sites are highly susceptible for degradation by RNase E. Once the RNase E degradation process is initiated in *E. coli*, it activates other exonucleases which

further degrade mRNA of the Unc-F gene. Thus the lack of hSGLT1 expression may be due to the instability of the mRNA.

The role of cyclic nucleotide regulation of Na⁺/glucose cotransporter (SGLT1) mRNA stability for the expression in LLC-PK1 cells was reported in the literature (Lee et al., 2000), same observations for the effect of mRNA stability on glucose transporter (GLUT1) gene expression were also mentioned in previous studies in mammalian cell lines (Qi and Pekala, 1999).

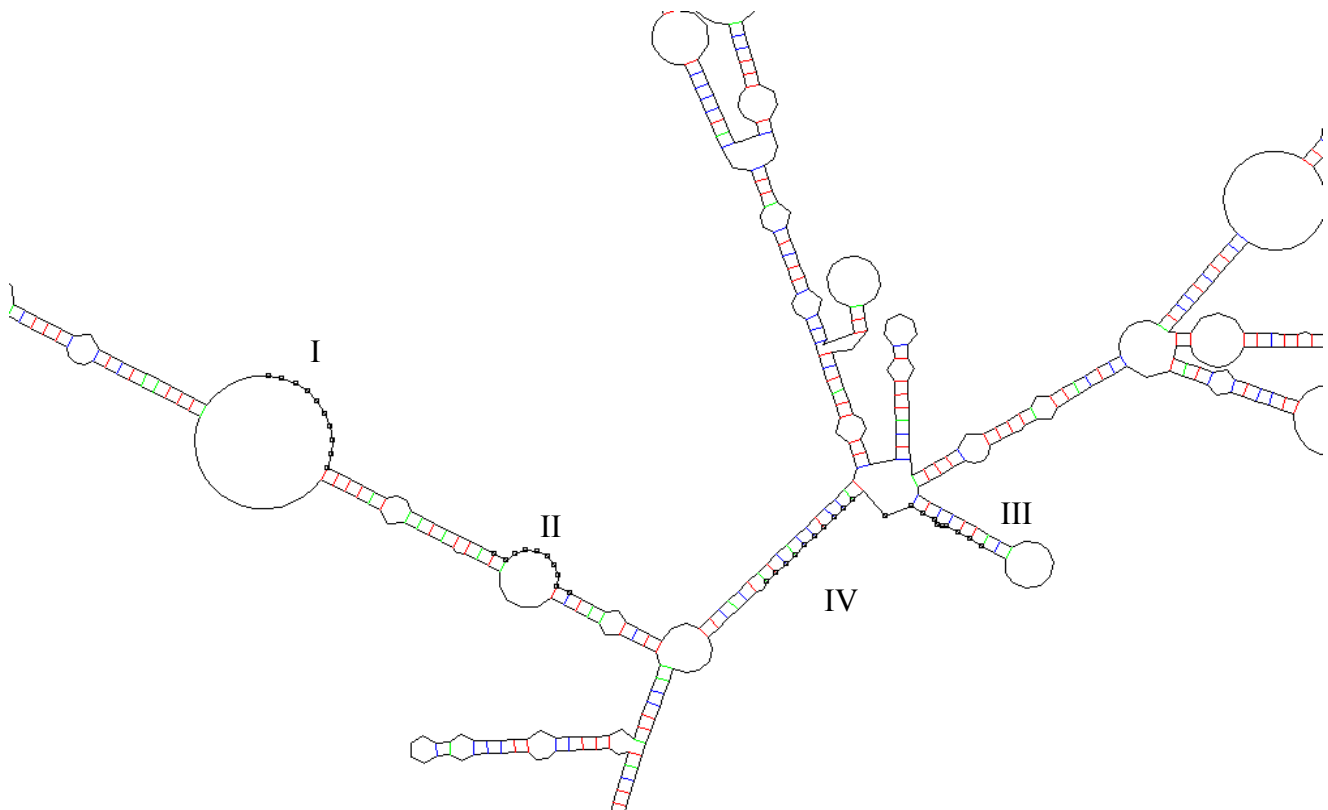


Figure 5.1 Part of hSGLT1 mRNA secondary structure indicating the positions of RNase E sites. Nucleotide sequences in this structure marked as 576, I (ACAAUUACAG); 600, II (GUGAUUUACA); 1488, III (GGGAUUUCAC); and 1500, IV (GAUUAUCUGU) indicates the positions of RNase E susceptible site in the mRNA of hSGLT1.

To our knowledge, this is the first time that possible implications of mRNA stability of hSGLT1 on its expression into *E. coli* are reported. The reason given by most of membrane protein molecular biologists to explain their unsuccessful attempts is that the membrane protein is synthesized in *E. coli* but due to the absence of specialized membrane protein folding machinery (Molecular Chaperones) and proper membrane targeting machinery in bacteria, expressed protein either accumulates as insoluble aggregates of improperly folded species called inclusion bodies, or proteolytic degradation of newly synthesized protein takes place due to improper targeting of protein. In our opinion, this statement does not hold true in

all conditions and the major culprit of our failure for hSGLT1 expression in *E. coli* is the mRNA stability of hSGLT1.

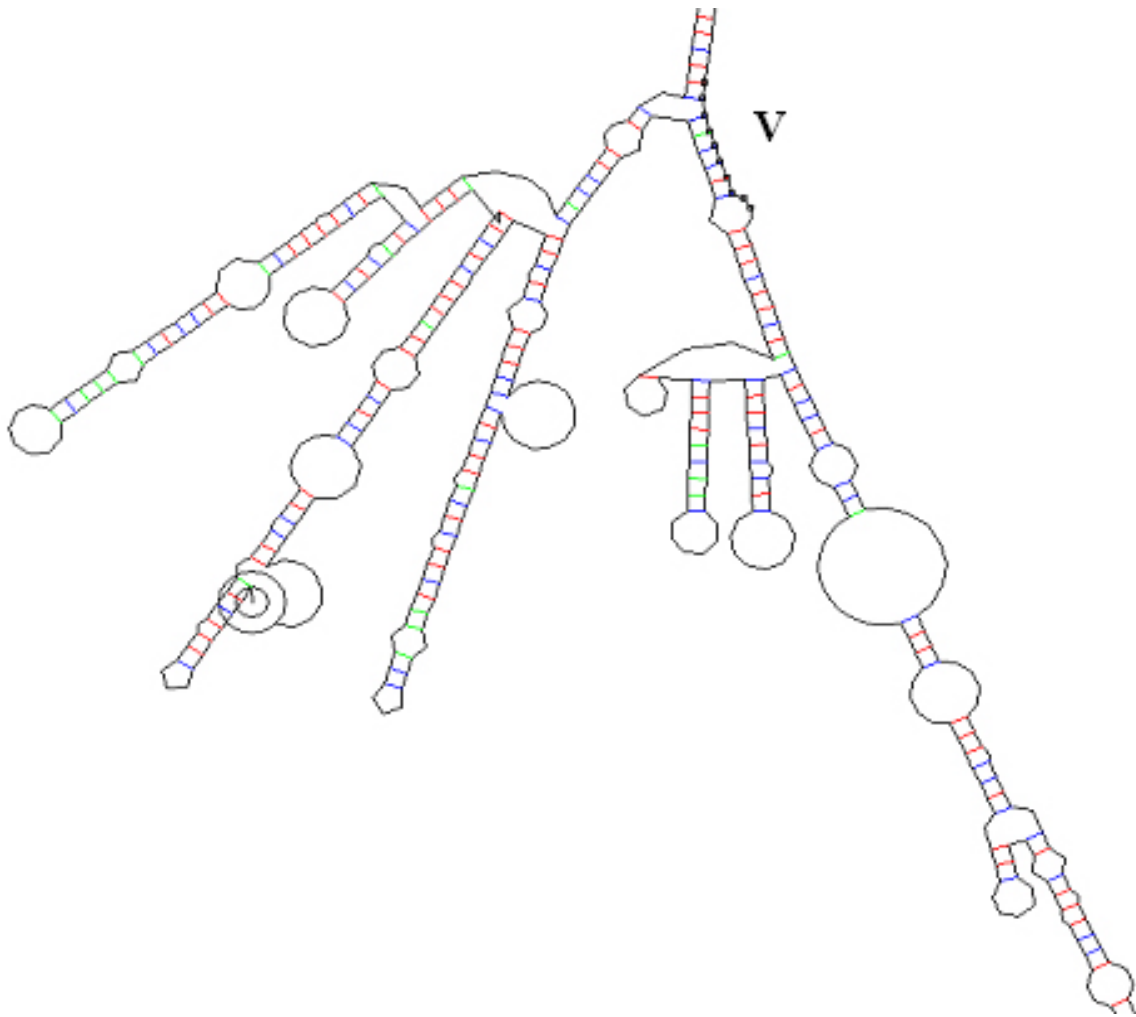


Figure 5.2 Part of hSGLT1 mRNA secondary structure indicating the position of RNase E site. Nucleotide sequence 1558 of hSGLT1 mRNA marked as V (GAUUAUCUGU) in this structure is highly prone for RNase E degradation due to presence of very high stem-loop structure adjacent to this site.

According to our mRNA degradation hypothesis, cDNA of hSGLT1 is transcribed into mRNA of hSGLT1 without any problem. At this point as mentioned above since hSGLT1 mRNA contains 5 RNase E sites, RNase E and other endoribonucleases start to degrade hSGLT1 mRNA from the 5'-3' end. RNase E degradation also activates other exonucleases like PNPase, RNase II, and RNase R. These active exonucleases start mRNA degradation from 3'-5' end of oligoribonucleotides generated by RNase E degradation into smaller parts. These smaller parts are further degraded into mononucleotides by oligoribonucleases.

5.1.1.4. Comparison to other attempts to express hSGLT1 in *E. coli*

In the year 2002, Quick and Wright (Quick and Wright, 2002) reported functional expression of hSGLT1 in *E. coli*. The authors of this study claimed that they obtained 1 mg functional hSGLT1 protein from 3-liters of bacterial culture. These results are only apparently contradictory to the results we obtained in *E. coli* expression host in the present study. We

analysed their plasmid construction strategy and results in a step by step manner to find out the probable reasons for their success. They used pTMH-6FH expression vector (Quick and Jung, 1998), a derivative of pT7-5 (*lacY*) (Bibi and Kaback, 1990) and it works under the *lac* promoter/operator (Bibi and Kaback, 1990; Quick and Jung, 1998), which is a mild promoter. Use of mild promoter does not seem to be real reason for their success because we also used pBAD expression vector, which works on the mild promoter P_{BAD} of the *araBAD* operon. The second important thing in their methodology was the use of growing temperatures below 20°C and the use of BL21 *E. coli* strains but we employed same growth conditions with same and different *E. coli* strains and could not get expression of hSGLT1 even in a small amount.

The most interesting and important aspect of their study is that, they shortened the N-terminal of hSGLT1 by 16 amino acids (sequence of hSGLT1 from 12-28 *aa*), this deletion increases the amount of hSGLT1 inserted into the membrane of *E. coli* by about fivefold. They reported that bacterial cotransporters possess significantly shorter N-terminal hydrophobic extensions than those in eukaryotes (Turk and Wright, 1997) so this deletion makes hSGLT1 more similar to its bacterial counterpart and its helps in hSGLT1 proper insertion into membrane. Another reason behind the fivefold increment in hSGLT1 expression and insertion into the membrane might, however, be stability of Δ N12-28hSGLT1 mRNA. Deletion of 48 nucleotide sequences at the N-terminal of hSGLT1 resulted in a secondary structure, which contains stem-loops at the N-terminal of gene (Figure 5.3). These N-terminal stem-loop structures prevent or delay the mRNA degradation by RNase E. Recently with the help of stem-loop addition at 5' end of mRNA, increased expression of genes has been described, which are either not possible to express (Paulus et al., 2004) or express at very low-level (Carrier et al., 1998; Carrier and Keasling, 1997a; Carrier and Keasling, 1997b; Carrier and Keasling, 1999; Smolke et al., 2000; Smolke and Keasling, 2002) in *E. coli*. Another important point of their strategy is the addition of glycophorin A transmembrane span (as a 15th transmembrane domain in hSGLT1 sequence) and of the green fluorescence protein (GFP) at the 3' end of hSGLT1 gene. It is a well-documented fact that GFP mRNA does not contain any RNase E sites (Smolke and Keasling, 2002). Presence of stem-loop structure at the 5' of Δ N12-28hSGLT1-Gly-GFP gene, protects it from RNase E degradation and due to the addition of GFP at the 3' of gene, provides protection to the gene from the exoribonuclease degradation, which acts from 3'-5' end. There are again evidences that indicate that mRNA stability was the decisive factor.

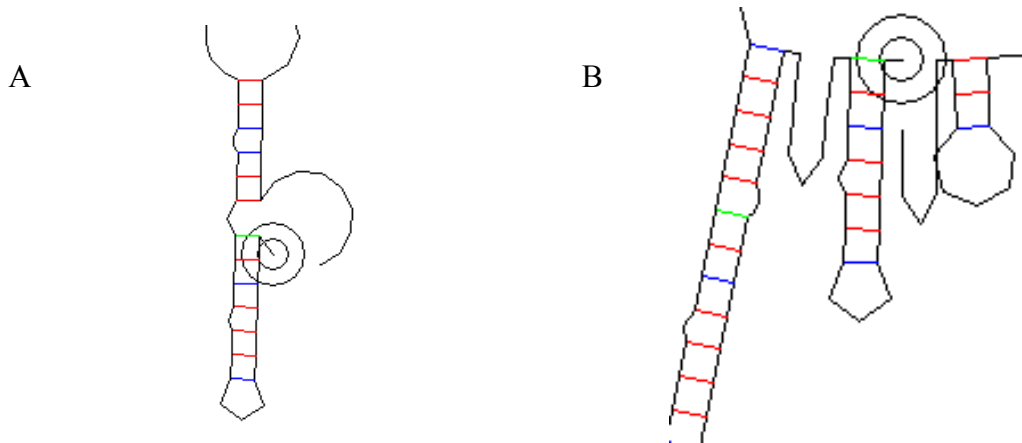


Figure 5.3 Secondary structure of a part of hSGLT1 mRNA, and Δ N12-28 hSGLT1 mRNA. (A) mRNA of hSGLT1 does not contain any stem-loop structure at its N-terminal so it is highly susceptible for RNase E degradation. (B) Deletion of amino acids from N-terminal of hSGLT1 results in a secondary structure, which contains stem-loop at N-terminal of gene, and these stem-loop structure protects the RNase E sites from RNase E degradation.

5.2. *P. pastoris* as an expression host

The methylotrophic yeast *P. pastoris* is a powerful tool for the heterologous expression of protein (Cereghino and Cregg, 2000). This system combines several advantages of prokaryotic and eukaryotic expression systems. The techniques needed for molecular genetic manipulation are similar to those well established for *S. cerevisiae*. *P. pastoris* can be easily grown to high cell densities using defined minimal media and is able to introduce eukaryotic posttranslational modifications. Another advantage of the *P. pastoris* expression system for structural analysis is the possibility of ^{13}C labeling of expressed proteins for nuclear magnetic resonance analysis. Feeding ^{13}C labeled methanol provides a cost-effective possibility to achieve incorporation levels of up to 98%.

5.2.1. Expression of hSGLT1 in *P. pastoris*

For the functional expression of hSGLT1 in *P. pastoris* FLAG tag was introduced in hSGLT1 by changing the native peptide sequence D₅₇₄ AEEEN to D₅₇₄YKDDDDK and a 10 amino acids long spacer was placed at C-terminal. Addition of spacer at C-terminal helps in the proper targeting of hSGLT1 in the membrane because if the His tag is directly present at the C-terminal of hSGLT1 it interferes with the insertion of proteins into the membrane (Turk et al., 2000) after its synthesis in the cytosol and we observed degradation of most of the protein under this condition. *P. pastoris* GS115 harboring a plasmid with hSGLT1 cDNA under the control of the *AOX* promoter proved to be most suitable for the high-level expression and stability of recombinant hSGLT1. The transporter was detected in the yeast cells by using a

FLAG antibody against the engineered FLAG epitope (Figure 4.9B), and it is active as judged by sodium-stimulated sugar (D-glucose) uptake.

5.2.2. Protein purification

For the purification of hSGLT1 we adopted a new strategy, which includes washing of hSGLT1 containing membranes with 4 M urea to get rid of most of peripheral and outer membrane proteins, which helps in the enrichment of hSGLT1. As judged by Western blot analysis during different stages of hSGLT1 purification, the hSGLT1 was properly inserted into the membrane because in the supernatant (Figure 4.9B, *lane S1*) and in urea washing (Figure 4.9B, *lane UW*), we could not detect any hSGLT1 protein, whereas all hSGLT1 was present in the pellet (Figure 4.9B, *lane P1*), and could be released into supernatant (Figure 4.9B, *lane S4*), which was obtained after solubilization of membranes in 1.2% FosCholine-12.

A variety of molecular signals or mechanisms have been reported for the specific localization of particular membrane proteins to specific membrane compartments (Bibi et al., 1992; Matter et al., 1992; Sandoval and Bakke, 1994; Weinglass and Kaback, 2000) but the mechanism by which hSGLT1 inserts into the membrane is still unclear. Recently, Quick and Wright (Quick and Wright, 2002) showed that shorter N-terminal of hSGLT1 increases the amount of hSGLT1 inserted into the *E. coli* membrane because bacterial cotransporters possess significantly shorter N-terminal hydrophilic extensions than those in eukaryotes (Turk and Wright, 1997). However in *P. pastoris* most of hSGLT1 inserted into membrane without any modification at its N-terminal as judged by Western blot analysis (Figure 4.9B). These results indicate that signal sequences encoded within hSGLT1 sequence are fully functional in the *P. pastoris*.

Purified hSGLT1 shows an apparent molecular mass of 55 kDa, which corresponds to the nonglycosylated transporter. Despite the apparent nonglycosylated status of hSGLT1 in *P. pastoris*, it shows biochemical properties that are indistinguishable from glycosylated hSGLT1. This finding also supports previous observations that N-glycosylation is not required for hSGLT1 activity (Quick and Wright, 2002; Turk et al., 1996).

Recombinant hSGLT1 was purified by Ni-affinity chromatography on a Protino column to more than 95% purity as judged by Coomassie Blue staining SDS-PAGE gel (Figure 4.9A). No degradation product was observed in the purified hSGLT1 (Figure 4.9A and B). About 3 mg of hSGLT1 was purified from 1 liter of *P. pastoris* culture. The yield of hSGLT1, which we obtained in this study, was higher than those reported for other membrane protein in *P. pastoris* expression system. The yield for other membrane protein reported in literature are as following, 2 mg of multidrug resistance protein1 (Cai et al., 2001), 0.7 mg of ATP-binding cassette transporter (Cai and Gros, 2003), 2.2 mg of NOP-1 (Bieszke et al., 1999), and 1 mg of 5HT_{5A}-serotonergic receptor (Weiss et al., 1998).

5.2.3. Reconstitution and functional analysis of recombinant hSGLT1

Purified recombinant hSGLT1 was reconstituted into performed detergent-destabilized liposomes made of 90% (w/v) asolectin soy lecithin and 10% (w/v) cholesterol with a detergent concentration adjusted to the onset of solubilization (Jung et al., 1998; Panayotova-Heiermann et al., 1999; Rigaud and Levy, 2003). 100 mM sodium stimulated uptake of 50 μ M α -MDG is completely blocked by 10 μ M phlorizin (Figure 4.10, Figure 4.11, Figure 4.12, and Figure 4.13). In order to further characterize recombinant hSGLT1 in proteoliposomes, we performed competitive uptake studies of 100 μ M α -MDG in the presence of inhibitor (100 μ M phlorizin) high-affinity substrates (10 mM D-glucose and D-galactose) and low-affinity substrates (10 mM 2-Deoxy-D-glucose, mannose, allose, and L-glucose) inhibited sugar uptake according to their affinity towards transporter (Table 4.3). hSGLT1 in proteoliposomes exhibits substrate specificity in the following order, Phlz \gg α -MDG \approx D-Glc \approx D-Gal \gg 2Doglc $>$ Man $>$ All $>$ L-Glc. Catalytic turnover of hSGLT1 based on the V_{max} of 3.4 μ mol \times mg hSGLT1⁻¹ \times min⁻¹ is 6 s⁻¹ (Table 4.4), which is in good agreement with that obtained in previous studies (Quick and Wright, 2002) and other Na⁺-dependent transporters [e.g., the Na⁺/ glucose transporter of *Vibrio parahaemolyticus* (vSGLT) (Turk et al., 2000), and Na⁺/ proline transporter of *Escherichia coli* (PutP) (Jung et al., 1998)]. The kinetics of recombinant hSGLT1 in intact cells or membrane vesicles, and reconstituted proteoliposomes, mirror those determined for hSGLT1 in native tissue and *Xenopus* oocytes.

5.2.4. Reasons for getting functional expression of hSGLT1 in *P. pastoris*

One obvious question that comes into mind, if mRNA of hSGLT1 is unstable in *E. coli* and contains five potential RNase E sites why did we get expression of hSGLT1 in *P. pastoris*. The best possible explanation of this question is that the mRNA half-life and underlying degradation mechanisms are different in *P. pastoris* as compared to *E. coli*. In yeast, the degradation of the transcript begins with the shortening of the poly (A) tail at the 3' end of mRNA (Muhlrad and Parker, 1992; Shyu et al., 1991). Shortening of the poly (A) tail primarily leads to removal of the 5'-cap structure (decapping), thereby exposing the transcript to digestion by a 5'-3' exonuclease. In addition to decapping and 5'-3' decay, transcripts can also be degraded in a 3'-5' direction following deadenylation (Anderson and Parker, 1998; Muhlrad et al., 1995). This process is catalyzed by a conserved complex of multiple 3'-5' exonucleases, termed the exosome that also performs a wide variety of RNA processing events. Currently, the available data suggest that the major mechanism of mRNA decay in yeast is by decapping and 5'-3' degradation (Beelman et al., 1996). Yeast mRNA can also be degraded by mechanisms that involve specific cleavage of transcript independent of prior poly (A) shortening.

Decapping is a key step in the yeast mRNA degradation for several reasons. First, in the 5'-3' pathway of mRNA degradation, it both precedes and permits the decay of the transcript body. Second, since individual mRNAs are decapped at different rates, decapping is also an important control point in mRNA decay. Third, decapping also plays a critical role in the process of mRNA surveillance wherein aberrant mRNAs containing nonsense codons are very rapidly decapped and degraded in a 5'-3' direction. The major difference in the mRNA degradation mechanism in *E. coli* and *P. pastoris* is that the decapping is the most crucial step in the mRNA degradation in yeast but in bacteria this step is not necessary for mRNA degradation. Average half-life of mRNA in yeast is around 3 h while in case of bacteria it is only 1.5 min.

Second explanation for hSGLT1 expression in *P. pastoris* can be given on the basis of difference in the codon usages in both expression systems. As mentioned previously, codon usage in *E. coli* are ~23% bias for hSGLT1 gene as compared to *H. sapiens*, while codon usage in *P. pastoris* are only 9.7% bias as compared to *H. sapiens*. Third possible explanation is that *P. pastoris* as a eukaryote organism shares many similarities with *H. sapiens* at the cellular level and molecular mechanisms underlying transcription, translation and membrane trafficking of membrane proteins compared to their prokaryote counterpart *E. coli*.

5.2.5. Advantages of our expression method

Our method of expression of hSGLT1 in *P. pastoris* has certain advantages over other methods of hSGLT1 expression. We expressed full-length hSGLT1 protein without any significant modification in hSGLT1 as compared to previously reported hSGLT1 in *E. coli* (Quick and Wright, 2002), in which N-terminal of hSGLT1 was shortened by deleting amino acid residues 12-28 and GFP was fused to its C-terminal but in our opinion hSGLT1 Δ N-GFP is not suitable for most of the biochemical and biophysical applications due to its very high molecular weight (\approx 100 kDa) and due to intense modifications in it. The amount of hSGLT1 (3 mg hSGLT1 per 1-liter of yeast culture) obtained in our expression system is the highest yield reported so far for hSGLT1 protein expression. The yield obtained in *E. coli* is only 1 mg of purified recombinant protein per 3-liter of cultured bacterial cells. For the better immunological detection and to provide ease in the purification two affinity tags are present in our protein. Our protein purification method is very simple and efficient. The initial step involving washing of the protein pellet with 4 M urea resulted in a much more enriched hSGLT1 protein pellet which was further solubilized in 1.2% FosCholine-12. Thus resultant solubilized supernatant gave more than 95% purified hSGLT1 protein without any degradation product on Ni-affinity purification on a Protino column, while the other reported procedure includes two steps protein purification, immuno-affinity chromatography followed by gel filtration (Quick and Wright, 2002). Advantages of our hSGLT1 expression methods clearly

demonstrate that our method is novel and unique, as it provides purified protein in less time with less expenditure.

5.3. Photoaffinity labeling of truncated loop 13

A photoaffinity probe should satisfy the following criteria for its successful utilization in target site identification. It should be small, so as not to cause unacceptable steric perturbation to the system under examination. It should be stable in the dark, and highly susceptible to light at a wavelength that does not cause photolytic damage to the biological sample. Finally, the reaction with biological targets should lead to stable products to enable their isolation, purification and analysis. Both diazirine and benzophenone based photo probes exhibit these major advantages over frequently used azido photoprobes (Bayley and Knowles, 1978; Gibbs et al., 1982; Lin et al., 1982). TIPDG, 6-AG and BzG come closer to satisfying the chemical and biological criteria required for most photo reagents (Brunner et al., 1980; Delfino et al., 1993; Dorman and Prestwich, 1994; Fang et al., 1998; Hatanaka et al., 1994; Nassal, 1984; Platz et al., 1991; Prestwich et al., 1997). All three photoprobes TIPDG, 6-AG and BzG can be photolysed at 350-360 nm, avoiding protein-damaging wavelengths. In TIPDG the electron withdrawing trifluoromethyl group may lead to an increased stability of the C-I bond. That this type of iodinated phenyldiazirine makes promising photolabeling reagents is inferred also from a number of studies with 3-(trifluoromethyl)-3-(3-[¹²⁵I]iodophenyl) diazirine, a reagents widely used in the past for labeling of the apolar phase of membranes (Brunner, 1989; Brunner and Semenza, 1981; Brunner et al., 1983). The superb selectivity of this reagent in labeling integral (versus peripheral) proteins may be a direct reflection of the C-I bond stability during diazirine photolysis.

Despite the early concerns about the photochemistry of aliphatic as opposed to aromatic diazirines (Brunner, 1993), they have now been successfully employed in the design of minimally perturbing photoaffinity probes (Kipp et al., 1997; Liessem et al., 1995). We, therefore, recently developed a novel photoreactive aliphatic diazirine-containing photoprobe 6-AG that mimic glucose, a high-affinity substrate transport by hSGLT1. In contrast to the bipolar azido group, no polarization of the aliphatic diazirine group can be observed. The carbon atom of the three membered aliphatic diazirine ring has a chemical shift of ~15 ppm in ¹³C NMR spectra, and the hydrogen atoms of vicinal methyl group have a chemical shift of ~1 ppm in ¹H NMR spectra. This data is typical for the chemical shifts usually observed in nonpolar alkyl groups. The nonpolar character of 6-AG seems to have a special benefit for the binding of modified substrates to hydrophobic membrane proteins.

BzG exhibits three distinct chemical and biochemical advantages over previously reported azido derivatives of phlorizin (Gibbs et al., 1982; Lin et al., 1982), which gave very inconsistent poor labeling results due to harsh photolysis conditions and low labeling efficiency caused by undesired side reactions. First BzG is more stable than azido derivatives

of phlorizin. Second BzG can be manipulated in ambient light and can be activated at 350-360 nm. Third BzG reacts preferentially with unreactive C-H bonds, even in the presence of solvent water and bulk nucleophiles. The relative inertness of the BzG triplet state to the water should guarantee that no BzG photoaffinity label will be lost to reaction with water, in contrast to carbene photoaffinity labels, where immediately or delayed hydrolysis has frequently been observed (Galardy et al., 1974; Hexter and Westheimer, 1971; Shafer et al., 1966).

Aryl azides are the most widely used photochemical reagents in the strategy of photoaffinity labeling receptors sites on proteins. Photoactivation of aryl azide yields several reactive intermediates, including singlet (half-life on the order of milliseconds) plus small fractions of the relatively long-lived triplet nitrenes. Special attention must, therefore, be given to minimize spurious labeling attendant with reactive species that can migrate from the original binding sites. Nitrenes are also thought to react preferentially with nucleophilic groups and rarely are involved in random, near-neighboring hydrogen extractions and insertion into C-H bonds. However, this feature is not necessarily a disadvantage in the employment of the phlorizin aryl azide derivative. For example, the receptor for 3-AP probably includes a polar group that serves as the specific interaction site for the $-N_3$ moiety. Our rationale for the synthesis of 3-AP photoprobe was based on previous results reported by Diedrich group (Diedrich, 1990; Gibbs et al., 1982; Hosang et al., 1981), using 4-azidophlorizin that introduction of the azido group into the phlorizin backbone neither changes its interactions mode with Na^+ /D-glucose cotransporter nor its inhibition kinetics.

The synthesis of the new photoactivable analogue of arbutin 9 features several noteworthy steps: (a) regioselective introduction of an iodine atom into the aromatic ring of compound 1 (Figure 3.2) in the presence of excess HgO affording aryl iodide 2 in high yield (Brunner et al., 1980; Hatanaka et al., 1994), (b) O-Demethylation of 2, followed by coupling of phenol 3, in the presence of mercuric cyanide to give keto compound 5 in very high yield (Ambroise et al., 2000). Regioselective introduction of the iodine atom into the aromatic ring of TIPDG can also serve the purpose of producing a radioactive analogue of TIPDG with a high specific activity by using the tritiodeiodination reaction (Ambroise et al., 2000) To check this possibility, we performed hydrodeiodination of TIPDG in the presence of molecular hydrogen and 10% Pd/C, which gave non iodinated form of TIPDG within 1 h without any significant loss of the diazirine moiety. Ambroise (Ambroise et al., 2000) synthesized [(4'-(3''-trifluoromethyldiazirinyloxy)phenoxy]-D-galactopyranoside by stannic tetrachloride-catalyzed glycosylation of β -D-galactose pentaacetate with [3-(4-hydroxyphenyl)-3-(trifluoromethyl)-3H-diazirine in 43% yield. The phenol [3-(4-hydroxy phenyl)-3-(trifluoromethyl)-3H-diazirine was synthesized in six steps by the previously reported procedure (Hatanaka et al., 1994), but the major drawback of this synthesis was the low yield (26%) of demethylation of [3-(4-methoxyphenyl)-3-(trifluoromethyl)-3H-diazirine with trimethylsilyl iodide and a prolonged reaction time 65 h (Hatanaka et al., 1994). In our method, demethylation of 3-Iodo-4-methoxy-trifluoroacetophenone 2 with LiCl gives phenol 3 in 88% yield and the coupling

reaction of phenol 3 with α -D-acetobromoglucose 4 in the presence of mercuric cyanide gives [(2'-Iodo-4'-trifluoroacetyl)phenoxy]-2,3,4,6-tetra-O-acetyl-D-glucopyranoside 5 in 75% yield. Thus, our method provides a simple and versatile approach for the synthesis of different sugar based photoaffinity probes.

The results on Na^+ -dependent glucose uptake show that TIPDG (Figure 4.20), BzG (Figure 4.19), 3-AP, and 6-AG (Figure 4.21) interact with the high affinity Na^+ /D-glucose cotransporter. It was further demonstrated that the K_i values of TIPDG ($22 \pm 5 \mu\text{M}$) and its prototype compound arbutin ($25 \pm 6 \mu\text{M}$), BzG ($12 \pm 2 \mu\text{M}$) and its respective model compound phlorizin ($8 \pm 1.2 \mu\text{M}$), 3-AP ($8.6 \pm 1.6 \mu\text{M}$) and its parent compound phlorizin ($8 \pm 1.2 \mu\text{M}$) and of 6-AG ($40 \pm 5 \mu\text{M}$) and its sibling D-glucose (1 mM) were essentially identical. Modification of phenyl ring OH group in arbutin into a trifluoromethyl diazirine group and mono iodination of its phenyl ring neither altered the affinity to the Na^+ /D-glucose cotransporter nor the mode of inhibition.

To further test the potential of TIPDG and BzG as a selective photoaffinity probe for SGLT1, we labeled the truncated loop 13 (amino acid 564-638 of SGLT1 amino acid sequence). MALDI-mass spectrometry analysis of photoaffinity labelled truncated loop 13 protein with TIPDG and with BzG clearly indicates that our probes successfully labeled the part of SGLT1 protein.

Site-directed mutagenesis studies suggest that a hydrophobic region located in the C-terminal loop 13 (amino acids 604-610) is critically involved in the binding of phlorizin (Novakova et al., 2001). The binding of phlorizin to loop 13 could be confirmed in solution by monitoring phlorizin-dependent fluorescence quenching of the endogenous tryptophan residue (Trp-561). It has been further demonstrated that the phloretin (but not the glucose) moiety of phlorizin interacts with loop13 (Xia et al., 2003). Phlorizin consists of a pyranoside ring and two aromatic rings joined by an alkyl spacer. The conformation of phlorizin in aqueous solutions was previously studied by two-dimensional NMR and pharmacophore analysis by Wielert-Badt (Wielert-Badt et al., 2000). Their model indicates that the interactions via hydrogen bonds from the 2-, 3-, 4-, and 6-hydroxyl groups of the pyranoside and the 4- and 6-OH groups of aromatic ring A are essential for phlorizin binding. This information can now be combined with the Trp fluorescence data (Raja et al., 2003) to estimate the dimensions of the phlorizin-binding and recognition region. We can assume that phlorizin binds to the region very close to position 611 by H-bonding probably with 4-OH group by acceptor/donor atom O-4 of aromatic ring A. Thus, position 611 is supposed to be very important in phlorizin recognition, as also suggested by the lower affinity of D611W mutant. The H-bonding of any one hydrophobic amino acid located in region 606-609 with 6-OH group by acceptor/donor atom O-6 of aromatic ring A of phlorizin also causes a strong interaction.

The combination of photoaffinity labeling, SDS-PAGE, enzymatic fragmentation, and MALDI-mass spectrometry analysis with resulting allocation of the attachment site of the ortho position of ring B of phlorizin to amino acid Arg-602 now defines directly the phlorizin

binding site in loop 13. Thus, an interaction of this region with the B ring of phlorizin can be assumed. Thereby the binding pocket could accommodate the phlorizin molecule in the predicted conformation. On the basis of photoaffinity labeling pattern of truncated loop 13 with 3-azidophlorizin, we could provide a generalized mechanism by which phlorizin inhibits sugar transport by SGLT1. According to our assumption, a phlorizin-binding region in SGLT1 is located between amino acids 601-611, in this region aromatic rings (A and B) of phlorizin interact with hydrophobic amino acids and the glucoside moiety of phlorizin is free to interact with sugar interaction sites of SGLT1 (Lo and Silverman, 1998; Panayotova-Heiermann et al., 1997).

In summary, this study provides first example of large-scale functional expression and purification of full-length human Na⁺/D-glucose cotransporter. Recombinant hSGLT1 retains full functionalities when reconstituted into proteoliposomes. The ability to purify functional cotransporter enables a battery of biochemical and biophysical experiments to probe the structure and function of hSGLT1, with results possibly relevant to other cotransporters in the SGLT family. We hope that our method of functional human membrane protein expression in *P. pastoris* presented in this study may also provide guidelines for the expression of other medically important human membrane proteins which thus far could not be expressed in prokaryote hosts.

5.4. Future prospective

In the life of a membrane protein molecular biologist the happiest day is the day when he/she gets functional expression of target protein. Our success in the functional expression of hSGLT1 open doors of new opportunities to work on hSGLT1. It would be an interesting and challenging task to decipher the molecular basis of the sugar transport and inhibitor binding. What are the responsible amino acids in the protein for sugar transport and inhibitor binding? What would be sugar translocation and inhibitor binding mechanisms? These and many other questions can now be readily answered because now we have an expression system, which provides sufficient amount of functional hSGLT1.

Photoaffinity labeling provides a promising approach for the identification of sugar translocation pathway and inhibitor binding sites (Raja et al., 2004; Raja et al., 2003; Tyagi and Kinne, 2003), so it would be a challenging and interesting task to performed equilibrium and time-dependent photoaffinity labeling studies with reconstituted recombinant hSGLT1 for the identification of critical amino acids responsible for sugar selectivity, uptake and for inhibitor binding.

It would be interesting to address the questions related to sugar translocation pathway and inhibitor binding mechanism by means of luminescence spectroscopy, which has proven informative in the case of some other transporter (Vazquez-Ibar et al., 2003) and which could

ultimately provide interesting insight concerning molecular mechanisms responsible for transport activity.

The ultimate goal of protein biologist working on structure-functional relationship of protein is to get the information about target protein structure by X-ray crystallography or Nuclear magnetic resonance spectroscopy, so it would be interesting and challenging tasks to work on this aspect of hSGLT1 structure with the help of protein obtained from our expression system.

6. Summary

Human sodium/D-glucose cotransporter (hSGLT1) is a member of solute carrier family (SLC5) and plays a central role in the homeostasis of glucose, salt, and water. During the course of this work, first the production of recombinant hSGLT1 transporter in *E. coli* and *P. pastoris* was evaluated.

A number of different expression vector constructs of hSGLT1 for its production in *E. coli* were prepared. Various affinity tags were appended to the transporter C-terminal to enable transporter detection and purification. We attempted expression of transporter in different expression vectors, in different conditions and in different *E. coli* strains but we could not get the expression of hSGLT1. During this process, we constructed clone pET22b-Unc-F-hSGLT1 containing Unc-F gene (encoding the β -subunit of *E. coli* ATP synthase), in this case also we could not find out any hSGLT1 expression but also no expression of β -subunit of the *E. coli* ATP synthase, which was expressed in large amounts in the control clone (pET22b-Unc-F). This finding along with the fact that hSGLT1 mRNA contains 5 RNase E sites suggests that in *E. coli* hSGLT1 mRNA is unstable and all mRNA is degraded by RNase E and other exoribonucleases before its translation into protein.

Heterologous expression of hSGLT1 was also carried out in *P. pastoris*. hSGLT1 gene containing FLAG tag and a 10 amino acids long spacer at its C-terminal was cloned into pPICZB plasmid and the resulted expression vector pPICZB-hSGLT1 was transformed into *P. pastoris* strain GS115 by electroporation. Purification of recombinant hSGLT1 by Nickel-affinity-chromatography yields about 3 mg of purified recombinant hSGLT1 per 1-liter of cultured *P. pastoris* cells. The purity of the hSGLT1 was more than 95% pure, as judged from Coomassie stained gels. Purified hSGLT1 migrates on SDS-PAGE at an apparent mass of 55 kDa, which corresponds to that of the nonglycosylated transporter. Reconstitution of purified hSGLT1 yields proteoliposomes active in Na^+ -dependent glucose uptake and sodium-stimulated uptake of 50 μM α -MDG is completely blocked by 10 μM phlorizin. The 1 min time course of α -MDG uptake in the proteoliposomes demonstrated a characteristic overshoot in the presence of Na^+ , indicating that sugar was concentrated within the proteoliposomes and that uptake was energised by Na^+ electrochemical gradient. In order to further characterize recombinant hSGLT1 in proteoliposomes, we performed competitive uptake studies of 100 μM α -MDG in the presence of inhibitor (100 μM phlorizin) high-affinity substrates (10 mM D-glucose and D-galactose) and low-affinity substrates (10 mM 2-Deoxy-D-glucose, mannose, allose, and L- glucose) that inhibited sugar uptake according to their affinity towards the transporter in cells and membranes. hSGLT1 in proteoliposomes exhibits substrate specificity in the following order, Phlz \gg α -MDG \approx D-Glc \approx D-Gal \gg 2Doglc $>$ Man $>$ All $>$ L-Glc. Recombinant reconstituted hSGLT1 shows stereospecificity as its preferred D-Glu over L-Glu, D-Glu inhibited 75% of α -MDG uptake L-Glu, inhibited only

2%. The equatorial orientation of the OH-group at the positions C-2 and C-3 of the D-glucose seems to be important for its recognition by hSGLT1 since the presence of mannose, 2-Deoxy-D-glucose and allose significant inhibitory effect on α -MDG uptake was observed. The 78% inhibition of α -MDG uptake in the presence of D-galactose indicates the orientation of OH-group at C-4 (equatorial in D-glucose and axial in D-galactose) is not that important for their recognition by cotransporter because D-Glu and D-Gal inhibited sugar uptake by transporter upto equal extent. Phlz inhibited 84% of α -MDG uptake in proteoliposomes. Catalytic turnover of hSGLT1 based on the V_{max} of $3.4 \mu\text{mol} \times \text{mg hSGLT1}^{-1} \times \text{min}^{-1}$ is 6 s^{-1} . These results clearly indicate that purified recombinant hSGLT1 posses the full functionalities in this reconstituted system.

For the identification of sugar-binding sites and phlorizin interactions sites in the transporter four new photoprobes were synthesized and subsequently evaluated for their effects on SGLT1 mediated α -MDG transport in rabbit small intestine brush border membrane vesicles. Results of these experiments shows that [(2'-Iodo-4'-(3''-trifluoromethyl-diazirinyloxy)phenoxy]-D-glucopyranoside (TIPDG), [(4'-Benzoyloxy)phenoxy]-D-glucopyranoside (BzG), 3-Azidophlorizin (3-AP), n-Methyl-6C-(Azimethyl)-D-glucopyranoside (6-AG) inhibit α -MDG uptake. The K_i values of TIPDG ($22 \pm 5 \mu\text{M}$) and its prototype compound arbutin ($25 \pm 6 \mu\text{M}$), BzG ($12 \pm 2 \mu\text{M}$) and its respective model compound phlorizin ($8 \pm 1.2 \mu\text{M}$), 3-AP ($8.6 \pm 1.6 \mu\text{M}$) and its parent compound phlorizin ($8 \pm 1.2 \mu\text{M}$) and of 6-AG ($40 \pm 5 \mu\text{M}$) and its sibling D-glucose (1 mM) were essentially identical. Photoaffinity labeling were performed with a functional domain of SGLT1 (amino acids 564-638 of the SGLT1 amino acid sequence, loop 13) with TIPDG, BzG, and 3-AP clearly demonstrated that our probes successfully labeled part of the SGLT1 protein.

3-AP was further used to identify phlorizin-binding sites in the truncated loop 13 by the combination of photoaffinity labeling, SDS-PAGE, enzymatic fragmentation, and MALDI-mass spectrometry analysis. The attachment site of the ortho position of ring B of phlorizin could be allocated to amino acid Arg-602, thus, an interaction of this region with the B ring of phlorizin can be assumed. Thereby the binding pocket could accommodate the phlorizin molecule in the previously predicted conformation.

To summarize, this study provides first example of large-scale functional expression and purification of full-length human Na^+/D -glucose cotransporter. Recombinant hSGLT1 retains full functionalities when reconstituted into proteoliposomes. The ability to purify functional cotransporter enables a battery of biochemical and biophysical experiments to probe the structure and function of hSGLT1, with results possibly relevant to other cotransporters in the SGLT family. The synthesis of four new photoaffinity probes provides tools for the identification of sugar translocation pathway and inhibitor binding in the recombinant hSGLT1.

7. Zusammenfassung

Der humane Na⁺/D-Glucose Kotransporter (hSGLT1) gehört zur Transporterfamilie SCL (solute carrier) 5 und spielt eine zentrale Rolle bei der Homöostase von Glucose, Salz und Wasser.

Ziel der vorliegenden Arbeit war zunächst die heterologe Expression des Transporters in *E. coli* und *P. pastoris*. Für die Expression in *E. coli* wurden verschiedene Expressionsvektoren verwendet und zur Detektion und Reinigung des Transporters unterschiedliche Affinitäts Tags an dessen C-Terminus angehängt.

Wir haben die Expression des Transporters mit verschiedenen Expressionsvektoren und *E. coli* Stämmen unter zahlreichen Bedingungen versucht, ohne dass die Expression von hSGLT1 gelang. Während dieser Versuche haben wir den Klon pET22b-Unc-F-hSGLT1 hergestellt, welcher das Unc-F Gen für die β -Untereinheit der *E. coli* ATP Synthase enthält. In diesem Fall konnten weder hSGLT1 noch ATPase Expression nachgewiesen werden, obwohl letztere in hohem Ausmaß im Kontrollklon (pET22b-Unc-F) exprimiert wurde. Zusammen mit der Tatsache, dass die mRNA des hSGLT1 5 RNase Sequenzen enthält, lässt dies den Schluß zu, dass die mRNA des hSGLT1 in *E. coli* instabil ist und dass die mRNA durch RNase E und andere Exoribonucleasen abgebaut wird, noch bevor die Translation zum Protein erfolgen kann.

Desweiteren wurde die heterologe Expression von hSGLT1 in *P. pastoris* durchgeführt. Das hSGLT1 Gen wurde mit einem C-terminalen FLAG Tag und einem 10 Aminosäuren langen Spacer in das Plasmid pPICZB kloniert. Mit dem erhaltenen Expressionsvektor pPICB-hSGLT1 wurde der *P. pastoris* Stamm GS115 durch Elektroporation transformiert. Durch Aufreinigung des hSGLT1 mittels Nickel-Affinitätschromatographie konnten 3 mg gereinigtes rekombinantes hSGLT1 Protein pro Liter *P. pastoris* Kultur angereichert werden. Die Reinheit des hSGLT1 lag bei über 95%.

Gereinigter hSGLT1 hat in SDS-PAGE Gelen ein scheinbares Molekulargewicht von 55 kDa, welches der Größe eines nicht-glykosilierten Transporters entspricht.

Nach Rekonstitution des gereinigten SGLT1 in Proteoliposomen konnte eine natriumgetriebene Akkumulation von α -Methyl-D-Glucose (α -MDG) nachgewiesen werden, die vollkommen durch 10 μ M Phlorizin gehemmt wurde.

Um rekombinanten hSGLT1 in Proteoliposomen näher zu charakterisieren, wurden kompetitive Aufnahmestudien mit 100 μ M α -MDG in der Gegenwart von Inhibitor (100 μ M Phlorizin), Substraten mit hoher Affinität (10 mM D-Glucose und D-Galactose) und Substraten mit geringer Affinität (10 mM 2-Deoxy-D-Glucose, Mannose, Allose und L-Glucose) durchgeführt, welche die Zuckeraufnahme entsprechend ihrer Affinität zum nativen Transporter inhibierten.

hSGLT1 in Proteoliposomen weist folgende Substratspezifität auf: Phlz >> α -MDG \approx D-Glc \approx D-Gal >> 2DoGlc > Man > All > L-Glc.

Die katalytische Umsatzrate des hSGLT1 beträgt 6 s^{-1} auf der Basis von $V_{\text{max}} = 3,4 \mu\text{mol} \times \text{mg hSGLT1}^{-1} \times \text{min}^{-1}$. Diese Ergebnisse zeigen deutlich dass gereinigter rekombinanter hSGLT1 in dem verwendeten System volle Funktionalität aufweist.

Für die Identifizierung der Bindungsstellen des Transporters für Zucker und der Interaktionsstellen mit Phlorizin wurden vier neue Photo-Proben synthetisiert und deren Wirkung auf den SGLT1-vermittelten α -MDG Transport in Vesikeln der Bürstensaummembran des Kaninchen-Dünndarms untersucht. Die Ergebnisse zeigten dass [(2'-Iodo-4'-(3''-trifluoromethyldiazirinyloxy)phenoxy]-D-glucopyranoside (TIPDG), [(4'-Benzoyloxy)phenoxy]-D-glucopyranoside (BzG), 3-Azidophlorizin (3-AP), n-Methyl-6C-(Azimethyl)-D-glucopyranoside (6-AG) die α -MDG Aufnahme inhibierten. Die K_i Werte der Ausgangsverbindungen und deren Derivate waren nahezu identisch; $25 \pm 6 \mu\text{M}$ für Arbutin und $22 \pm 5 \mu\text{M}$ für TIPDG, $8 \pm 1,2 \mu\text{M}$ für die Ausgangsverbindung Phlorizin und $12 \pm 2 \mu\text{M}$ für BzG und $8,6 \pm 1,2 \mu\text{M}$ für 3-AP als deren Derivate und 1 mM für die Ausgangsverbindung D-Glucose und $40 \pm 5 \mu\text{M}$ für 6-AG.

Photoaffinitäts-Markierungen wurden mit einer funktionellen, rekombinant exprimierten Domäne des SGLT1 (Aminosäuren 564-638 des loop 13) mit TIPDG, BzG und 3-AP durchgeführt. Es konnte deutlich gezeigt werden, dass die Proben erfolgreich Teile des SGLT1 Proteins markierten.

Um die Phlorizin-Bindestellen des Loop 13 zu identifizieren wurde im weiteren 3-AP in einer Kombination von Photoaffinitäts Markierungen, SDS-PAGE, enzymatischer Fragmentierung und MALDI Massenspektrometrie verwendet. Die Anlagerungsstelle des Ring B von Phlorizin konnte der Aminosäure Arg-602 zugeordnet werden. Folglich kann eine Wechselwirkung dieser Region mit dem Phlorizin B-Ring angenommen werden. Dadurch könnte die Bindungstasche das Phlorizinmolekül in der zuvor vorhergesagten Konformation beherbergen.

In dieser Studie konnte zum ersten mal der humane Na^+ /D-Glucose Kotransporter in großem Maßstab funktionell exprimiert und gereinigt werden. Dabei konnte gezeigt werden, dass rekombinanter hSGLT1 bei der Rekonstitution in Proteoliposomen die volle Funktionalität beibehält. Die Fähigkeit den funktionellen Kotransporter zu reinigen, eröffnet viele Möglichkeiten die Struktur und Funktion des hSGLT1 mit Hilfe biochemischer und biophysikalischer Methoden zu untersuchen. Durch die Herstellung von vier neuen Photoaffinitäts-Proben ist es in Zukunft möglich den Transportweg von Zucker zu verfolgen und Inhibitor Bindestellen zu identifizieren. Die daraus resultierenden Erkenntnisse sind möglicherweise übertragbar auf andere Ko-Transporter der SGLT Familie.

8. Reference list

Addona, G. H., Husain, S. S., Stehle, T., and Miller, K. W. (2002). Geometric isomers of a photoactivable general anesthetic delineate a binding site on adenylate kinase. *J Biol Chem* 277, 25685-25691.

Ambroise, Y., Mioskowski, C., Leblanc, G., and Rousseau, B. (2000). Syntheses and properties of photoactivatable sugar derivatives designed to probe the sugar-binding site of melibiose permease. *Bioorg Med Chem Lett* 10, 1125-1127.

Anderson, J. S., and Parker, R. P. (1998). The 3' to 5' degradation of yeast mRNAs is a general mechanism for mRNA turnover that requires the SKI2 DEVH box protein and 3' to 5' exonucleases of the exosome complex. *Embo J* 17, 1497-1506.

Arechaga, I., Miroux, B., Karrasch, S., Huijbregts, R., de Kruijff, B., Runswick, M. J., and Walker, J. E. (2000). Characterisation of new intracellular membranes in *Escherichia coli* accompanying large scale over-production of the b subunit of F₁F₀ ATP synthase. *FEBS Lett* 482, 215-219.

Arkowitz, R. A., and Bassilana, M. (1994). Protein translocation in *Escherichia coli*. *Biochim Biophys Acta* 1197, 311-343.

Armstrong, C. M. (2003). Voltage-gated K channels. *Sci STKE*, re10.

Barnett, J., Chow, J., Ives, D., Chiou, M., Mackenzie, R., Osen, E., Nguyen, B., Tsing, S., Bach, C., Freire, J., and et al. (1994). Purification, characterization and selective inhibition of human prostaglandin G/H synthase 1 and 2 expressed in the baculovirus system. *Biochim Biophys Acta* 1209, 130-139.

Bayley, H. (1983). *Photogenerated Reagents in Biochemistry and Molecular Biology* (Amsterdam, Elsevier Science publisher B.V.).

Bayley, H., and Knowles, J. R. (1977). Photoaffinity labeling. *Methods Enzymol* 46, 69-114.

Bayley, H., and Knowles, J. R. (1978). Photogenerated reagents for membrane labeling. 1. Phenylnitrene formed within the lipid bilayer. *Biochemistry* 17, 2414-2419.

Beelman, C. A., Stevens, A., Caponigro, G., LaGrandeur, T. E., Hatfield, L., Fortner, D. M., and Parker, R. (1996). An essential component of the decapping enzyme required for normal rates of mRNA turnover. *Nature* 382, 642-646.

Bibi, E., and Kaback, H. R. (1990). *In vivo* expression of the lacY gene in two segments leads to functional lac permease. *Proc Natl Acad Sci U S A* 87, 4325-4329.

- Bibi, E., Stearns, S. M., and Kaback, H. R. (1992). The N-terminal 22 amino acid residues in the lactose permease of *Escherichia coli* are not obligatory for membrane insertion or transport activity. *Proc Natl Acad Sci U S A* 89, 3180-3184.
- Bieszke, J. A., Spudich, E. N., Scott, K. L., Borkovich, K. A., and Spudich, J. L. (1999). A eukaryotic protein, NOP-1, binds retinal to form an archaeal rhodopsin-like photochemically reactive pigment. *Biochemistry* 38, 14138-14145.
- Binda, C., Newton-Vinson, P., Hubalek, F., Edmondson, D. E., and Mattevi, A. (2002). Structure of human monoamine oxidase B, a drug target for the treatment of neurological disorders. *Nat Struct Biol* 9, 22-26.
- Birnir, B., Lee, H. S., Hediger, M. A., and Wright, E. M. (1990). Expression and characterization of the intestinal Na⁺/glucose cotransporter in COS-7 cells. *Biochim Biophys Acta* 1048, 100-104.
- Borhan, B., Souto, M. L., Imai, H., Shichida, Y., and Nakanishi, K. (2000). Movement of retinal along the visual transduction path. *Science* 288, 2209-2212.
- Borst, P., and Elferink, R. O. (2002). Mammalian ABC transporters in health and disease. *Annu Rev Biochem* 71, 537-592.
- Bracey, M. H., Hanson, M. A., Masuda, K. R., Stevens, R. C., and Cravatt, B. F. (2002). Structural adaptations in a membrane enzyme that terminates endocannabinoid signaling. *Science* 298, 1793-1796.
- Brunner, J. (1989). Photochemical labeling of apolar phase of membranes. *Methods Enzymol* 172, 628-687.
- Brunner, J. (1993). New photolabeling and crosslinking methods. *Annu Rev Biochem* 62, 483-514.
- Brunner, J., and Semenza, G. (1981). Selective labeling of the hydrophobic core of membranes with 3-(trifluoromethyl)-3-(m-[¹²⁵I]iodophenyl)diazirine, a carbene-generating reagent. *Biochemistry* 20, 7174-7182.
- Brunner, J., Senn, H., and Richards, F. M. (1980). 3-Trifluoromethyl-3-phenyldiazirine. A new carbene generating group for photolabeling reagents. *J Biol Chem* 255, 3313-3318.
- Brunner, J., Spiess, M., Aggeler, R., Huber, P., and Semenza, G. (1983). Hydrophobic labeling of a single leaflet of the human erythrocyte membrane. *Biochemistry* 22, 3812-3820.
- Burckhardt, G., and Kinne, R. K. H. (1992). Transport Proteins – Co- and Counter-Transporters. In *The Kidney: Physiology and Pathophysiology*, D. W. Seldin, and G. Giebisch, eds. (New York, Raven Press), pp. 537-586.

- Cai, J., Daoud, R., Georges, E., and Gros, P. (2001). Functional expression of multidrug resistance protein 1 in *Pichia pastoris*. *Biochemistry* 40, 8307-8316.
- Cai, J., and Gros, P. (2003). Overexpression, purification, and functional characterization of ATP-binding cassette transporters in the yeast, *Pichia pastoris*. *Biochim Biophys Acta* 1610, 63-76.
- Carpousis, A. J., Van Houwe, G., Ehretsmann, C., and Krisch, H. M. (1994). Copurification of *E. coli* RNAase E and PNPase: evidence for a specific association between two enzymes important in RNA processing and degradation. *Cell* 76, 889-900.
- Carrier, T., Jones, K. L., and Keasling, J. D. (1998). mRNA stability and plasmid copy number effects on gene expression from an inducible promoter system. *Biotechnol Bioeng* 59, 666-672.
- Carrier, T. A., and Keasling, J. D. (1997a). Controlling messenger RNA stability in bacteria: strategies for engineering gene expression. *Biotechnol Prog* 13, 699-708.
- Carrier, T. A., and Keasling, J. D. (1997b). Engineering mRNA stability in *E. coli* by the addition of synthetic hairpins using a 5' cassette system. *Biotechnol and Bioeng* 55, 577-580.
- Carrier, T. A., and Keasling, J. D. (1999). Library of synthetic 5' secondary structures to manipulate mRNA stability in *Escherichia coli*. *Biotechnol Prog* 15, 58-64.
- Cereghino, J. L., and Cregg, J. M. (2000). Heterologous protein expression in the methylotrophic yeast *Pichia pastoris*. *FEMS Microbiol Rev* 24, 45-66.
- Chen, T.-Y. (2003). Coupling gating with ion permeation in ClC channels. *Sci STKE*, pe23.
- Chiara, D. C., Dangott, L. J., Eckenhoff, R. G., and Cohen, J. B. (2003). Identification of nicotinic acetylcholine receptor amino acids photolabeled by the volatile anesthetic halothane. *Biochemistry* 42, 13457-13467.
- Church, R. F., Maleike, R. R., and Weiss, M. J. (1972). Diazirines. 3. Synthesis of a series of diazirine-containing molecules and their pharmacological evaluation. *J Med Chem* 15, 514-518.
- Church, R. F. R., and Weiss, M. J. (1970). Diazirines. II. Synthesis and properties of small functionalized diazirine molecules. Observations on the reaction of a diaziridine with the iodine-iodide ion system. *J Org Chem* 35, 2465-2471.
- Clare, J. J., Rayment, F. B., Ballantine, S. P., Sreekrishna, K., and Romanos, M. A. (1991). High-level expression of tetanus toxin fragment C in *Pichia pastoris* strains containing multiple tandem integrations of the gene. *Biotechnology (N Y)* 9, 455-460.
- Coburn, G. A., and Mackie, G. A. (1999). Degradation of mRNA in *Escherichia coli*: an old problem with some new twists. *Prog Nucleic Acid Res Mol Biol* 62, 55-108.

Cregg, J. M., Cereghino, J. L., Shi, J., and Higgins, D. R. (2000). Recombinant protein expression in *Pichia pastoris*. *Mol Biotechnol* *16*, 23-52.

Darbandi-Tonkabon, R., Hastings, W. R., Zeng, C. M., Akk, G., Manion, B. D., Bracamontes, J. R., Steinbach, J. H., Mennerick, S. J., Covey, D. F., and Evers, A. S. (2003). Photoaffinity labeling with a neuroactive steroid analogue. 6-azi-pregnanolone labels voltage-dependent anion channel-1 in rat brain. *J Biol Chem* *278*, 13196-13206.

Decoursey, T. E. (2003). Voltage-gated proton channels and other proton transfer pathways. *Physiol Rev* *83*, 475-579.

Delfino, J. M., Schreiber, S. L., and Richards, F. M. (1993). Design, synthesis, and properties of a photoactivatable membrane-spanning phospholipidic probe. *J Am Chem Soc* *115*, 3458-3474.

Diedrich, D. F. (1966). Competitive inhibition of intestinal glucose transport by phlorizin analogs. *Arch Biochem Biophys* *117*, 248-256.

Diedrich, D. F. (1990). Photoaffinity-labeling analogs of phlorizin and phloretin: synthesis and effects on cell membranes. *Methods Enzymol* *191*, 755-780.

Diez-Sampedro, A., Loo, D. D., Wright, E. M., Zampighi, G. A., and Hirayama, B. A. (2004). Coupled sodium/glucose cotransport by SGLT1 requires a negative charge at position 454. *Biochemistry* *43*, 13175-13184.

Diez-Sampedro, A., Lostao, M. P., Wright, E. M., and Hirayama, B. A. (2000). Glycoside binding and translocation in Na⁺-dependent glucose cotransporters: comparison of SGLT1 and SGLT3. *J Membr Biol* *176*, 111-117.

Diez-Sampedro, A., Wright, E. M., and Hirayama, B. A. (2001). Residue 457 controls sugar binding and transport in the Na⁺/glucose cotransporter. *J Biol Chem* *276*, 49188-49194.

Do, H., Falcone, D., Lin, J., Andrews, D. W., and Johnson, A. E. (1996). The cotranslational integration of membrane proteins into the phospholipid bilayer is a multistep process. *Cell* *85*, 369-378.

Doring, F., Klapper, M., Theis, S., and Daniel, H. (1998). Use of the glyceraldehyde-3-phosphate dehydrogenase promoter for production of functional mammalian membrane transport proteins in the yeast *Pichia pastoris*. *Biochem Biophys Res Commun* *250*, 531-535.

Dorman, G., and Prestwich, G. D. (1994). Benzophenone photophores in biochemistry. *Biochemistry* *33*, 5661-5673.

Dorman, G., and Prestwich, G. D. (2000). Using photolabile ligands in drug discovery and development. *Trends Biotechnol* *18*, 64-77.

Driessen, A. J. (1994). How proteins cross the bacterial cytoplasmic membrane. *J Membr Biol* *142*, 145-159.

Driessen, A. J., Manting, E. H., and van der Does, C. (2001). The structural basis of protein targeting and translocation in bacteria. *Nat Struct Biol* *8*, 492-498.

D'Silva, P. R., and Lala, A. K. (2000). Organization of diphtheria toxin in membranes. A hydrophobic photolabeling study. *J Biol Chem* *275*, 11771-11777.

Dunbar, L. A., and Caplan, M. J. (2000). The cell biology of ion pumps: sorting and regulation. *Eur J Cell Biol* *79*, 557-563.

Evers, C., Haase, W., Murer, H., and Kinne, R. (1978). Properties of brush border vesicles isolated from rat kidney cortex by calcium precipitation. *Membr Biochem* *1*, 203-219.

Fang, K., Hashimoto, M., Jockusch, S., Turro, N. J., and Nakanishi, K. (1998). A bifunctional photoaffinity probe for ligand/receptor interaction studies. *J Am Chem Soc* *120*, 8543-8544.

Firnges, M. A., Lin, J. T., and Kinne, R. K. (2001). Functional asymmetry of the sodium-D-glucose cotransporter expressed in yeast secretory vesicles. *J Membr Biol* *179*, 143-153.

Fleming, K. G. (2000). Riding the wave: structural and energetic principles of helical membrane proteins. *Curr Opin Biotechnol* *11*, 67-71.

Galardy, R. E., Craig, L. C., Jamieson, J. D., and Printz, M. P. (1974). Photoaffinity labeling of peptide hormone binding sites. *J Biol Chem* *249*, 3510-3518.

Gibbs, E. M., Hosang, M., Reber, B. F., Semenza, G., and Diedrich, D. F. (1982). 4-Azidophlorizin, a high affinity probe and photoaffinity label for the glucose transporter in brush border membranes. *Biochim Biophys Acta* *688*, 547-556.

Guarna, M. M., Lesnicki, G. J., Tam, B. M., Robinson, J., Radziminski, C. Z., Hasenwinkle, D., Boraston, A., Jervis, E., MacGillivray, R. T. A., Turner, R. F. B., and Kilburn, D. G. (1997). Online monitoring and control of methanol concentration in shake-flask cultures of *Pichia pastoris*. *Biotechnol Bioeng* *56*, 279-286.

Hagenbuch, B., and Meier, P. J. (2004). Organic anion transporting polypeptides of the OATP/ SLC21 family: phylogenetic classification as OATP/ SLCO superfamily, new nomenclature and molecular/functional properties. *Pflugers Arch* *447*, 653-665.

Hatanaka, Y., Hashimoto, M., Kurihara, H., Nakayama, H., and Kanaoka, Y. (1994). A novel family of aromatic diazirines for photoaffinity labeling. *J Org Chem* *59*, 383-387.

Hediger, M. A., Coady, M. J., Ikeda, T. S., and Wright, E. M. (1987). Expression cloning and cDNA sequencing of the Na⁺/glucose co-transporter. *Nature* *330*, 379-381.

- Hediger, M. A., Romero, M. F., Peng, J. B., Rolfs, A., Takanaga, H., and Bruford, E. A. (2004). The ABCs of solute carriers: physiological, pathological and therapeutic implications of human membrane transport proteins. *Pflugers Arch* 447, 465-468.
- Heinrich, S. U., Mothes, W., Brunner, J., and Rapoport, T. A. (2000). The Sec61p complex mediates the integration of a membrane protein by allowing lipid partitioning of the transmembrane domain. *Cell* 102, 233-244.
- Hexter, C. S., and Westheimer, F. H. (1971). S-carboxymethylcysteine from the photolysis of diazoacyl trypsin and chymotrypsin. *J Biol Chem* 246, 3934-3938.
- Higgins, D. R., and Cregg, J. M. (1998). Introduction to *Pichia pastoris*. *Methods Mol Biol* 103, 1-15.
- Hosang, M., Gibbs, E. M., Diedrich, D. F., and Semenza, G. (1981). Photoaffinity labeling and identification of (a component of) the small-intestinal Na⁺,D-glucose transporter using 4-azidophlorizin. *FEBS Lett* 130, 244-248.
- Ikeda, T. S., Hwang, E. S., Coady, M. J., Hirayama, B. A., Hediger, M. A., and Wright, E. M. (1989). Characterization of a Na⁺/glucose cotransporter cloned from rabbit small intestine. *J Membr Biol* 110, 87-95.
- Ishida, N., and Kawakita, M. (2004). Molecular physiology and pathology of the nucleotide sugar transporter family (SLC35). *Pflugers Arch* 447, 768-775.
- Jahn, O., Eckart, K., Brauns, O., Tezval, H., and Spiess, J. (2002). The binding protein of corticotropin-releasing factor: ligand-binding site and subunit structure. *Proc Natl Acad Sci U S A* 99, 12055-12060.
- Jiang, Y., Ruta, V., Chen, J., Lee, A., and MacKinnon, R. (2003). The principle of gating charge movement in a voltage-dependent K⁺ channel. *Nature* 423, 42-48.
- Jung, H., Tebbe, S., Schmid, R., and Jung, K. (1998). Unidirectional reconstitution and characterization of purified Na⁺/proline transporter of *Escherichia coli*. *Biochemistry* 37, 11083-11088.
- Kachalsky, S. G., Jensen, B. S., Barchan, D., and Fuchs, S. (1995). Two subsites in the binding domain of the acetylcholine receptor: an aromatic subsite and a proline subsite. *Proc Natl Acad Sci U S A* 92, 10801-10805.
- Kasahara, M., Maeda, M., Hayashi, S., Mori, Y., and Abe, T. (2001). A missense mutation in the Na⁺/glucose cotransporter gene SGLT1 in a patient with congenital glucose-galactose malabsorption: normal trafficking but inactivation of the mutant protein. *Biochim Biophys Acta* 1536, 141-147.

- King, P. A., Betts, J. J., Horton, E. D., and Horton, E. S. (1993). Exercise, unlike insulin, promotes glucose transporter translocation in obese Zucker rat muscle. *Am J Physiol* 265, R447-452.
- Kinne, R. (1976). Properties of the glucose transport system in the renal brush border membrane. *Current Topics in Membranes and Transport* 8, 209-267.
- Kipp, H., Kinne, R. K., and Lin, J. T. (1997). Synthesis of the photoaffinity label [1'-¹⁴C]-6C-(azimethyl)octylglucoside and its reaction with isolated renal brush border membranes. *Anal Biochem* 245, 61-68.
- Kurumbail, R. G., Stevens, A. M., Gierse, J. K., McDonald, J. J., Stegeman, R. A., Pak, J. Y., Gildehaus, D., Miyashiro, J. M., Penning, T. D., Seibert, K., *et al.* (1996). Structural basis for selective inhibition of cyclooxygenase-2 by anti-inflammatory agents. *Nature* 384, 644-648.
- Lam, J. T., Martin, M. G., Turk, E., Hirayama, B. A., Bosshard, N. U., Steinmann, B., and Wright, E. M. (1999). Missense mutations in SGLT1 cause glucose-galactose malabsorption by trafficking defects. *Biochim Biophys Acta* 1453, 297-303.
- Lee, W. Y., Loflin, P., Clancey, C. J., Peng, H., and Lever, J. E. (2000). Cyclic nucleotide regulation of Na⁺/glucose cotransporter (SGLT1) mRNA stability. Interaction of a nucleocytoplasmic protein with a regulatory domain in the 3'-untranslated region critical for stabilization. *J Biol Chem* 275, 33998-34008.
- Lehmann, J., and Thieme, R. (1986). Synthesis of 6-C-aza-6-deoxy-D-glucose and -D-galactose for photoaffinity labelling of carbohydrate-binding proteins. *Liebigs Annalen der Chemie*, 525-532.
- Leite, J. F., Blanton, M. P., Shahgholi, M., Dougherty, D. A., and Lester, H. A. (2003). Conformation-dependent hydrophobic photolabeling of the nicotinic receptor: electrophysiology-coordinated photochemistry and mass spectrometry. *Proc Natl Acad Sci U S A* 100, 13054-13059.
- Li de La Sierra, I. M., Gally, J., Vincent, M., Bertrand, T., Briozzo, P., Barzu, O., and Gilles, A. M. (2000). Substrate-induced fit of the ATP binding site of cytidine monophosphate kinase from *Escherichia coli*: time-resolved fluorescence of 3'-anthraniloyl-2'-deoxy-ADP and molecular modeling. *Biochemistry* 39, 15870-15878.
- Liessem, B., Glombitza, G. J., Knoll, F., Lehmann, J., Kellermann, J., Lottspeich, F., and Sandhoff, K. (1995). Photoaffinity labeling of human lysosomal beta-hexosaminidase B. Identification of Glu-355 at the substrate binding site. *J Biol Chem* 270, 23693-23699.
- Lin, J., Kormanec, J., Homerova, D., and Kinne, R. K. (1999). Probing transmembrane topology of the high-affinity Sodium/Glucose cotransporter (SGLT1) with histidine-tagged mutants. *J Membr Biol* 170, 243-252.

- Lin, J. T., Hahn, K. D., and Kinne, R. (1982). Synthesis of phlorizin derivatives and their inhibitory effect on the renal sodium/D-glucose cotransport system. *Biochim Biophys Acta* 693, 379-388.
- Lin, J. T., Kormanec, J., Wehner, F., Wielert-Badt, S., and Kinne, R. K. (1998). High-level expression of Na⁺/D-glucose cotransporter (SGLT1) in a stably transfected Chinese hamster ovary cell line. *Biochim Biophys Acta* 1373, 309-320.
- Lin-Chao, S., and Cohen, S. N. (1991). The rate of processing and degradation of antisense RNAI regulates the replication of *ColE1*-type plasmids *in vivo*. *Cell* 65, 1233-1242.
- Lo, B., and Silverman, M. (1998). Cysteine scanning mutagenesis of the segment between putative transmembrane helices IV and V of the high affinity Na⁺/Glucose cotransporter SGLT1. Evidence that this region participates in the Na⁺ and voltage dependence of the transporter. *J Biol Chem* 273, 29341-29351.
- Loll, P. J. (2003). Membrane protein structural biology: the high throughput challenge. *J Struct Biol* 142, 144-153.
- Loo, D. D., Hazama, A., Supplisson, S., Turk, E., and Wright, E. M. (1993). Relaxation kinetics of the Na⁺/glucose cotransporter. *Proc Natl Acad Sci U S A* 90, 5767-5771.
- Loo, D. D., Hirayama, B. A., Gallardo, E. M., Lam, J. T., Turk, E., and Wright, E. M. (1998). Conformational changes couple Na⁺ and glucose transport. *Proc Natl Acad Sci U S A* 95, 7789-7794.
- Lostao, M. P., Hirayama, B. A., Panayotova-Heiermann, M., Sampogna, S. L., Bok, D., and Wright, E. M. (1995). Arginine-427 in the Na⁺/glucose cotransporter (SGLT1) is involved in trafficking to the plasma membrane. *FEBS Lett* 377, 181-184.
- Lucke, H., Berner, W., Menge, H., and Murer, H. (1978). Sugar transport by brush border membrane vesicles isolated from human small intestine. *Pflugers Arch* 373, 243-248.
- Lynch, B. A., Lambeng, N., Nocka, K., Kensel-Hammes, P., Bajjalieh, S. M., Matagne, A., and Fuks, B. (2004). The synaptic vesicle protein SV2A is the binding site for the antiepileptic drug levetiracetam. *Proc Natl Acad Sci U S A* 101, 9861-9866.
- Mackie, G. A. (1998). Ribonuclease E is a 5'-end-dependent endonuclease. *Nature* 395, 720-723.
- Mallee, J. J., Atta, M. G., Lorica, V., Rim, J. S., Kwon, H. M., Lucente, A. D., Wang, Y., and Berry, G. T. (1997). The structural organization of the human Na⁺/myo-inositol cotransporter (SLC5A3) gene and characterization of the promoter. *Genomics* 46, 459-465.
- Mangroo, D., and Gerber, G. E. (1992). Photoaffinity labeling of fatty acid-binding proteins involved in long chain fatty acid transport in *Escherichia coli*. *J Biol Chem* 267, 17095-17101.

- Martin, M. G., Lostao, M. P., Turk, E., Lam, J., Kreman, M., and Wright, E. M. (1997). Compound missense mutations in the sodium/D-glucose cotransporter result in trafficking defects. *Gastroenterology* *112*, 1206-1212.
- Martin, M. G., Turk, E., Lostao, M. P., Kerner, C., and Wright, E. M. (1996). Defects in Na⁺/glucose cotransporter (SGLT1) trafficking and function cause glucose-galactose malabsorption. *Nat Genet* *12*, 216-220.
- Matter, K., Hunziker, W., and Mellman, I. (1992). Basolateral sorting of LDL receptor in MDCK cells: the cytoplasmic domain contains two tyrosine-dependent targeting determinants. *Cell* *71*, 741-753.
- McDowall, K. J., Kaberdin, V. R., Wu, S. W., Cohen, S. N., and Lin-Chao, S. (1995). Site-specific RNase E cleavage of oligonucleotides and inhibition by stem-loops. *Nature* *374*, 287-290.
- Meinild, A. K., Loo, D. D., Hirayama, B. A., Gallardo, E., and Wright, E. M. (2001). Evidence for the involvement of Ala 166 in coupling Na⁺ to sugar transport through the human Na⁺/glucose cotransporter. *Biochemistry* *40*, 11897-11904.
- Melefors, O., and von Gabain, A. (1988). Site-specific endonucleolytic cleavages and the regulation of stability of *E. coli* ompA mRNA. *Cell* *52*, 893-901.
- Mothes, W., Heinrich, S. U., Graf, R., Nilsson, I., von Heijne, G., Brunner, J., and Rapoport, T. A. (1997). Molecular mechanism of membrane protein integration into the endoplasmic reticulum. *Cell* *89*, 523-533.
- Muhlrاد, D., Decker, C. J., and Parker, R. (1995). Turnover mechanisms of the stable yeast PGK1 mRNA. *Mol Cell Biol* *15*, 2145-2156.
- Muhlrاد, D., and Parker, R. (1992). Mutations affecting stability and deadenylation of the yeast MFA2 transcript. *Genes Dev* *6*, 2100-2111.
- Muller, V., and Gruber, G. (2003). ATP synthases: structure, function and evolution of unique energy converters. *Cell Mol Life Sci* *60*, 474-494.
- Napoli, R., Hirshman, M. F., and Horton, E. S. (1995). Mechanisms and time course of impaired skeletal muscle glucose transport activity in streptozocin diabetic rats. *J Clin Invest* *96*, 427-437.
- Nassal, M. (1984). 4'-(1-Azi-2,2,2-trifluoroethyl)phenylalanine, a photolabile carbene-generating analog of phenylalanine. *J Am Chem Soc* *106*, 7540-7545.
- Nielsen, H., Engelbrecht, J., Brunak, S., and von Heijne, G. (1997). Identification of prokaryotic and eukaryotic signal peptides and prediction of their cleavage sites. *Protein Eng* *10*, 1-6.

- Novakova, R., Homerova, D., Kinne, R. K., Kinne-Saffran, E., and Lin, J. T. (2001). Identification of a region critically involved in the interaction of phlorizin with the rabbit sodium-D-glucose cotransporter SGLT1. *J Membr Biol* 184, 55-60.
- Okuda, T., Haga, T., Kanai, Y., Endou, H., Ishihara, T., and Katsura, I. (2000). Identification and characterization of the high-affinity choline transporter. *Nat Neurosci* 3, 120-125.
- Panayotova-Heiermann, M., Eskandari, S., Turk, E., Zampighi, G. A., and Wright, E. M. (1997). Five transmembrane helices form the sugar pathway through the Na⁺/glucose cotransporter. *J Biol Chem* 272, 20324-20327.
- Panayotova-Heiermann, M., Leung, D. W., Hirayama, B. A., and Wright, E. M. (1999). Purification and functional reconstitution of a truncated human Na⁺/glucose cotransporter (SGLT1) expressed in *E. coli*. *FEBS Lett* 459, 386-390.
- Panayotova-Heiermann, M., Loo, D. D., Kong, C. T., Lever, J. E., and Wright, E. M. (1996). Sugar binding to Na⁺/glucose cotransporters is determined by the carboxyl-terminal half of the protein. *J Biol Chem* 271, 10029-10034.
- Parent, L., Supplisson, S., Loo, D. D., and Wright, E. M. (1992a). Electrogenic properties of the cloned Na⁺/glucose cotransporter: I. Voltage-clamp studies. *J Membr Biol* 125, 49-62.
- Parent, L., Supplisson, S., Loo, D. D., and Wright, E. M. (1992b). Electrogenic properties of the cloned Na⁺/glucose cotransporter: II. A transport model under nonrapid equilibrium conditions. *J Membr Biol* 125, 63-79.
- Paulus, M., Haslbeck, M., and Watzele, M. (2004). RNA stem-loop enhanced expression of previously non-expressible genes. *Nucleic Acids Res* 32, e78.
- Peerce, B. E., and Wright, E. M. (1984). Conformational changes in the intestinal brush border sodium-glucose cotransporter labeled with fluorescein isothiocyanate. *Proc Natl Acad Sci U S A* 81, 2223-2226.
- Peterson, G. L. (1977). A simplification of the protein assay method of Lowry et al. which is more generally applicable. *Anal Biochem* 83, 346-356.
- Platz, M., Admasu, A. S., Kwiatkowski, S., Crocker, P. J., Imai, N., and Watt, D. S. (1991). Photolysis of 3-aryl-3-(trifluoromethyl)diazirines: a caveat regarding their use in photoaffinity probes. *Bioconjug Chem* 2, 337-341.
- Pohlschroder, M., Prinz, W. A., Hartmann, E., and Beckwith, J. (1997). Protein translocation in the three domains of life: variations on a theme. *Cell* 91, 563-566.
- Pratt, M. B., Husain, S. S., Miller, K. W., and Cohen, J. B. (2000). Identification of sites of incorporation in the nicotinic acetylcholine receptor of a photoactivatable general anesthetic. *J Biol Chem* 275, 29441-29451.

- Prestwich, G. D., Dorman, G., Elliott, J. T., Marecak, D. M., and Chaudhary, A. (1997). Benzophenone photoprobes for phosphoinositides, peptides and drugs. *Photochem Photobiol* 65, 222-234.
- Qi, C., and Pekala, P. H. (1999). The influence of mRNA stability on glucose transporter (GLUT1) gene expression. *Biochem Biophys Res Commun* 263, 265-269.
- Quick, M., and Jung, H. (1998). A conserved aspartate residue, Asp187, is important for Na⁺-dependent proline binding and transport by the Na⁺/proline transporter of *Escherichia coli*. *Biochemistry* 37, 13800-13806.
- Quick, M., and Wright, E. M. (2002). Employing *Escherichia coli* to functionally express, purify, and characterize a human transporter. *Proc Natl Acad Sci U S A* 99, 8597-8601.
- Raja, M. M., Kipp, H., and Kinne, R. K. (2004). C-terminus loop 13 of Na⁺ glucose cotransporter SGLT1 contains a binding site for alkyl glucosides. *Biochemistry* 43, 10944-10951.
- Raja, M. M., Tyagi, N. K., and Kinne, R. K. (2003). Phlorizin recognition in a C-terminal fragment of SGLT1 studied by tryptophan scanning and affinity labeling. *J Biol Chem* 278, 49154-49163.
- Rigaud, J. L., and Levy, D. (2003). Reconstitution of membrane proteins into liposomes. *Methods Enzymol* 372, 65-86.
- Rigaud, J. L., Pitard, B., and Levy, D. (1995). Reconstitution of membrane proteins into liposomes: application to energy-transducing membrane proteins. *Biochim Biophys Acta* 1231, 223-246.
- Roll, P., Massacrier, A., Pereira, S., Robaglia-Schlupp, A., Cau, P., and Szepetowski, P. (2002). New human sodium/glucose cotransporter gene (KST1): identification, characterization, and mutation analysis in ICCA (infantile convulsions and choreoathetosis) and BFIC (benign familial infantile convulsions) families. *Gene* 285, 141-148.
- Romanos, M., Scorer, C., Sreekrishna, K., and Clare, J. (1998). The generation of multicopy recombinant strains. *Methods Mol Biol* 103, 55-72.
- Rudnick, G., Kaback, H. R., and Weil, R. (1975). Photoinactivation of the beta-galactoside transport system in *Escherichia coli* membrane vesicles with 2-nitro-4-azidophenyl-1-thio-beta-D-galactopyranoside. *J Biol Chem* 250, 1371-1375.
- Sakaguchi, M. (1997). Eukaryotic protein secretion. *Curr Opin Biotechnol* 8, 595-601.
- Sambrook, J., and Russell, D. W. (2001). *Molecular Cloning A Laboratory manual*, 3 edn, Cold Spring Harbor Laboratory Press, New York).

Sandoval, I. V., and Bakke, O. (1994). Targeting of membrane proteins to endosomes and lysosomes. *Trends Cell Biol* 4, 292-297.

Sawyer, G. W., Chiara, D. C., Olsen, R. W., and Cohen, J. B. (2002). Identification of the bovine gamma-aminobutyric acid type A receptor alpha subunit residues photolabeled by the imidazobenzodiazepine [³H]Ro15-4513. *J Biol Chem* 277, 50036-50045.

Schultz, S. G., and Curran, P. F. (1970). Coupled transport of sodium and organic solutes. *Physiol Rev* 50, 637-718.

Shafer, J., Baronowsky, P., Laursen, R., Finn, F., and Westheimer, F. H. (1966). Products from the photolysis of diazoacetyl chymotrypsin. *J Biol Chem* 241, 421-427.

Shyu, A. B., Belasco, J. G., and Greenberg, M. E. (1991). Two distinct destabilizing elements in the c-fos message trigger deadenylation as a first step in rapid mRNA decay. *Genes Dev* 5, 221-231.

Smith, C. D., Hirayama, B. A., and Wright, E. M. (1992). Baculovirus-mediated expression of the Na⁺/glucose cotransporter in Sf9 cells. *Biochim Biophys Acta* 1104, 151-159.

Smolke, C. D., Carrier, T. A., and Keasling, J. D. (2000). Coordinated, differential expression of two genes through directed mRNA cleavage and stabilization by secondary structures. *Appl Environ Microbiol* 66, 5399-5405.

Smolke, C. D., and Keasling, J. D. (2002). Effect of gene location, mRNA secondary structures, and RNase sites on expression of two genes in an engineered operon. *Biotechnol Bioeng* 80, 762-776.

Staros, J. V., and Knowles, J. R. (1978). Photoaffinity inhibition of dipeptide transport in *Escherichia coli*. *Biochemistry* 17, 3321-3325.

Strugatsky, D., Gottschalk, K. E., Goldshleger, R., Bibi, E., and Karlish, S. J. (2003). Expression of Na⁺,K⁺-ATPase in *Pichia pastoris*: analysis of wild type and D369N mutant proteins by Fe²⁺-catalyzed oxidative cleavage and molecular modeling. *J Biol Chem* 278, 46064-46073.

Takagaki, Y., Radhakrishnan, R., Gupta, C. M., and Khorana, H. G. (1983). The membrane-embedded segment of cytochrome b5 as studied by cross-linking with photoactivatable phospholipids. *J Biol Chem* 258, 9128-9135.

Talmont, F., Sidobre, S., Demange, P., Milon, A., and Emorine, L. J. (1996). Expression and pharmacological characterization of the human mu-opioid receptor in the methylotrophic yeast *Pichia pastoris*. *FEBS Lett* 394, 268-272.

Tate, C. G. (2001). Overexpression of mammalian integral membrane proteins for structural studies. *FEBS Lett* 504, 94-98.

Terman, B. I., and Insel, P. A. (1986). Photoaffinity labeling of alpha 1-adrenergic receptors of rat heart. *J Biol Chem* 261, 5603-5609.

Thiele, C., Hannah, M. J., Fahrenholz, F., and Huttner, W. B. (2000). Cholesterol binds to synaptophysin and is required for biogenesis of synaptic vesicles. *Nat Cell Biol* 2, 42-49.

Tomcsanyi, T., and Apirion, D. (1985). Processing enzyme ribonuclease E specifically cleaves RNA I. An inhibitor of primer formation in plasmid DNA synthesis. *J Mol Biol* 185, 713-720.

Trosper, T., and Levy, D. (1977). Photocatalyzed labeling of adipocyte plasma membranes with an aryl azide derivative of glucose. *J Biol Chem* 252, 181-186.

Turk, E., Kerner, C. J., Lostao, M. P., and Wright, E. M. (1996). Membrane topology of the human Na⁺/glucose cotransporter SGLT1. *J Biol Chem* 271, 1925-1934.

Turk, E., Kim, O., le Coutre, J., Whitelegge, J. P., Eskandari, S., Lam, J. T., Kreman, M., Zampighi, G., Faull, K. F., and Wright, E. M. (2000). Molecular characterization of *Vibrio parahaemolyticus* vSGLT: a model for sodium-coupled sugar cotransporters. *J Biol Chem* 275, 25711-25716.

Turk, E., Martin, M. G., and Wright, E. M. (1994). Structure of the human Na⁺/glucose cotransporter gene SGLT1. *J Biol Chem* 269, 15204-15209.

Turk, E., and Wright, E. M. (1997). Membrane topology motifs in the SGLT cotransporter family. *J Membr Biol* 159, 1-20.

Turk, E., Zabel, B., Mundlos, S., Dyer, J., and Wright, E. M. (1991). Glucose/galactose malabsorption caused by a defect in the Na⁺/glucose cotransporter. *Nature* 350, 354-356.

Tyagi, N. K., and Kinne, R. K. (2003). Synthesis of photoaffinity probes [2'-iodo-4'-(3"-trifluoromethyldiazirinyloxy)phenoxy]-D-glucopyranoside and [(4'-benzoyloxy)phenoxy]-D-glucopyranoside for the identification of sugar-binding and phlorizin-binding sites in the sodium/D-glucose cotransporter protein. *Anal Biochem* 323, 74-83.

van Veen, H. W., Margolles, A., Muller, M., Higgins, C. F., and Konings, W. N. (2000). The homodimeric ATP-binding cassette transporter LmrA mediates multidrug transport by an alternating two-site (two-cylinder engine) mechanism. *Embo J* 19, 2503-2514.

Vazquez-Ibar, J. L., Guan, L., Svrakic, M., and Kaback, H. R. (2003). Exploiting luminescence spectroscopy to elucidate the interaction between sugar and a tryptophan residue in the lactose permease of *Escherichia coli*. *Proc Natl Acad Sci U S A* 100, 12706-12711.

von Ballmoos, C., Brunner, J., and Dimroth, P. (2004). The ion channel of F-ATP synthase is the target of toxic organotin compounds. *Proc Natl Acad Sci U S A* 101, 11239-11244.

Walker, J. E., Saraste, M., and Gay, N. J. (1982). *E. coli* F1-ATPase interacts with a membrane protein component of a proton channel. *Nature* 298, 867-869.

Wang, D., Chiara, D. C., Xie, Y., and Cohen, J. B. (2000). Probing the structure of the nicotinic acetylcholine receptor with 4-benzoylbenzoylcholine, a novel photoaffinity competitive antagonist. *J Biol Chem* 275, 28666-28674.

Wang, H., Dutta, B., Huang, W., Devoe, L. D., Leibach, F. H., Ganapathy, V., and Prasad, P. D. (1999). Human Na⁺-dependent vitamin C transporter 1 (hSVCT1): primary structure, functional characteristics and evidence for a non-functional splice variant. *Biochim Biophys Acta* 1461, 1-9.

Weinglass, A. B., and Kaback, H. R. (2000). The central cytoplasmic loop of the major facilitator superfamily of transport proteins governs efficient membrane insertion. *Proc Natl Acad Sci U S A* 97, 8938-8943.

Weiss, H. M., Haase, W., and Reilander, H. (1998). Expression of an integral membrane protein, the 5HT_{5A} receptor. *Methods Mol Biol* 103, 227-239.

Wielert-Badt, S., Hinterdorfer, P., Gruber, H. J., Lin, J. T., Badt, D., Wimmer, B., Schindler, H., and Kinne, R. K. (2002). Single molecule recognition of protein binding epitopes in brush border membranes by force microscopy. *Biophys J* 82, 2767-2774.

Wielert-Badt, S., Lin, J. T., Lorenz, M., Fritz, S., and Kinne, R. K. (2000). Probing the conformation of the sugar transport inhibitor phlorizin by 2D-NMR, molecular dynamics studies, and pharmacophore analysis. *J Med Chem* 43, 1692-1698.

Wright, E. M., Hirayama, B. A., Loo, D. D. F., Turk, E., and Hager, K. (1994). Intestinal Sugar Transport. In *Physiology of Gastrointestinal Tract*, L. R. Johnson, ed. (New York, Raven Press), pp. 1751-1772.

Wright, E. M., and Loo, D. D. (2000). Coupling between Na⁺, sugar, and water transport across the intestine. *Ann N Y Acad Sci* 915, 54-66.

Wright, E. M., Martín, G. M., and Turk, E. (2001). Familial Glucose-Galactose Malabsorption and Hereditary Renal Glycosuria. In *Metabolic Basis of Inherited Disease*, C. R. Scriver, A. L. Beaudet, W. S. Sly, and D. Valle, eds. (McGraw-Hill, New-York), pp. 4891-4908.

Wright, E. M., and Turk, E. (2004). The sodium/glucose cotransport family SLC5. *Pflugers Arch* 447, 510-518.

Wright, E. M., Turk, E., and Martin, M. G. (2002). Molecular basis for glucose-galactose malabsorption. *Cell Biochem Biophys* 36, 115-121.

Xia, X., Lin, J. T., and Kinne, R. K. (2003). Binding of phlorizin to the isolated C-terminal extramembranous loop of the Na⁺/glucose cotransporter assessed by intrinsic tryptophan fluorescence. *Biochemistry* 42, 6115-6120.

Yu, F. H., and Catterall, W. A. (2003). Overview of the voltage-gated sodium channel family. *Genome Biol* 4, 207.

Zhang, S. P., Zubay, G., and Goldman, E. (1991). Low-usage codons in *Escherichia coli*, yeast, fruit fly and primates. *Gene* 105, 61-72.

Ziebell, M. R., Nirthanan, S., Husain, S. S., Miller, K. W., and Cohen, J. B. (2004). Identification of binding sites in the nicotinic acetylcholine receptor for [³H]azietomidate, a photoactivatable general anesthetic. *J Biol Chem* 279, 17640-17649.

Erklärung

Erklärung

Hiermit erkläre ich, das ich die Dissertation selbständig verfasst habe und keine anderen Hilfsmittel als die in der Dissertation angegebenen verwendet habe.

Dortmund, den 25.02.05

Navneet Kumar Tyagi

Acknowledgements

I take this opportunity to convey my deepest sense of gratitude to all those who helped in my venture.

First and foremost, I would like to thank Prof. Dr. Rolf K.H. Kinne for his ardent support and guidance throughout my PhD career. It is indeed an honor to have carried out my doctoral research under his supervision. He has introduced me to a multitude of fields including the most exciting field of membrane protein biochemistry and molecular biology. The experience has been an enlightening one, thereby making me a penchant for various aspects of this field, besides being cognizant of other areas of studies carried out at the interface of chemistry and biology. He has always lended me a patient and helping attitude. Many a time it has been his elegant creativity and grand experience in the field of science that helped me tackle the problem with ease. Thanks to his timely suggestions at various stages of this work, which has truly helped and managed to mould the work undertaken into its present shape.

I am also grateful to late Prof. Dr. Anil K. Lala (Indian Institute of Technology, Bombay, India) for inculcating in me, a working philosophy that is necessary for doing cutting edge research. I have gained an invaluable experience through my association with him, on how to approach, how not to and finally tackle the problem at hand.

My special thanks to Prof. Dr. Wolfgang Siess (Ludwing Maxmillian University, Munich, Germany) for his kind permission to perform my experiments related to the expression of human sodium/glucose cotransporter in his lab. His immense support and encouragements has helped me to succeed in high-level expression of this protein.

I thank Prof. Dr. Keith W. Miller (Harvard Medical School/ Massachusetts General Hospital, Boston, USA), and all his group member for a wonderful collaboration and supportive discussions.

I thank Prof. Dr. Herbert Waldmann for being in my examination committee.

I wish to thank Dr. Pankaj Goyal for his wonderful advices and support for the expression of hSGLT1 protein, without whom this work would not have taken a complete shape.

Special thanks to my expert molecular biologist friends Dr. Patrick R. D`Silva, Dr. Rana Roy, and Dr. Suneel Kateriya for their valuable advices.

I wish to thank Dr. Jutta Rötter for her support, and managing all the bureaucratic matters especially money matters for me.

I thank International Max-Planck Research School in Chemical Biology for providing me fellowship and for generous travel grants.

I thank Natascha and Niklas for their assistance in official matters and for giving me loads of information.

I wish to thank my special friends Manish Verma and Deepali Gupta for their encouragement, advices, affection and support. I have spent three wonderful and memorable years with them.

I wish to thank Dr. Ritu Dhawan for carefully proofreading the entire thesis.

Acknowledgements

I wish to thank all my friends namely, Dharemendra Pandey, Dr. Heidrun Olsen, Dr. Okram Barun, Dr. Anupam Bhattacharya, Dr. Ankur Kulshertha and all others for their excellent support.

I thank all the staff members of the Epithelial cell physiology department for their kind assistance during the course of this work.

I owe to my parents for their continuous support and blessings. Special appreciations are due to my loving brothers, Vikas, Adarsh and Azad, bhabhis, Vineta and Bina, my wonderful sister, Poonam and Jijaji subodh, for their love and care bestowed upon me. I cannot forget affection given by Abhinav (Vishu), Appoorva (Chinu), Soumya (Anya), Abhijay (Abhi), Saahil (Arnav) and Aryan.

Curriculum Vitae

Name: Navneet Kumar Tyagi
Date of birth: July 13, 1977
Place of birth: Meerut, India
Nationality: Indian

Education:

July 1990- June 1992 10th Std. (St. Charls Inter College Sardhana, India)
July 1992- June 1994 12th Std. (St. Charls Inter College Sardhana, India)
July 1994- June 1997 BS, Biology (SGPG College, Saraapur Khurd, India)
July 1997-June 1999 MS, Chemistry (University of Roorkee, Roorkee, India)
July 1999- June 2001 Project Assistant in the Department of Chemistry, Indian Institute of Technology, Bombay, India
Nov. 2001- present Ph. D Thesis at the Department of Epithelial Cell Physiology, Max-Planck Institute for Molecular Physiology, Dortmund, Germany, Under the Supervision of Prof. Dr. Dr. h.c. Rolf K.H. Kinne

Awards/Achievements and experiences:

2004 Worked for 9 months Collaboration project with **Prof. Dr. Wolfgang Siess**, Institute for Prevention of Cardiovascular Diseases in Ludwig Maximilians University Munich, Germany
2003 Worked for 5 months Collaboration project with **Prof. Keith W. Miller**. in the department of Anesthesia and Critical care, Massachusetts General Hospital/Harvard Medical School, Boston, USA.
2003 Recipient of Martin-Schmeisser fellowship from university of Dortmund Germany
2002-2004 Awarded fellowship for Ph. D program by International Max-Planck Research School in Chemical Biology.
2001 Worked as a Visiting scientist in Department of Neurobiology, Heidelberg University, Germany.
1999-2001 Worked as a junior research assistant in Indian Institute of Technolgy, Bombay, India.
1999 Awarded Junior Research Fellowship by Department of Science and Technology, Government of India.

Curriculum vitae

1999 Qualified for Graduate aptitude test in Engineering (GATE) with score of 94.43 in the year 1999.

Publications:

1. **Navneet K. Tyagi**; and Rolf K. H. Kinne (2003) "Synthesis of Photoaffinity Probe [(2'-Iodo-4'-(3"-trifluoromethyldiaziranyl) Phenoxy)]-D-Glucopyranoside (TIPDG) and [(4'-Benzoyl) Phenoxy)]-D-Glucopyranoside for the Identification of Sugar Binding and Phlorizin Binding Sites in the Sodium/D-Glucose Cotransporter Protein (SGLT1)." *Anal. Biochem.* **323**, 74-83.
2. M. Mobeen. Raja; **Navneet K. Tyagi**; and Rolf K. H. Kinne (2003) "Phlorizin Recognition in a C-terminal Fragments of SGLT1 Studied by Trp Scanning and Affinity Labeling." *J. Biol. Chem.* **278**, 49154-49163.
3. **Navneet K. Tyagi**; Pankaj Goyal; Dharemendra Pandey; Wolfgang Siess; and Rolf K. H. Kinne (2005) "Functional Expression, Purification, and Characterization of Human Na⁺/D-Glucose Transporter (hSGLT1) in *Pichia pastoris*" *J. Biol. Chem.* (Communicated).
4. **Navneet K. Tyagi**; Pankaj Goyal; Wolfgang Siess; and Rolf K. H. Kinne (2005) "Messenger RNA Stability is the Major Hurdle in the Expression of Human Membrane Proteins in *E. coli*" (Under Preparation).
5. Azad Kumar; **Navneet K. Tyagi**; Pankaj Goyal; Wolfgang Siess; and Rolf K. H. Kinne (2005) "Ligand-Dependent Conformational Changes in Human Sodium/Glucose Cotransporter1 in Solution and in Reconstituted Forms as Studied by Fluorescence Spectroscopy" (Under Preparation).
6. Dharemendra Pandey; Pankaj Goyal; **Navneet K. Tyagi**; Rolf K. H. Kinne; and Wolfgang Siess (2005) "Over-expression, Purification, and Functional Characterization of Human LIMK-2 in the Yeast, *Pichia pastoris*" (Under Preparation).
7. Pankaj Goyal; Dharemendra Pandey; **Navneet K. Tyagi**; Rolf K. H. Kinne; and Wolfgang Siess (2005) "Identification and Characterization of Nuclear and Nucleolus Signal Sequences in LIMK2" (Under Preparation).